Title
Adaptive Rejection of Narrow Band Disturbance in Hard Disk Drives

Author
Zheng, Qixing

Publication Date
2009

Peer reviewed|Thesis/dissertation

Adaptive Rejection of Narrow Band Disturbance in Hard Disk Drives

by

Qixing Zheng

A dissertation submitted in partial satisfaction of the

requirements for the degree of

Doctor of Philosophy

in

Engineering-Mechanical Engineering

in the

Graduate Division

of the

University of California, Berkeley

Committee in charge:

Professor Masayoshi Tomizuka, Chair
Professor Roberto Horowitz
Professor Avideh Zakhor

Fall 2009

Adaptive Rejection of Narrow Band Disturbance in Hard Disk Drives

Abstract

Adaptive Rejection of Narrow Band Disturbance in Hard Disk Drives

by

Qixing Zheng

Doctor of Philosophy in Engineering-Mechanical Engineering

University of California at Berkeley

Professor Masayoshi Tomizuka, Chair

The hard disk drive (HDD) industry strives for higher storage densities and capacities. The critical factor for the performance of HDDs in this regard is the track mis-registration (TMR) which is the statistical number to indicate the performance of track-following control. After traditional track-following servo control, several visible frequency components remain in the spectrum of non-repeatable position error signal (PES). The dominant ones among these frequency components are a main contributor to the TMR. The rejection of these dominant components via servo control is difficult due to the fact that the frequency of the dominant component is not exactly known.

This dissertation introduces several adaptive control schemes to reject the dominant frequency component (narrow band disturbance with the largest magnitude) to reduce TMR for higher achievable areal density of HDDs.

A natural approach to narrow band disturbance rejection is indirect adaptive control, which involves two steps both performed in real time. At the first step, the frequency of the dominant component is estimated. Two frequency estimation methods are investigated in this dissertation. The discrete Fourier transform (DFT) method results in fast and accurate frequency estimation, but its large computational amount makes it an impratical approach for on-line identification. The least mean squares (LMS) algorithm is a computationally simple method for frequency identification. Carefully choosing the step size profile, the frequency estimate converges within one revolution and the resulting bias is small. The second step of the indirect adaptive control is to apply an add-on compensator based on the frequency estimate to reject the dominant component. Two choices for the add-on compensator are discussed in this dissertation. One is to identify the magnitude and phase of the dominant component. With the identified frequency, magnitude and phase, an estimate of the dominant component is constructed and then canceled by the control signal. This scheme is further extended to rejecting multiple frequency components. Another proposed compensator adopts the structure of a disturbance observer (DOB). The Q filter in DOB is selected to be a narrow band-pass filter centered at the estimated frequency. A deep notch in the error rejection function is introduced by the DOB with such a Q filter to reject the dominant component.

Two direct adaptive control schemes, which adapt compensator parameters directly, are also applied to compensate for the dominant component. One scheme applies a finite-impulse-response (FIR) Q filter built around the baseline servo controller to reject the dominant component based on Youla-Kucera parameterization. The coefficients of the Q filter are updated

in such a way that the resulting controller incorporates the internal model of the narrow-band disturbance. To make the scheme suited for HDD systems, two modifications are proposed: 1) adding a pre-specified term to the Q filter to avoid large transient oscillation, and 2) cascading a bandpass filter to the Q filter to deal with inaccurate HDD plant model as well as to limit the waterbed effect to a certain frequency range. Another direct adaptive controller adopts the disturbance observer (DOB) loop with a narrow bandpass Q filter. The frequency parameter of the Q filter is directly adapted to the optimal value in the sense of minimizing the track-following TMR.

Realistic simulation tools are used to show that all adaptive control schemes described in this dissertation are effective in terms of rejecting narrow band disturbances to achieve smaller TMR. The advantages and disadvantages of each scheme are also discussed.

Contents

List of Figures

Chapter 1

Introduction

Hard disk drives (HDDs) continue to be the dominant large-capacity storage system. This dissertation is concerned with the advanced control algorithms to reject the narrow band disturbance in HDDs to improve the track-following servo performance. A brief introduction of the HDD components is given in Section 1.1. Section 1.2 provides an overview of the HDD servo system. The outline of the dissertation is provided in Section 1.3.

1.1 Hard Disk Drive Components

The first hard disk was brought to market by IBM in 1956 ([2]). Since then, the cost per megabytes of HDD has been constantly decreasing, while the capacity has been constantly increasing and the performance of data access has been constantly improving. All these progresses owe to great advances in many disciplines, including servo control. The servo problem for HDDs is very challenging as visualized using the following analogy ([57]).

> *Imagine an airplane flying at 5M miles per hour but only 1/16 inch above the ground on a highway with 100,000 lanes where the width of each lane is only fraction of an inch. The challenge of the problem is further intensified by the fact that the airplane is expected to switch lanes frequently and then follow the new lane with the same precision. A scaled down version of this scenario is what one finds in the head positioning servomechanism of an HDD.*

Before we introduce the servo control system for HDDs, we should first look inside our control object, the HDD system. Figure 1.1 shows the servo-related main components of a hard disk drive. The user data is stored in concentric rings called tracks on the surface of the round flat disks. Tracks are further divided into sectors. In addition to the data sectors that hold user data, there are also servo sectors, which can provide the relative position of the head to the HDD

servo system. The disks are stacked on top of one another along a spindle and are rotated by a spindle motor. The data is accessed (read from or written to the disk) by a magneto-resistive read head and a thin film inductive write head, which are mounted on head sliders that are carried by suspensions. The suspensions are mounted on the actuator arm or E-block. The heads, the sliders, the suspensions, and the E-block together are known as the head stack assembly (HSA). During the read/write operation, the whole HSA is moved or maintained position by an actuator, the voice coil motor (VCM) shown in Fig. 1.1.

Figure 1.1: HDD components: 1) disks; 2) a track; 3) spindle; 4) head slider; 5) suspension; 6) actuator arm or E-block; 7) pivot bearing; 8) voice coil motor (VCM).

1.2 Hard Disk Drive Servo System

There are two parts in the HDD servo system: the spindle motor servo and the VCM servo. In this dissertation, we will be focusing on VCM servo control and the term "servo system" always refers to the VCM servo system.

The VCM servo operation has two major modes: track seeking and track following. When the HDD receives a read/write request from the host like a personal computer, the requested data can be stored anywhere, i.e. any track, on the disk. If the track that holds the requested data is not the track that the read/write head is currently at, a command will be generated to move the head from the current track to the target track by applying current to the VCM actuator. This operation is called track-seeking control. After the head arrives at the target track, the position of the head must be maintained close enough to the track center for accurate

read/write operation. This regulation of the head position is called track-following control.

The block diagram of the simplified VCM servo control loop is illustrated in Fig. 1.2. The plant includes the power amplifier, the VCM and the HSA. The output of the plant is the head position, which is measured at discrete time samples from the servo information stored in servo sectors. The sampling time of the position measurement depends on how fast the disks rotate and how many servo sectors there are in one revolution (called the sector number). The rotating speed of the disks is usually evaluated by the number of revolutions per minute (RPM). If the HDD has 7200 RPM and 200 servo sectors per revolution, then the sampling time is calculated by 60/7200/200, which is about 41.7 microseconds. The position measurement is compared to the reference to generate the position error signal (PES). The reference is equal to the distance between the target track and the current track for track-seeking control and zero for track-following control. The PES is then passed into the servo controller to calculate the VCM control signal, which is converted to an analog signal and gets amplified by the power amplifier to drive the VCM. Usually different servo controllers are used for track seeking and track following.

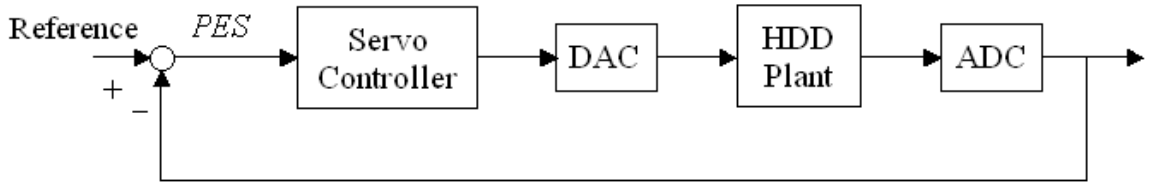

Figure 1.2: Block diagram of HDD servo system (DAC: digital-to-analog converter; ADC: analog-to-digital converter).

The performance measure for the track-seeking control is the seek time, which must be as small as possible. There are several track-seeking control algorithms developed over the past twenty years. The time optimal control or bang-band control is a well-known solution to minimize seek time with control input saturation ([67]). The proximate time optimal servomechanism proposed by Workman ([89]) is an improved version of time optimal control widely used in the HDD industry. Other popular seeking controllers include mode switching control with initial value compensation ([63], [92], [93]) and two-degrees-of-freedom control ([96], [97]), which work for both track seeking and track following.

The focus of this dissertation is the track-following control for accurate read/write operation under large narrow band disturbances. The performance of a track-following controller is measured by the track mis-registration (TMR), a statistical property of the PES, defined as

$$\text{TMR} = 3\sqrt{\frac{1}{N}\sum_{k=1}^{N} PES(k)^2}\ , \tag{1.1}$$

for a sequence of PES with length N. For accurate read/write operation, the TMR is required to be less than 10% of the track pitch (or track width), under the adverse influence of multiple disturbances (also called TMR sources) that will be discussed in Chapter 2. Most commonly used track-following control in the HDD industry is the proportional-integral-derivative (PID) controller, which is a second-order system and usually suffices the need of attenuating low frequency disturbances. There are several resonance mode mainly at high frequencies need to be suppressed using notch filters ([26]) to stabilize the closed-loop system. The track-following controller can be designed by applying modern methodologies such as H_2-optimal control [20], H_∞-optimal control [21] and LQG/LTR loop shaping [16].

1.3 Outline of the Dissertation

This chapter has provided a brief introduction to HDD inside components and VCM servo system. Chapter 2 will introduce disturbances in HDD system, especially the narrow band disturbances. Some existing methods of rejecting HDD disturbances will also be reviewed. Chapter 3 provides an overview of adaptive controllers. Then in Chapter 4, some indirect adaptive controllers will be described and applied to reject HDD narrow band disturbances. Another kind of adaptive control algorithms, direct adaptive control, will be introduced to reject narrow band disturbances in Chapter 5. The conclusions of this dissertation and some future research topics related to the rejection of HDD narrow band disturbances will be provided in Chapter 6.

Chapter 2

Narrow Band Disturbance

This chapter describes the narrow band disturbances in the HDD system. The various sources of the narrow band disturbances are discussed in Section 2.1. The narrow band disturbances exist in both repeatable runout (RRO) and non-repeatable runout (NRRO) and the methods of handling such disturbance in RRO and in NRRO are usually different. Some popular methods to reject the narrow band disturbances in the RRO are given in Section 2.2.1, while some traditional ways of rejecting the narrow band disturbances in the NRRO are discussed in detail in Section 2.2.2.

2.1 Narrow Band Disturbance Overview

As introduced in Section 1.1, the performance of the HDD track-following control is measured by the TMR. The source of TMR is the disturbances in HDD, including repeatable runout (RRO) and non-repeatable runout (NRRO). Narrow band disturbances contribute a lot to both the repeatable and the non-repeatable runouts, but the narrow band disturbances in these two runouts are different in nature.

Some of the HDD disturbances repeat from revolution to revolution. Thus, they are called RRO. The RRO is mainly due to the track eccentricity and the spindle eccentricity. The PES caused by the RRO is called repeatable PES (RPES). Figure 2.1 shows the spectral density of a sequence of RPES, which consists of a fundamental frequency component and its higher harmonics. Obviously all RRO harmonics can be considered as narrow band disturbances. The RRO is locked to the spindle rotation in both frequency and phase, which makes the frequency and phase of the narrow-band disturbances in the RRO time-invariant.

The RPES is the deterministic part at each servo sector by definition, which keeps showing up in PES at every revolution. Thus, it can be estimated by taking average of the PES

for each sector. After removing the RPES from PES, we obtain the non-repeatable part of PES ([95]), known as non-repeatable PES (NRPES), the source of which is called non-repeatable runout (NRRO). The NRRO contains both broadband and narrow band components as shown in Figure 2.2. To further decompose the NRRO, we can use the famous PES Pareto method ([3], [4], [5]). The known sources of NRPES include but not limited to:

1. Power amplifier noise that is significant at low frequencies;
2. Windage, which is a broadband disturbance usually below 1000 Hz;
3. White sensor noise, which dominates the high frequency PES;
4. Disk modes excited by air turbulence;
5. External shock and vibration.

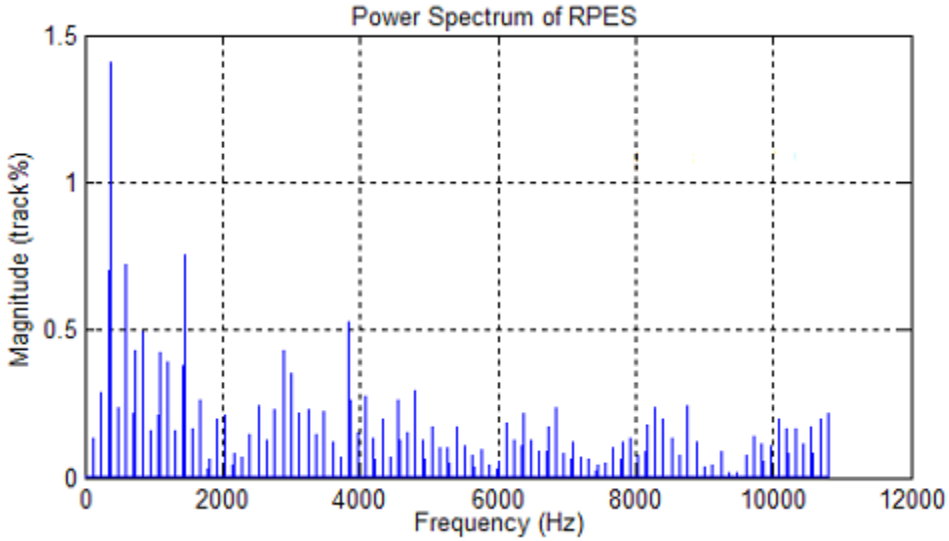

Figure 2.1: An example of repeatable PES spectrum after standard servo control.

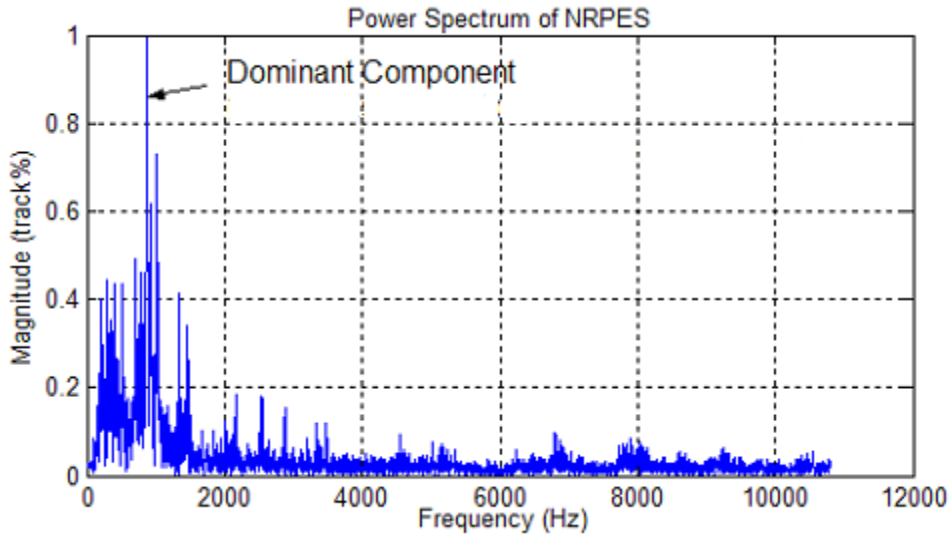

Figure 2.2: An example of non-repeatable PES spectrum after standard servo control.

Among all these sources, both disk modes and external vibration can result in sharp peaks, or narrow band components, in the PES spectrum. There are many disk modes in the HDD system and most of them are caused by disk flutter ([23]), which is the vibration in the axial direction of the disk due to internal windage excitation during the disk operation. This axial vibration can be translated to the head off-track in the radial direction and shows up as narrow band peaks in the NRPES spectrum. HDDs, especially small form-factor ones, are very sensitive to external shock and vibration, which are also narrow band disturbances and mainly show up as large peaks at low frequencies in the PES spectrum. To make the situation worse, the head off-track concentrated in [350 Hz, 2000 Hz] is amplified by the error rejection function ([23]). This amplification along with the rapid growth in track density and spindle motor speed makes narrow band disturbances in this frequency range a major contribution to the NRRO and thus to the TMR. Moreover, the NRRO present during self-servo writing process will be transformed into RRO afterwards. Therefore, the narrow band disturbances must be properly rejected to meet the stringent TMR budget.

2.2 Dominant Frequency Component

This dissertation is focused on rejecting the narrow band disturbances of NRRO in the mid-high frequency range around 300 Hz to 1800 Hz. We call the largest narrow band frequency component in the NRPES spectrum as the dominant frequency component. Throughout the dissertation, we will use “narrow band disturbance” and “dominant frequency component” interchangeably unless otherwise stated.

To reject the dominant component of NRRO, it is required to know its nature in the frequency domain. Figure 2.3 shows that the frequency of the dominant component varies from one zone to another (different head or different track). The magnitude and the phase are both

time-varying for the dominant component at a fixed zone as depicted in Fig. 2.4. Therefore, the dominant frequency component of NRRO can be modeled as a sinusoidal signal with slowly time-varying magnitude and phase at varying frequency for different zones in an HDD.

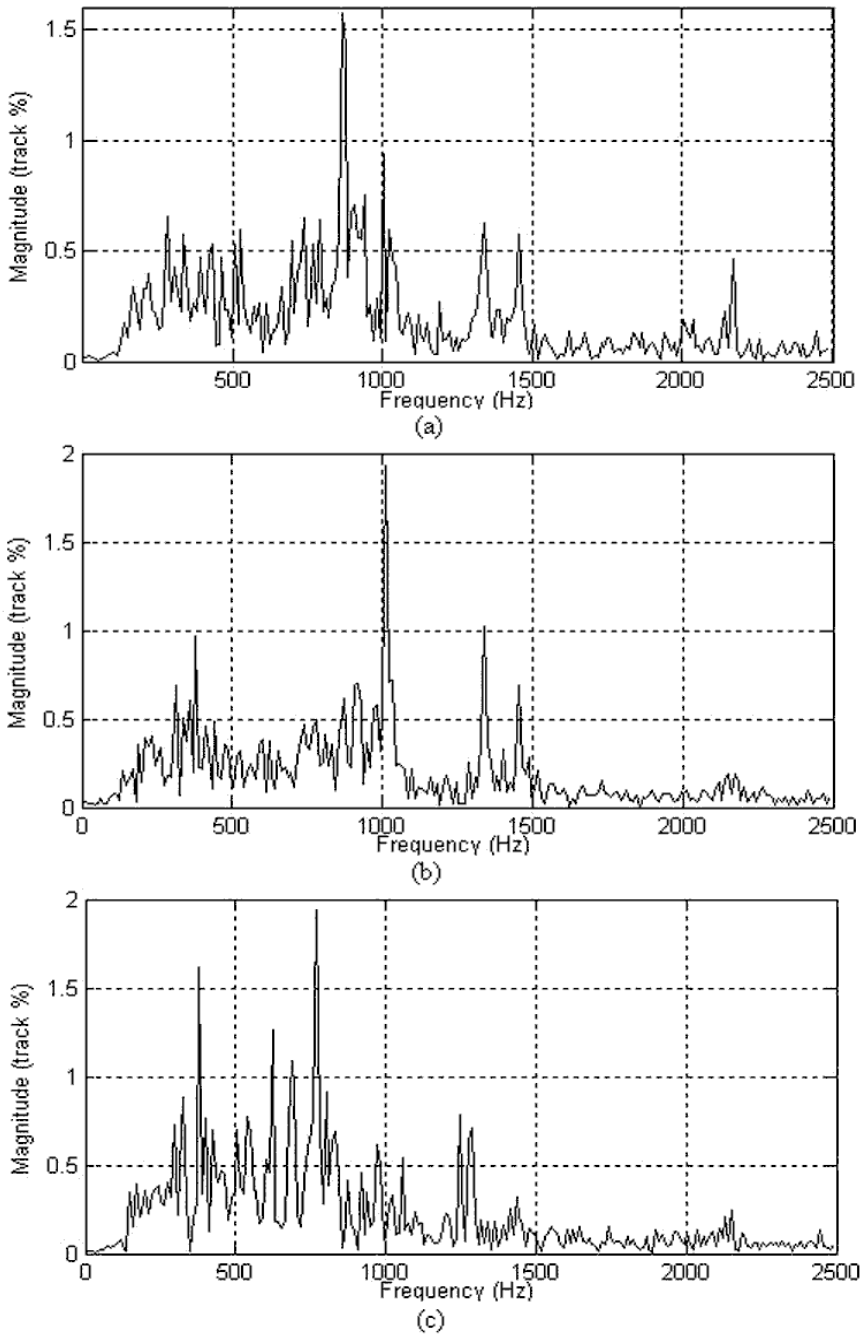

Figure 2.3: Power spectra of NRPES in three different zones: (a) In zone No.1 (dominant component exists at 870Hz); (b) In zone No.2 (at 1000Hz); (c) In zone No.3 (at 750Hz).

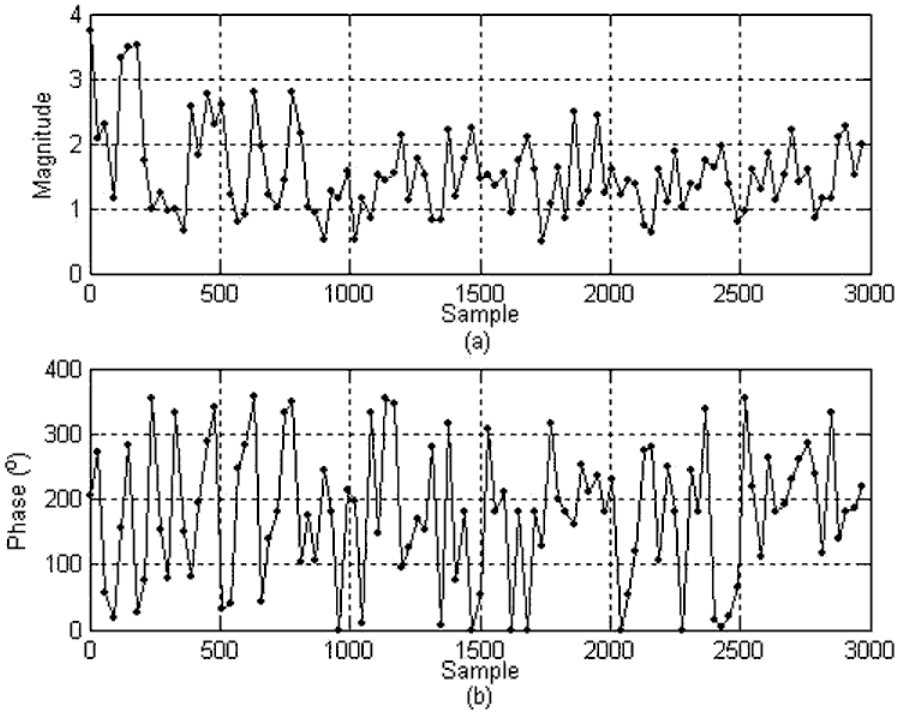

Figure 2.4: Spectral analysis (discrete Fourier transform) of the dominant component in every 30 sample non-repeatable PES measurement from a disk drive: (a) Time trace of magnitude; (b) Time trace of phase.

2.3 Traditional Narrow Band Disturbance Rejection

RRO and NRRO are totally different in nature. So the effective algorithms that reject the narrow band disturbances in them are different. In this section some traditional servo methods to reject RRO and NRRO narrow band disturbances will be discussed.

2.3.1 RRO Rejection

RRO is locked to the spindle rotation in both frequency and phase. RRO can be rejected either by improving the precision of the servo-writer during the manufacturing processes or by servo control algorithms, like repetitive control ([40]) and adaptive feedforward control ([91]).

2.3.2 NRRO Rejection

Unlike RRO, NRRO contains broadband noise and narrow band frequency components with time-varying phases and magnitudes at known and often unknown frequencies as discussed in Section 2.2. In this dissertation, we focus on rejecting the narrow band frequency components.

There exist several mechanical approaches to suppressing narrow band NRRO disturbance due to disk flutter. Examples of such mechanical re-design include novel aerodynamic designs of the shroud (like decreasing disk-to-shroud spacing [35], smoothening the shroud contour and reducing the shroud opening [29]), squeeze air bearing damping [17], feedback [34] and feedforward [24] control using additional sensors, feedback control with piezoelectric actuator patches [85], and optimal HSA design [64]. The external vibration induced PES can be effectively rejected by the use of a shock sensor or an accelerometer ([19], [107]). Most of these approaches yield significant TMR reduction.

However, all these time-consuming redesign of mechanical structures of HDD will greatly increase the cost of disk drives. Instead, rejecting narrow band NRRO via servo algorithms is more preferable. The traditional servo methods of rejecting narrow-band disturbances in the NRRO include different kinds of peak filters ([43], [90], [100]). The difficulty of determining the center frequency of the peak filters remains for these methods.

Since the frequency or the model of the narrow band disturbance of interest is unknown, the most appropriate and effective compensation algorithm is the adaptive control scheme, including indirect adaptive control and direct adaptive control, which will be discussed in detail in the following chapters.

2.4 Summary

In this chapter, the properties of various disturbances in the HDD system have been reviewed. The disturbances of interest in this dissertation, the narrow band disturbances in NRRO, are caused by disk flutters and external vibration. The frequencies of the NRRO narrow band disturbances are usually unknown and can be different at different tracks and disks. Moreover, their phase and magnitude are slowly time varying. In order to reject these disturbances, either additional mechanical components should be applied or the track-following servo controller should be redesigned. The latter is a preferred approach from the viewpoint of implementation cost.

Chapter 3

Adaptive Control Overview

This chapter gives an overview of adaptive control theory. The definitions and some famous examples of adaptive control are given in Section 3.1, which is divided into two subsections, 3.1.1 about indirect adaptive control and 3.1.2 about direct adaptive control, respectively. Section 3.2 lists some important moments in the history of adaptive control. Section 3.3 describes several adaptive controllers that have been applied to HDD systems.

3.1 Definitions and Examples

The compensation methods discussed in Section 2.3 are all effective on rejecting narrow band disturbance, only if part (such as frequency) or whole of the model of the disturbance is exactly known. As seen in Section 2.2, however, the frequency of the NRRO narrow band disturbance of interest is often unknown and even time varying. Then all the traditional compensation schemes that require known frequency do not work on its own for rejecting such disturbance.

A natural and popular control method of dealing with unknown or changing parameters of a controlled plant is adaptive control, which was defined in [49] as the following.

Definition 3.1: An adaptive control system measures a certain performance index of the control system using the inputs, the states, the outputs and the known disturbances. From the comparison of the measured performance index and a set of given ones, the adaptation mechanism modifies the parameters of the adjustable controller and/or generates an auxiliary control in order to maintain the performance index of the control system close to the set of given ones (i.e., within the set of acceptable ones).

A simplified definition given in [11] stated that an adaptive controller is a controller

with adjustable parameters and a mechanism for adjusting the parameters. Depending on the way that the controller parameters are adjusted, adaptive control can be categorized into indirect adaptive control and direct adaptive control, the definitions and a few examples of which will be given in Subsections 3.1.1 and 3.1.2. In Chapter 4 and Chapter 5, both indirect and direct adaptive controllers will be applied to reject NRRO narrow band disturbance in the HDD system.

3.1.1 Indirect Adaptive Control

When the controller parameters are calculated based on the plant model identification, the adaptive controller is called indirect [11]. The indirect adaptive control works as a two-step approach: the plant model or parameters are identified first and then the controller parameters are determined accordingly.

One popular indirect adaptive controller is the explicit self-tuning control system represented in Fig. 3.1. The identifier block takes the plant input and the plant output to estimate the plant model or parameters, usually by an appropriate parameter adaptation algorithm (PAA). These identified parameters are treated as the true parameters of the plant, based on which the controller parameters are computed according to the specification. The controller with these computed parameters is then applied to the closed-loop system. The controller parameters are often determined by pole placement [10] in the deterministic case or by minimum variance design [68] in the stochastic case.

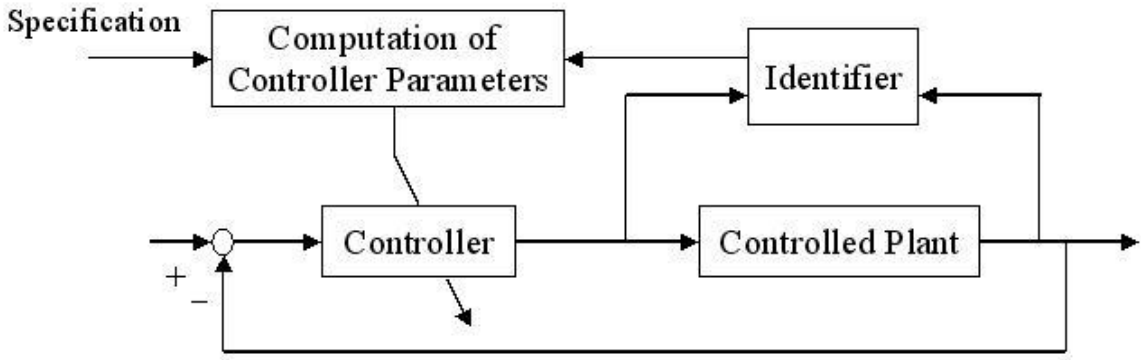

Figure 3.1: Self-tuning control structure.

3.1.2 Direct Adaptive Control

When the controller parameters are adjusted directly without plant model identification, the adaptive controller is called direct. One example of direct adaptive controller is the model reference adaptive control scheme depicted in Fig. 3.2. The controller parameters are updated in such a way that the controlled closed-loop system behaves like the reference model.

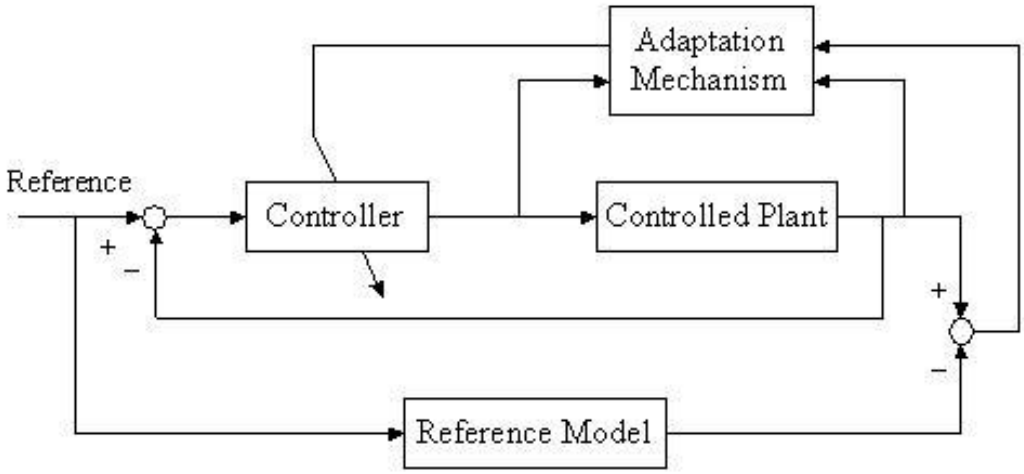

Figure 3.2: Model reference adaptive control structure.

In many cases, the direct adaptive control is accomplished by an appropriate parameterization (re-parameterization) of the plant equation in terms of the controller parameters. In general, direct adaptive control provided more attenuation than indirect adaptive control [48]. However, for some plants, such as plants that possess unstable zeros, the plant re-parameterization becomes impossible. Then only indirect adaptive control can be applied to such plants.

3.2 Brief History of Adaptive Control

Adaptive control has a history of more than fifty years. It first appeared in 1950s with extensive research related to high performance aircraft. In 1958, Whitaker et al. proposed the model reference adaptive control and presented a well-known parameter adjustment mechanism called the "MIT-rule", which updates the parameter vector by setting its time derivative equal to a constant adaptation gain or step size multiplied by the model error and the negative gradient of the model error. The indirect adaptive control emerged around the same time period by Kalman's self-optimizing control design for digital process control system [39], which is considered to be the first publication on the self-tuning idea.

In 1960s, the adaptive control research was greatly stimulated by the advancement of many control theories, such as state space, stochastic control, Lyapunov's stability theory and dynamic programming. As part of adaptive control theory, system identification and parameter estimation were also well developed in that time period.

From the late 1960s to 1970s, Landau provided an input-output approach known as hyperstability or positivity to prove the stability of model reference adaptive systems ([45], [46]). In 1973, the term "self-tuning" was first created in [9], which boosted development of the indirect adaptive control approach.

In 1980s, the research of adaptive control was focusing on the robustness analysis of adaptive control systems under the influence of unmodeled dynamics, noise and disturbance. There were several modifications of adaptation algorithms proposed for the robustness consideration, including using normalized signals [66] and adding leakage [36].

3.3 Adaptive Control for HDD

Adaptive controllers have been constantly finding its way into the HDD systems, although they are often considered to be too computationally involved for the very limited computing time allocated for control algorithm in HDDs.

There is one adaptive control algorithm that plays an important role in HDD systems, the adaptive feedforward cancellation (AFC) algorithm ([14], [91]). The AFC is a continuous-time adaptive approach commonly applied in HDD systems to reject RRO harmonics. It has been shown in [14] that the AFC algorithm is equivalent to the internal model principle scheme. In [15], Bodson and Douglas combined the AFC scheme with a frequency estimation of the disturbance to form an indirect adaptive controller for the rejection of sinusoidal disturbances with unknown frequency.

Horowitz and Li ([32]) introduced a Wiener filter based adaptive controller as a track-following add-on compensator to reject stochastic disturbances through two parameter adaptation algorithms running simultaneously: one identifies the plant and noise model and the other estimates the parameters of a Wiener filter.

A robust track-following controller design was presented in [38] to handle VCM gain variation. The authors first adopted an Internal Model Control (IMC) structure for robust stability against unmodeled plant dynamics and then applied the model reference adaptive control to adapt a gain variable to handle the plant gain variation.

In [44], Krishnamoorthy and Tsao proposed a robust adaptive and repetitive control scheme for HDD track following. They used an LQG controller as the baseline track-following controller, which was augmented by a plug-in two-period repetitive controller for the repeatable disturbances and an adaptive-Q controller for the remaining non-repeatable disturbances.

3.4 Summary

An overview of the adaptive control theory has been given in this chapter. The definition of adaptive control as well as a brief note on the history of adaptive control was provided. Two popular adaptive controllers were discussed: the self-tuning control and the model reference adaptive control, which respectively belong to the category of the indirect adaptive control and the direct adaptive control. Several applications of the adaptive control theory in HDD servo systems were also discussed.

Chapter 4

Indirect Adaptive Rejection of Narrow Band Disturbance

In this chapter the indirect adaptive control scheme introduced in Chapter 3 is applied in HDD systems to reject narrow band disturbance with unknown frequency. The structure of the rejection scheme is described in Section 4.1. Basically there are two major components in the structure: frequency identifier and add-on narrow band disturbance compensator. Section 4.2 describes frequency identification of the narrow band disturbance, which is critical to successfully rejecting the disturbance. The algorithms discussed there include discrete Fourier transform (DFT) and least mean squares (LMS). With an accurate frequency identification result, several methods can be applied to reject the disturbance, including the basis function method and the disturbance observer (DOB), which are introduced in Sections 4.3 and 4.4, respectively. A realistic simulation tool is used to demonstrate the performance of indirect adaptive compensators.

4.1 Structure of Indirect Adaptive Rejection System for Narrow Band Disturbance

As introduced in Section 3.1.1, indirect adaptive control is a two-step approach. For the rejection of disturbance, the first step of indirect adaptive control is to identify the disturbance model. Since a narrow band disturbance can be represented by its frequency, phase and magnitude, we can consider them as the model parameters of a narrow band disturbance. Moreover, the impact of a peak in the disturbance on the output of a linear time-invariant closed-loop system is determined by the gain of the loop at the frequency of the peak. So usually we only need to identify the frequency of the narrow band disturbance. The second step of indirect adaptive control usually involves designing a feedback controller based on the identification results from the first step. However, since the HDD system is not only disturbed by the narrow

band disturbance (dominant frequency component) but also many other kinds of noise as described in Chapter 2, it is more desirable to use an add-on compensator than to replace the existing or baseline feedback controller with a new one solely for the purpose of rejecting narrow band disturbance. The other reason for using an add-on compensator is that in this way it is very easy to turn off or on the narrow band disturbance rejection, based on the existence of the disturbance. This rejection scheme is represented by the closed-loop structure shown in Fig. 4.1.

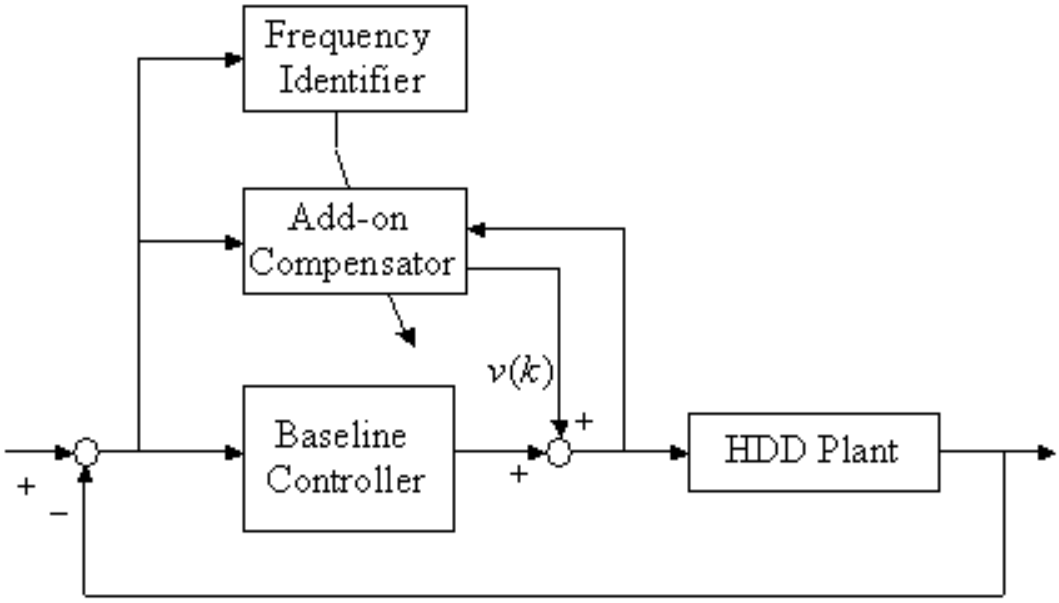

Figure 4.1: Structure of the indirect adaptive compensation for narrow band disturbance.

4.2 Frequency Identification

Frequency identification of sinusoidal signals buried in noise is an important problem, which has numerous applications in communications, sonar, speech analysis and many other areas. One category of frequency identification methods, such as the Pisarenko harmonic decomposition ([69]), the reformed Pisarenko harmonic decomposition ([75], [76], [77]), and the multiple signal classification method ([72]), is based on eigendecomposition of the autocorrelation matrix. The maximum likelihood algorithm is another candidate of estimating frequency of sinusoids in noise ([1], [41], [88]). A popular and not too computationally intensive method for frequency identification is adaptive notch filter ([61], [54], [12], [13]). In this section, we will describe the theoretically most accurate but computationally complex discrete Fourier transform (DFT) method and a computationally simple least mean squares method for frequency identification.

4.2.1 Narrow Band Signal Enhancement

The only available direct head position measurement in an HDD system, the PES, is used for the frequency identification. As introduced in Chapter 2, the PES contains not only the NRRO narrow band disturbance we want to reject but also broadband noise and many other frequency components. When we identify the frequency of the dominant frequency component (considered as signal for identification), all other frequency components are considered as noise. In order to isolate the frequency band of the dominant component from other components as well as to enhance the signal-to-noise ratio (SNR) for identification, the PES is filtered by an infinite-impulse-response (IIR) bandpass filter. The pass band of the filter should cover the frequency band that the dominant frequency component resides. Figure 4.2 shows an example of such filter with pass band [700Hz, 1100Hz]. The PES spectra before and after the bandpass filter are compared in Fig. 4.3. All frequency components outside the pass band are effectively attenuated by the filter.

The frequency of the dominant component needs to be identified on-line, because it varies from track to track. Furthermore, since the read-write head does not stay on one track for many revolutions during operation, the frequency identification should be completed within a short time window. Therefore, the frequency identification algorithm must be computationally simple and converges fast. Moreover, we assume that there is only one dominant component in the filtered PES.

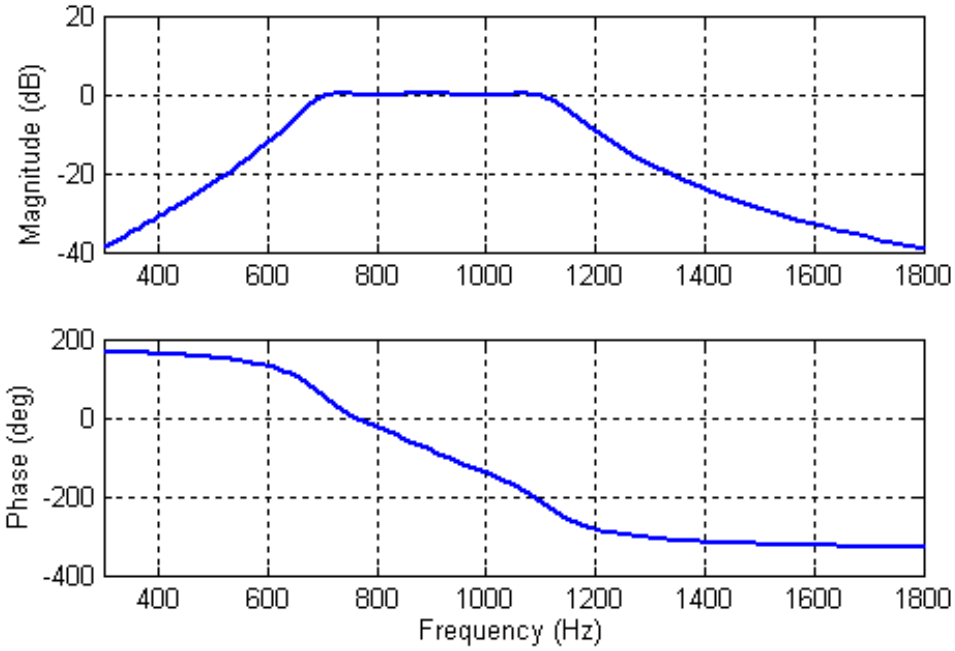

Figure 4.2: Frequency response of a bandpass filter with pass band [700Hz, 1100Hz] for the frequency identification.

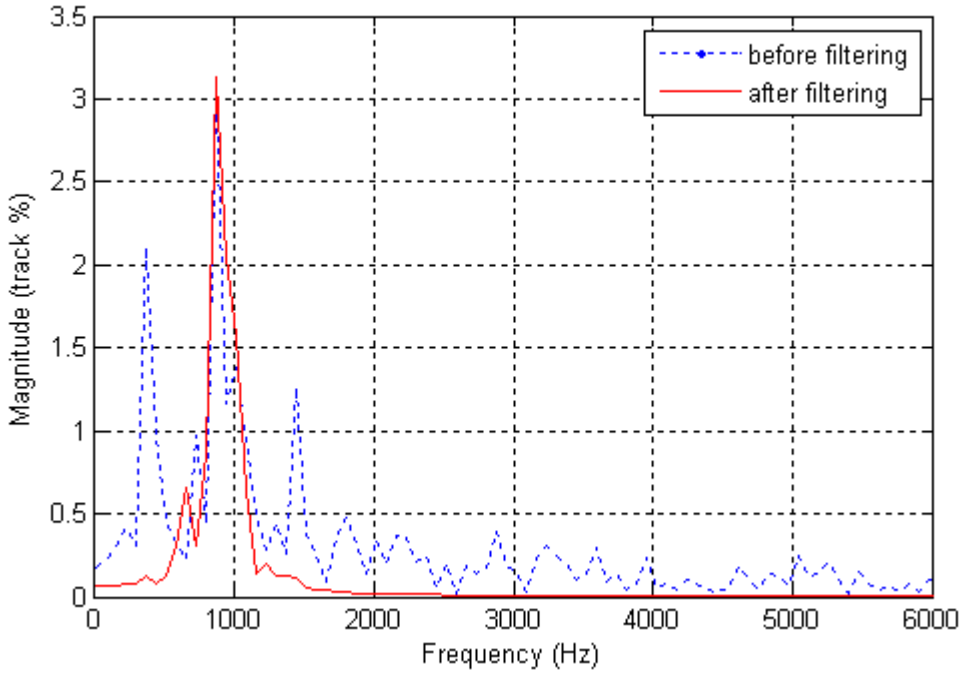

Figure 4.3: PES spectra before and after the bandpass filter.

4.2.2 Discrete Fourier Transform

The narrow band disturbance is basically a sinusoidal signal. To estimate its frequency, it would be better to resort to frequency domain analysis or Fourier analysis.

For any discrete-time absolutely summable sequence $x(n)$, its discrete-time Fourier transform (DTFT) is defined as

$$X(e^{j\omega}) = \sum_{n=-\infty}^{\infty} x(n)e^{-j\omega n} . \tag{4.1}$$

Noticing that $e^{-j2\pi n} = 1$, $X(e^{j\omega})$ is periodic with period 2π. The sequence $x(n)$ can be represented by its DTFT:

$$x(n) = \frac{1}{2\pi}\int_{-\pi}^{\pi} X(e^{j\omega})e^{-j\omega n} d\omega . \tag{4.2}$$

Equation (4.2) is called the synthesis formula, since it determines how much of each frequency component is required to synthesize $x(n)$.

For a discrete-time sinusoidal signal given by

$$x(n) = \cos(\omega_0 n + \phi), \tag{4.3}$$

where n ranges from $-\infty$ to ∞, its DTFT is nonzero only at $\omega = \pm\omega_0 + 2k\pi$, for any integer k, which implies that the absolution value (usually termed magnitude) of $X(e^{j\omega})$ can be used to find the frequency of a sinusoidal signal. In practice, it is impossible to get an infinitely long signal. So the DTFT of a sequence $x(n)$ that is collected only for a finite duration $n = 0, \ldots, L-1$, is given by

$$X(e^{j\omega}) = \sum_{n=0}^{L-1} x(n)e^{-j\omega n} . \tag{4.4}$$

The DTFT of a finite-duration sinusoidal signal at frequency ω_0 is no longer impulses at $\omega = \pm\omega_0 + 2k\pi$. The sharp impulses are smoothed out into the entire ω domain (spectral leakage pattern), but the magnitudes of the DTFT at $\omega = \pm\omega_0 + 2k\pi$ are much larger than the values at other frequencies if the sequence is long enough. In general, the longer the sequence, the smaller the spectral leakage. Thus, the DTFT is still a good way of estimating frequency of a

finite-length sinusoidal sequence. But it is still impractical to calculate $X(e^{j\omega})$ for any real ω with limited computation power. So for most of the times, $X(e^{j\omega})$ is only evaluated at uniformly-spaced finitely many points over one period:

$$X_L(k) = \sum_{n=0}^{N-1} x(n) e^{\frac{-j2\pi kn}{N}}, \text{ for } k = 0, 1, \ldots, N-1. \tag{4.5}$$

The subscript L means that the length of $x(n)$ is L. The number of frequency points, N, is usually chosen to be no less than the length of $x(n)$ and $x(n)$ is padded with zeros for $n \geq L$. $X_L(k)$ gives value of $X(e^{j\omega})$ at $\omega = \frac{2\pi k}{N}$ and is called the discrete Fourier transform (DFT) of $x(n)$.

When $x(n)$ only takes real value, $X_L(k)$ becomes complex conjugate to $X_L(N-k)$, which means that $X_L(k)$ and $X_L(N-k)$ have the same magnitude. So only the first half of $X_L(k)$ needs to be calculated for the purpose of estimating frequency of a sinusoidal sequence or a narrow band signal. Moreover, for a discrete-time sinusoidal signal of length L, the magnitude of $X_L(k)$ at the frequency of the signal is equal to $L/2$. Thus, the normalized DFT given by

$$\overline{X}_L(k) = \frac{2X_L(k)}{L}, \text{ for } k = 0, 1, \ldots, M, \tag{4.6}$$

is used for frequency identification. The constant M is obtained from N by

$$M = \begin{cases} \frac{N}{2} - 1, \text{if } N \text{ is even} \\ \frac{N+1}{2}, \text{if } N \text{ is odd} \end{cases} \tag{4.7}$$

Suppose the frequency identification begins at time 0. Then at each control sample, an N-point DFT is performed for all available PES (denoted by $x(n)$) that has been collected since the identification starts. Then at time $L-1$, the frequency estimate (in the unit of Hz) is given by

$$\hat{f}(L-1) = \frac{1}{NT_s} \underset{k \in \{0,1,\ldots,M\}}{\arg\max} \left| \overline{X}_L(k) \right|^2, \tag{4.8}$$

where $\overline{X}_L(k)$ is the normalized DFT of $x(n)$ ($n = 0, 1, \ldots, L-1$) calculated by Eq. (4.6) and

(4.5). Notice that the resolution of the frequency estimate is $\frac{1}{NTs}$. So N must be chosen to be a large integer to achieve enough resolution for accurate frequency estimation. In our case, N = 2048. Moreover, since we know that the dominant frequency component is within certain frequency range, the DFT only needs to be carried out for those k's such that $\frac{k}{NTs}$ lies in the frequency range that the dominant component resides. Suppose the lower bound and the upper bound of k are k_l and k_u, respectively. At sample L (length of $x(n)$ is L+1), Eq. (4.5) can be re-written as

$$\begin{aligned} X_{L+1}(k) &= \sum_{n=0}^{L} x(n) e^{\frac{-j2\pi kn}{N}} \\ &= \sum_{n=0}^{L-1} x(n) e^{\frac{-j2\pi kn}{N}} + x(L) e^{\frac{-j2\pi kL}{N}} \\ &= X_L(k) + x(L) e^{\frac{-j2\pi kL}{N}}, \end{aligned} \tag{4.9}$$

for $k = 0, 1, \ldots, N-1$. The same relation applies to the normalized DFT:

$$\overline{X}_{L+1}(k) = \overline{X}_L(k) + x(L) e^{\frac{-j2\pi kL}{N}}, \tag{4.10}$$

for $k = k_l, k_l + 1, \ldots, k_u$, which means that the DFT can be calculated recursively as new measurement comes in. So at each control sample L, only $x(L) e^{\frac{-j2\pi kL}{N}}$ for $k = k_l, k_l + 1, \ldots, k_u$, need to be calculated and added to $\overline{X}_L(k)$ to obtain $\overline{X}_{L+1}(k)$, which is used at the next sample to calculate $\overline{X}_{L+2}(k)$ and so on.

The frequency identification algorithm using DFT is applied to a set of PES measurement collected from a hard drive with 7200 RPM and 180 servo sectors per track to demonstrate its performance. It is assumed that the frequency of the dominant component is in the range [700Hz, 1100Hz]. The 2048-point DFT is calculated recursively by Eq. (4.10) for the frequency identification. The lower bound and upper bound of k are $k_l = 67$ and $k_u = 104$ in this case. The identification result is shown in Fig. 4.4. The frequency estimate oscillates in the beginning due to the significant spectral leakage effect for small sample size. After 0.8 revolution, the estimate converges to the accurate frequency of the dominant component.

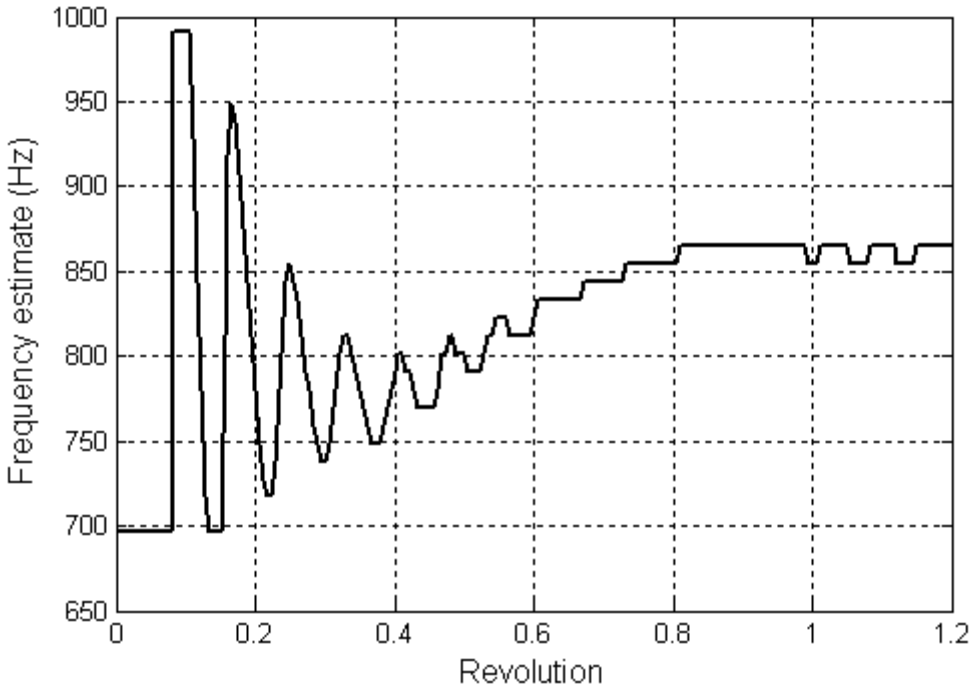

Figure 4.4: Frequency identification result using the DFT method.

The DFT is the frequency-domain representation for a sequence of discrete-time signal. Without any prior knowledge of the signal, the DFT provides the most accurate and straightforward frequency estimate. This method can also be called spectral analysis of the signal, since it is based on the spectral density of the signal. However, it is not suited for on-line identification due to its impractically large amount of computation for calculating DFT. For example, in our simulation, when $k_l = 67$ and $k_u = 104$, 38 complex-number multiplications and additions are required to calculate $\overline{X}_L(k)$ at each control interval, which is usually not acceptable in a HDD system. A computationally simple method is preferred for real time frequency identification.

4.2.3 Least Mean Squares Method

This method is based on the parametric model of a sinusoidal signal. Let $z(k)$ and $x(k)$ represent the filtered PES and the dominant frequency component, respectively. All other frequency components contained in $z(k)$ are treated as noise $n(k)$, i.e., $z(k) = x(k) + n(k)$. Although the phase and magnitude of the dominant component are usually slowly time varying, we suppose that the component can be expressed as

$$x(k) = A\cos(\omega_0 T_s k + \phi), \tag{4.11}$$

where ω_0 is the frequency (in radian/second) of the dominant component and A and ϕ are magnitude and phase, respectively. It is easy to verify that the following equations hold

$$\begin{aligned} x(k) &= A\cos[\omega_0 T_S(k-1+1)+\phi] \\ &= A\cos\{[\omega_0 T_S(k-1)+\phi]+\omega_0 T_S\} \\ &= A\cos[\omega_0 T_S(k-1)+\phi]\cos(\omega_0 T_S) - A\sin[\omega_0 T_S(k-1)+\phi]\sin(\omega_0 T_S) \end{aligned} \tag{4.12}$$

$$\begin{aligned} x(k-2) &= A\cos[\omega_0 T_S(k-1-1)+\phi] \\ &= A\cos\{[\omega_0 T_S(k-1)+\phi]-\omega_0 T_S\} \\ &= A\cos[\omega_0 T_S(k-1)+\phi]\cos(\omega_0 T_S) + A\sin[\omega_0 T_S(k-1)+\phi]\sin(\omega_0 T_S) \end{aligned} \tag{4.13}$$

Adding these two equations together yields

$$x(k)+x(k-2) = 2A\cos[\omega_0 T_S(k-1)+\phi]\cos(\omega_0 T_S). \tag{4.14}$$

Noticing that

$$A\cos[\omega_0 T_S(k-1)+\phi] = x(k-1), \tag{4.15}$$

we have

$$x(k)+x(k-2) = 2\cos(\omega_0 T_S)x(k-1). \tag{4.16}$$

Define the estimation error as

$$e(k) = z(k)+z(k-2)-\hat{\lambda}(k)z(k-1). \tag{4.17}$$

where the frequency coefficient $\hat{\lambda}(k)$ is defined as

$$\hat{\lambda}(k) = 2\cos\left[\hat{\omega}(k)T_S\right]. \tag{4.18}$$

Here the estimate of the frequency ω_0 at sample k is denoted as $\hat{\omega}(k)$.

With the definition of estimation error (4.17), the LMS [28] algorithm is applied to obtain the estimate of this frequency coefficient:

$$\hat{\lambda}(k+1) = \hat{\lambda}(k) - \mu\frac{\partial e(k)}{\partial\hat{\lambda}(k)}e(k), \tag{4.19}$$

where μ is the step size. The partial derivative of $e(k)$ is given by

$$\frac{\partial e(k)}{\partial \hat{\lambda}(k)} = -z(k-1). \tag{4.20}$$

Therefore, $\hat{\lambda}(k)$ is finally updated according to

$$\hat{\lambda}(k+1) = \hat{\lambda}(k) + \mu\, z(k-1)e(k). \tag{4.21}$$

From Eq. (4.18) the frequency estimate at the (k+1)-th sample is given by

$$\hat{\omega}(k+1) = (\cos^{-1}[\hat{\lambda}(k+1)/2])/T_s. \tag{4.22}$$

It is important for an algorithm to be stable and to converge. So the proof of the stability and convergence of this algorithm of frequency identification is provided as follows.

Let λ denote the true value of the frequency coefficient, i.e., $\lambda = 2\cos(\omega_0 T_s)$. Suppose that $z(k)$ can be expressed as

$$\begin{aligned} z(k) &= 2\cos(\omega_0 T_s)z(k-1) - z(k-2) + \xi(k) \\ &= \lambda z(k-1) - z(k-2) + \xi(k), \end{aligned} \tag{4.23}$$

where $\xi(k)$ is considered as the modeling error of $z(k)$. After subtracting λ from the both sides of (4.21), substituting $e(k)$ by (4.17) and substituting $z(k)$ by (4.23), we can get the dynamic model of the frequency coefficient error $\bar{\lambda}(k) = \hat{\lambda}(k) - \lambda$ as

$$\bar{\lambda}(k+1) = (1 - \mu[z(k-1)]^2)\bar{\lambda}(k) + \mu\, z(k-1)\xi(k). \tag{4.24}$$

The PES in HDD is bounded and so is the filtered PES $z(k)$. Since $\xi(k)$ depends only on $z(k)$, $z(k-1)$, $z(k-2)$, and λ, it must also be bounded. Therefore, there exists a positive constant M satisfying $|z(k-1)\xi(k)| \le M$ for all k.

Suppose that

$$\left|1 - \mu[z(k-1)]^2\right| \le \eta, \tag{4.25}$$

for all k and some positive constant η. Then we have

$$\left|\bar{\lambda}(k+1)\right| \le \eta\left|\bar{\lambda}(k)\right| + \mu M, \tag{4.26}$$

which yields an upper bound for $|\bar{\lambda}(k)|$:

$$|\bar{\lambda}(k)| \le C\eta^k + \frac{\mu M}{1-\eta}, \tag{4.27}$$

where constant C depends on the initial absolute error $|\bar{\lambda}(0)|$. Thus, if the step size μ satisfies

$$0 < \mu < \frac{2}{\max_k [z(k)]^2}, \tag{4.28}$$

then $0 < \eta < 1$ and

$$\lim_{k\to\infty} |\bar{\lambda}(k)| \le \frac{\mu M}{1-\eta}. \tag{4.29}$$

The bound in (4.29) can be made small by choosing small μ, whereas large μ (but still less than $(\max_k [z(k)]^2)^{-1}$) is desired for fast convergence.

On the other hand, $z(k)$ can be considered as a random process with bounded value. Suppose that (4.25) still holds. Then from (4.24), we have

$$E(|\bar{\lambda}(k+1)|) \le \eta E(|\bar{\lambda}(k)|) + \mu\, E(|z(k-1)\xi(k)|). \tag{4.30}$$

If $\mu E(|z(k-1)\xi(k)|) = 0$, then $\hat{\lambda}(k)$ is an asymptotically unbiased estimate of λ. Since $\mu E(|z(k-1)\xi(k)|)$ is small in our case, the bias of $\hat{\lambda}(k)$ is also small.

The performance of the frequency identification by LMS algorithm is determined by the step size μ: a large step size results in fast convergence and large fluctuation after convergence and vice versa. Figure 4.5 compares the frequency estimates for $\mu = 0.01$ and $\mu = 0.001$. In the simulation, we allow one revolution for the frequency estimate to converge and use the estimated frequency at the end of the first revolution to build the add-on compensator.

In order to achieve both fast convergence at the beginning and small fluctuation after convergence, we use a time-varying step size as depicted in Fig. 4.6. The step size μ remains 0.01 for the first 1/4 revolution, and then it is ramped down, according to the equation

$$\mu(k+1) - 0.0001 = 0.9[\mu(k) - 0.0001]. \tag{4.31}$$

This makes μ exponentially converge to 0.0001. With this step size, the frequency estimate converges within one revolution and is similar to the result of spectral analysis (discrete Fourier transform) as shown in Fig. 4.7. The converged frequency estimate by the LMS algorithm after one revolution is 861 Hz, which is very close to 854 Hz, the frequency of the dominant component with the largest magnitude in the spectrum of one revolution of the filtered PES. This identified frequency is then used to build the add-on compensator in Fig. 4.1 to reject the dominant frequency component.

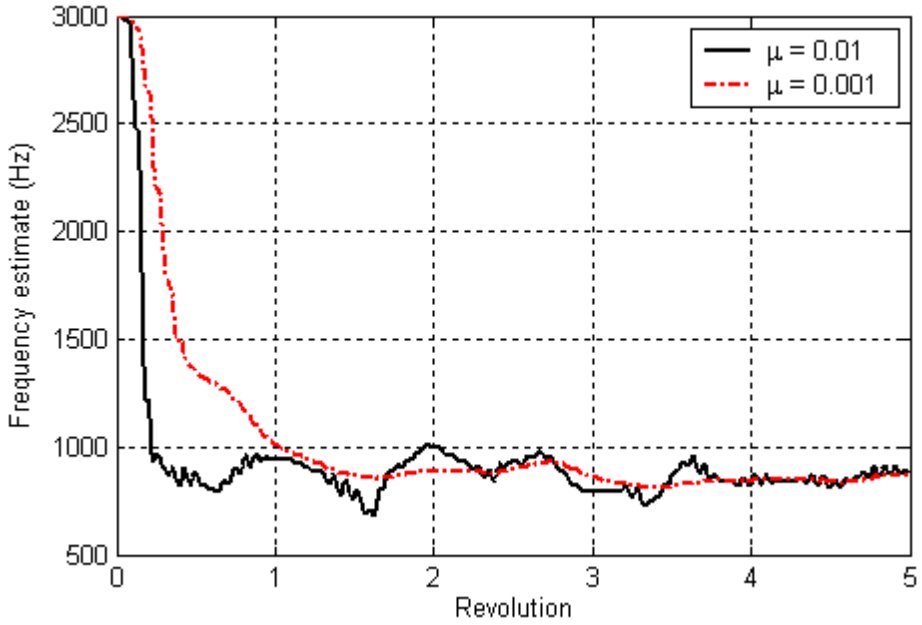

Figure 4.5: Frequency identification by the LMS algorithm with different values of the step size. The identification begins at Revolution 0.

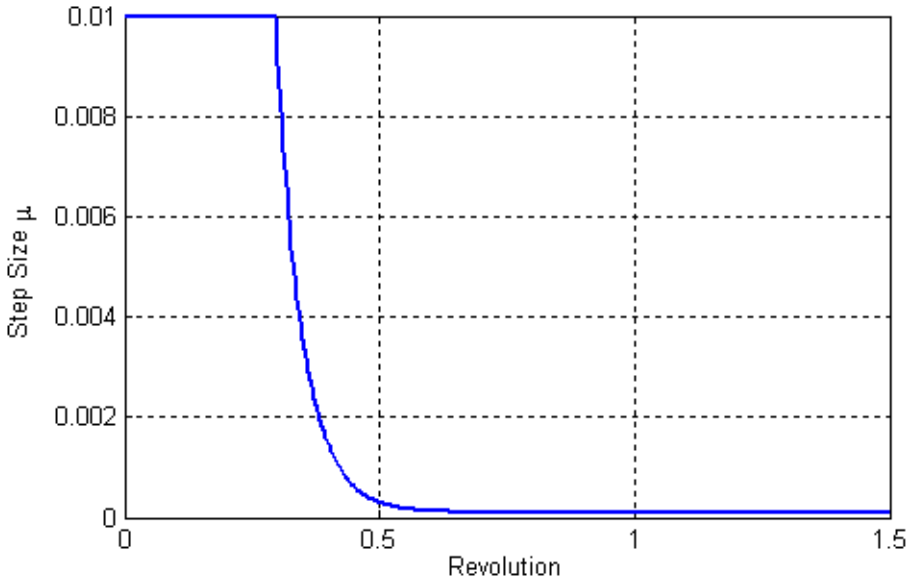

Figure 4.6: Trajectory of the time-varying step size for frequency estimation.

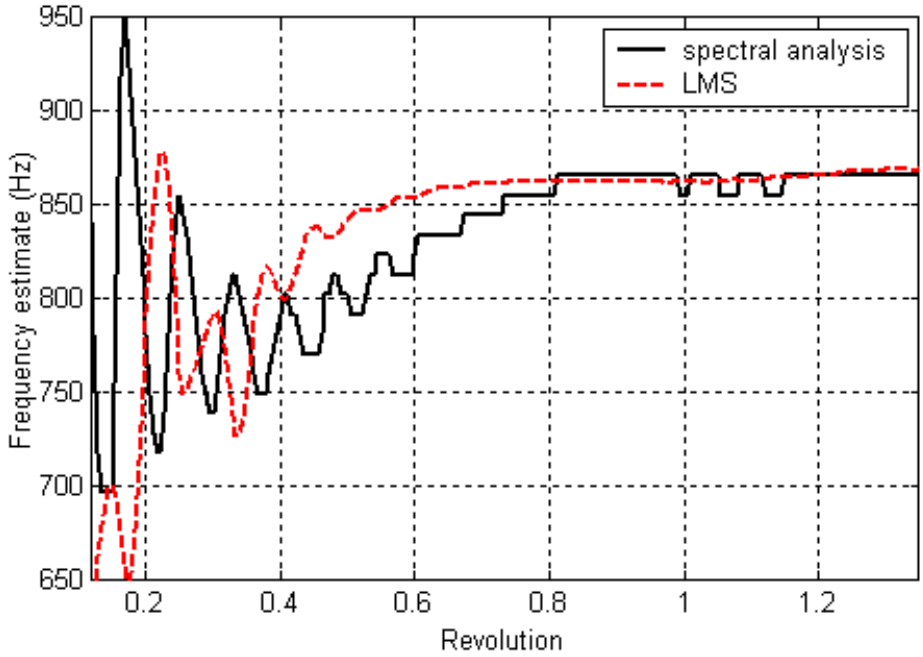

Figure 4.7: Simulation result of the frequency identification by spectral analysis and by LMS algorithm.

4.3 Basis Function Algorithm

The second step of the indirect adaptive control is the add-on compensator design. One compensation scheme was proposed by Kim et al. [42]. They added a 2nd order peak filter to the servo loop in parallel with the existing controller to achieve certain attenuation at the center frequency of the filter. With their compensation scheme, the dominant component was reduced by 50% and the TMR improvement was limited. In this section and the next section, two other compensators will be introduced to deal with the dominant frequency component: the basis function algorithm and the narrow band disturbance observer, respectively.

4.3.1 Magnitude and Phase Identification

The narrow band disturbance of interest can be modeled as a sinusoidal signal, which is completely described by its frequency, magnitude and phase. With the frequency estimate obtained from the frequency identification, if we can further estimate its magnitude and phase, the signal can be constructed and removed from the servo loop to reject the disturbance.

For magnitude and phase identification, it is convenient to let the disturbance (TMR source) enter at the input to the plant as shown in Fig. 4.8. In reality, the disturbance can enter anywhere in between the control signal and the PES measurement, but for any disturbance, there is an equivalent signal that enters at the input to the plant and generates the same PES as the original disturbance. So it is reasonable to assume that all disturbances enter at the input to the plant.

The exact transfer function of the plant is usually unknown or very complicated. But we always have a plant model, the transfer function of which is supposed to be $z^{-m}P_n(z^{-1})$, where m is the pure delay steps of the system and

$$P_n(z^{-1}) = \frac{B(z^{-1})}{A(z^{-1})}. \tag{4.32}$$

The polynomials $A(z^{-1})$ and $B(z^{-1})$ are equal to $1 + a_1 z^{-1} + \cdots + a_n z^{-n}$ and $b_0 + b_1 z^{-1} + \cdots + b_n z^{-n}$ ($b_0 \neq 0$), respectively. Since in the HDD system the plant modeling uncertainty is very small in the frequency range [200Hz, 1100Hz], we can assume that

$$P(z^{-1}) = z^{-m}P_n(z^{-1}) \tag{4.33}$$

holds in [200Hz, 1100Hz].

A delayed estimate of the disturbance can be generated by inverting the plant model transfer function without the pure delay. When there are unstable zeros in the plant model, the zero-phase error-tracking (ZPET) algorithm ([80], [81]) can be used to get approximate inversion.

Suppose that the inverse of the plant model without pure delay is $P_n^{-1}(z^{-1})$ ($P_n^{-1}(z^{-1}) = A(z^{-1})/B(z^{-1})$, if there are no unstable zeros). The disturbance estimate at ($k - m$)-th sample is then given by

$$\hat{d}(k-m) = P_n^{-1}(z^{-1})y(k) - u(k-m). \tag{4.34}$$

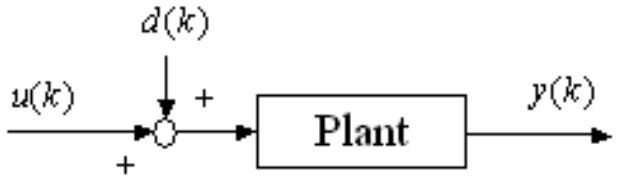

Figure 4.8: Plant model with disturbance at input.

With the identified frequency $\hat{\omega}$, obtained by the frequency identification scheme described in the previous section, we can employ a bandpass filter given by

$$G_{bpf}(z^{-1}) = (1-\eta)\frac{1-\eta z^{-2}}{1-2\eta\cos(\hat{\omega}T_s)z^{-1}+\eta^2 z^{-2}} \tag{4.35}$$

to get rid of the frequency components other than the dominant one contained in $\hat{d}(k-m)$. Notice that at $\hat{\omega}$, $G_{bpf}(z^{-1}) = 1$, which guarantees that at the steady state the filtering does not change the magnitude and the phase of the dominant component and by choosing η close to and less than 1, the pass band is made narrow. Then the filtered $\hat{d}(k-m)$ (denoted by $\hat{d}'(k-m)$) is approximately equal to the value of the dominant component delayed by m samples, which is denoted by $x'(k-m)$.

The time-varying phase and magnitude of $x'(k-m)$ must be identified to successfully reject the disturbance. The method for phase and magnitude identification is the basis function algorithm ([58], [82], [83]), which is based on a Fourier expansion of the dominant component:

$$\begin{aligned} x'(k-m) &= \alpha\cos[(k-m)\hat{\omega}T_s] + \beta\sin[(k-m)\hat{\omega}T_s] \\ &= \Theta^T\Phi(k-m), \end{aligned} \tag{4.36}$$

where $\Phi^T(k) = [\cos(\hat{\omega}T_s k)\ \sin(\hat{\omega}T_s k)]$, $\Theta^T = [\alpha\ \beta]$, and α and β are unknown coefficients, which are related to magnitude and phase of the dominant component. The objective is to

correctly identify these coefficients in Θ. Let an estimate of Θ be denoted by

$$\hat{\Theta}^T(k) = [\alpha(k) \;\; \beta(k)]. \tag{4.37}$$

Then the *a priori* estimate of $x'(k-m)$ is given by

$$\hat{x}^0(k-m) = \hat{\Theta}^T(k-1)\Phi(k-m) \tag{4.38}$$

and the *a priori* estimation error is defined by

$$\begin{aligned} \varepsilon^0(k) &= \hat{d}'(k-m) - \hat{x}^0(k-m) \\ &\approx \Theta^T\Phi(k-m) - \hat{\Theta}^T(k-1)\Phi(k-m). \end{aligned} \tag{4.39}$$

The parameter estimate vector, $\hat{\Theta}(k)$, is updated at every sample using the recursive least squares parameter adaptation algorithm ([47]) as

$$\hat{\Theta}(k) = \hat{\Theta}(k-1) + \frac{F(k)\Phi(k-m)\varepsilon^0(k)}{1+\Phi^T(k-m)F(k)\Phi(k-m)} \tag{4.40}$$

$$F(k+1) = \frac{1}{\lambda_1}\left[F(k) - \frac{F(k)\Phi(k-m)\Phi^T(k-m)F(k)}{\lambda_1 + \Phi^T(k-m)F(k)\Phi(k-m)}\right], \tag{4.41}$$

where λ_1 is the forgetting factor.

The convergence of $\hat{\Theta}(k)$ yields an accurate representation of the dominant component and this estimate, $\hat{x}(k) = \hat{\Theta}^T(k)\Phi(k)$, is removed from the input of the plant to compensate for the dominant frequency component by letting

$$v(k) = -\hat{x}(k), \tag{4.42}$$

where $v(k)$ is the compensation signal shown in Fig. 4.1.

4.3.2 Simulation Results

To see how the TMR is improved by the proposed compensation scheme, a simulation is performed by running the basis function algorithm for five revolutions to reject the dominant frequency component. The first thing to do for the basis function algorithm is to compute the disturbance estimate using (4.34) by filtering the measurement or the output of the plant through the inverse of the plant and then comparing with the delayed control signal. The inverse of the full-order plant model is not practical due to the large amount of computation. In the simulation,

the inverse of a 4th order simplified plant model is used to get the disturbance estimate. The simplified plant model is a double-integrator with the butterfly resonance mode at around 5,000 Hz. The magnitude and the phase of the simplified model differ from those of the full order model only at high frequencies. The inverse of the simplified plant works almost the same as the accurate inverse, since the difference at high frequencies is reduced by the bandpass filter (4.35). The coefficient η in (4.35) is set to 0.95 in the simulation. The forgetting factor λ_1 of the recursive least squares parameter adaptation algorithm in (4.41) is chosen to be a small value 0.3 representing strong forgetting, since the magnitude and the phase of the dominant component vary fast.

As mentioned before, the compensation scheme is mainly for the track following control, which means that the reference is zero. In the spectrum of the PES shown in Fig. 4.9, we can see that the dominant component is almost completely removed by the proposed compensation scheme with small amplification in [1300 Hz, 2300 Hz] and the TMR is reduced by 17% (the standard deviation of the PES before and after compensation are 3.36 and 2.78 in the unit of track percentage, respectively).

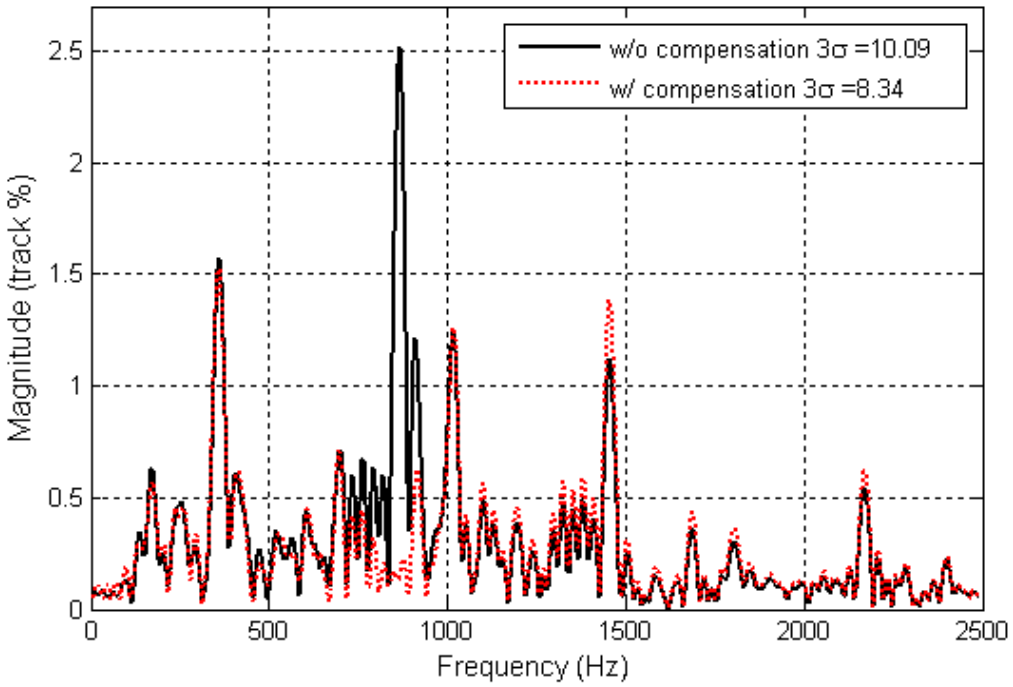

Figure 4.9: PES spectra with and without compensation.

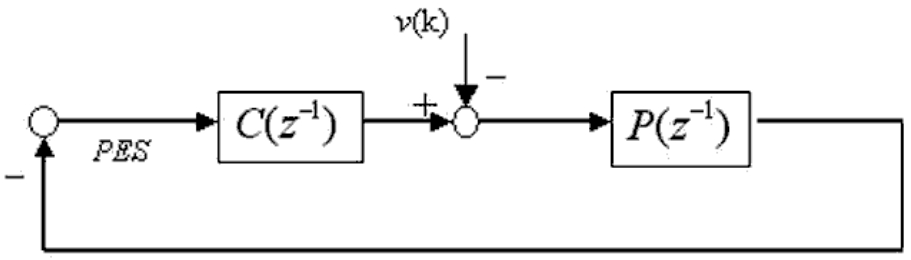

Figure 4.10: Block diagram of a simulation system for checking effect of compensation.

It is important to confirm that the proposed scheme is capable to track the time-varying magnitude and phase of the dominant frequency component. This point was studied by simulation as follows. First, the time traces of magnitude and phase of the dominant component at 861 Hz in the original system (without compensation) are obtained by calculating DFT of every 30 sample PES. The traces are represented by the dots in Fig. 4.11. Then run a simulation with compensation and store the compensation signal (v(k) in Fig. 4.1). To see the effect of the compensation signal, we simulate the system shown in Fig. 4.10 with the previously stored compensation signal as the only input, obtaining the time traces of magnitude and phase of the frequency component at 861 Hz in the negative PES. These time traces are then compared with the original time traces without compensation. As shown Fig. 4.11, the magnitude and the phase of the frequency component at 861 Hz in the negative PES caused by the compensation signal alone are close to those of the dominant component of the uncompensated case. Because the system is linear, the dominant component is canceled by the compensation signal.

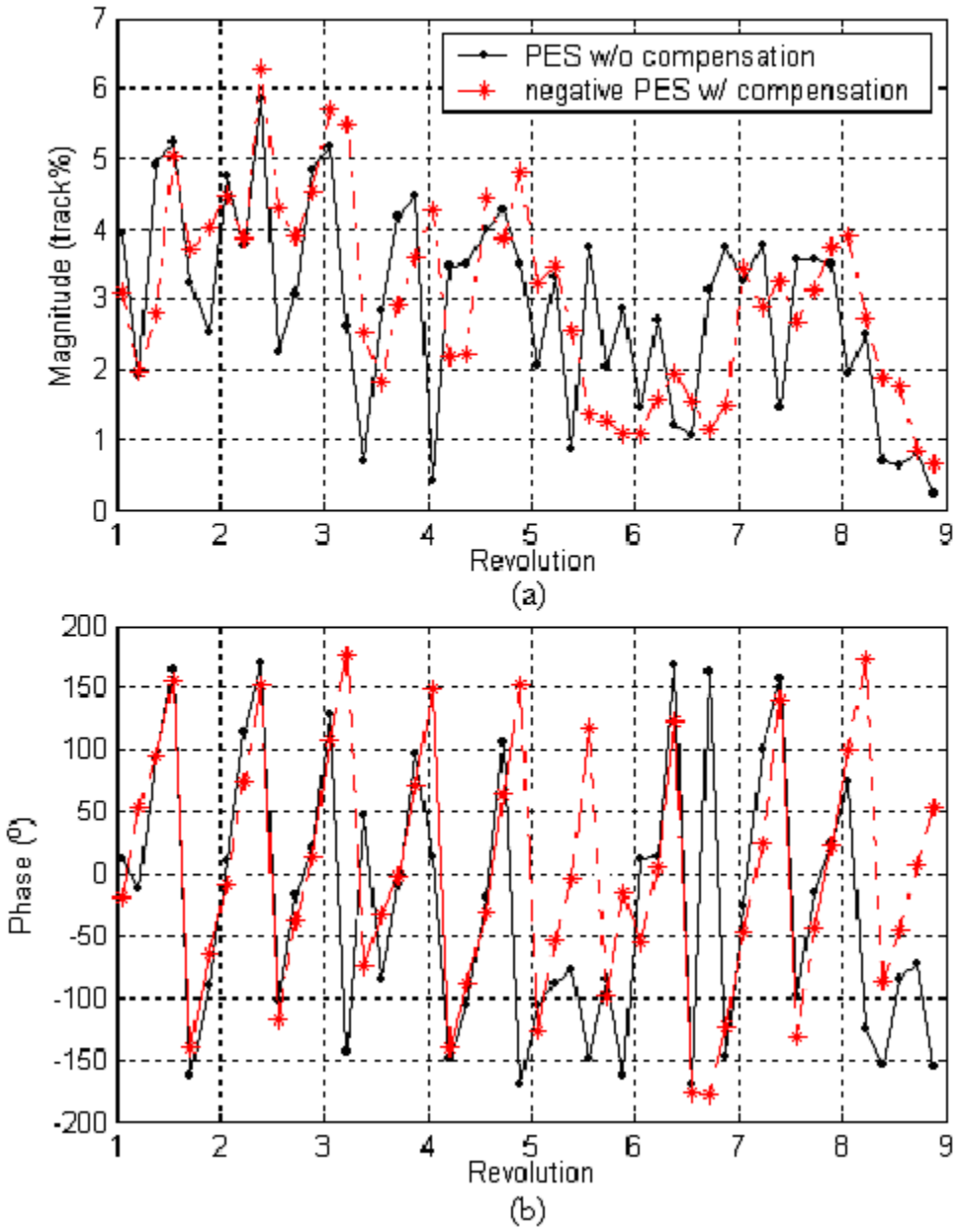

Figure 4.11: Time traces of (a) magnitude and (b) phase of the frequency component at 861 Hz in the original PES spectrum and in the negative PES spectrum generated by the compensation signal.

4.3.3 Multiple Component Compensation

One advantage of the basis function algorithm is that it can be extended to deal with multiple frequency components. Figure 4.12 shows the structure of three-component compensation. The PES is now filtered by three bandpass filters (one of which is actually a low pass filter) with disjoint pass bands as shown in Fig. 4.13 to select the frequency range of interest. Assume that in the PES spectrum there is only one dominant component in each pass band. Then each component can be removed by the single component compensation scheme introduced in Section 4.3.1. The compensation blocks in Fig. 4.12 are identical to each other, involving frequency estimation by LMS method and magnitude and phase identification using the basis function algorithm.

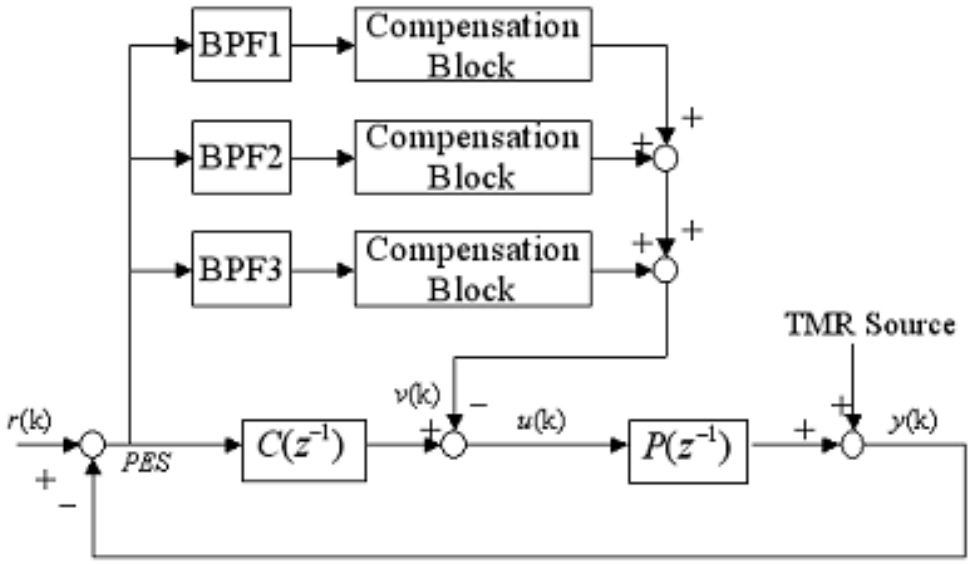

Figure 4.12: Structure of multiple component compensation (BPF: bandpass filter with different pass band).

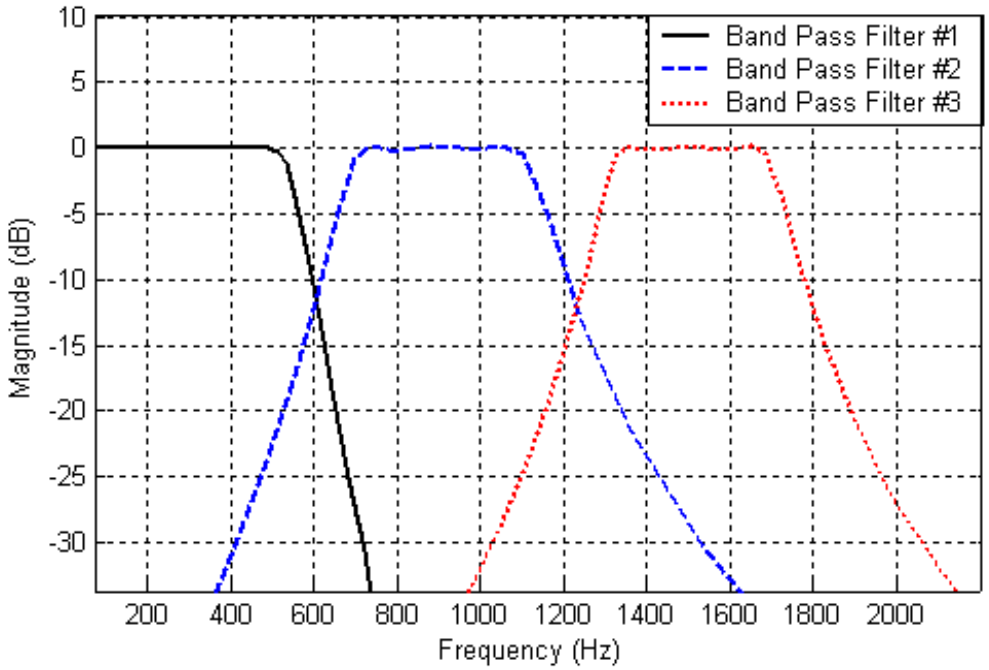

Figure 4.13: Magnitude of the frequency responses of three bandpass filters with disjoint pass bands [0 Hz, 500 Hz], [700 Hz, 1100 Hz], and [1300 Hz, 1700 Hz].

Suppose that the PES spectrum without filtering is shown in Fig. 4.14(a). Component No.1 is the dominant one in frequency range [0 Hz, 500 Hz], No.2 in [700 Hz, 1100 Hz], and No.3 in [1300 Hz, 1700 Hz]. In Fig. 4.14(b) it is clearly shown that the spectrum of the output of each bandpass filter has only one dominant frequency component.

Same as before, the first revolution of simulation is dedicated to the frequency identification by the LMS algorithm. It is shown in Fig. 4.15 that the frequency estimate for every component converges within one revolution and is close to the result of spectral analysis. The converged frequency estimates for the three dominant components after one revolution are 377 Hz, 861 Hz, and 1468 Hz, respectively, which are all close to their true values 360 Hz, 854 Hz, and 1450 Hz. With these frequency estimates, the magnitude and the phase of each dominant component are identified and then used to construct the compensation signal. The compensation runs for these three components for 5 revolutions and the spectrum of the resulting PES is calculated and compared to the original spectrum. As shown in Fig. 4.16, all three components have been greatly attenuated by the proposed compensation scheme and 25% TMR improvement is achieved in total (the standard deviation of the PES is reduced from 3.36 to 2.53 in the unit of track percentage).

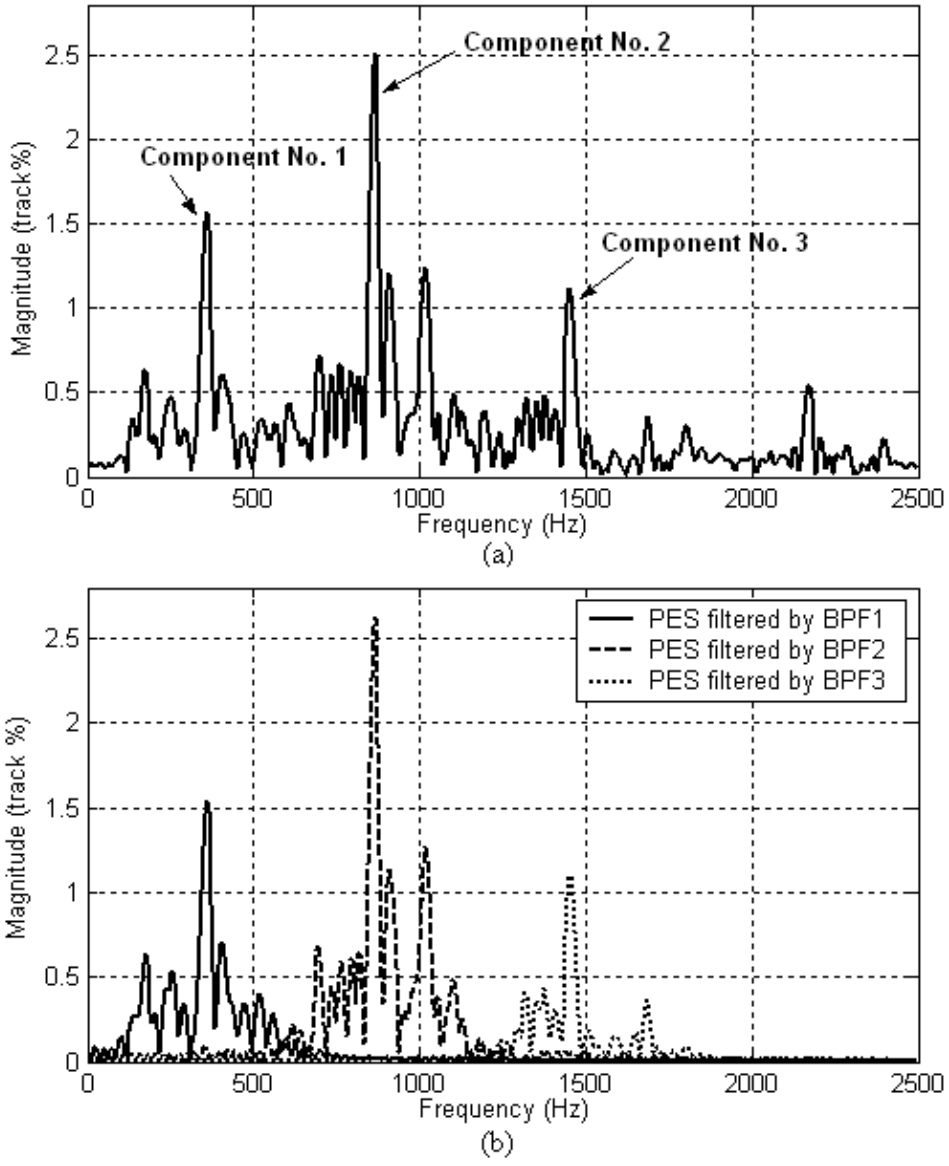

Figure 4.14: PES spectra: (a) original; (b) filtered by different bandpass filters.

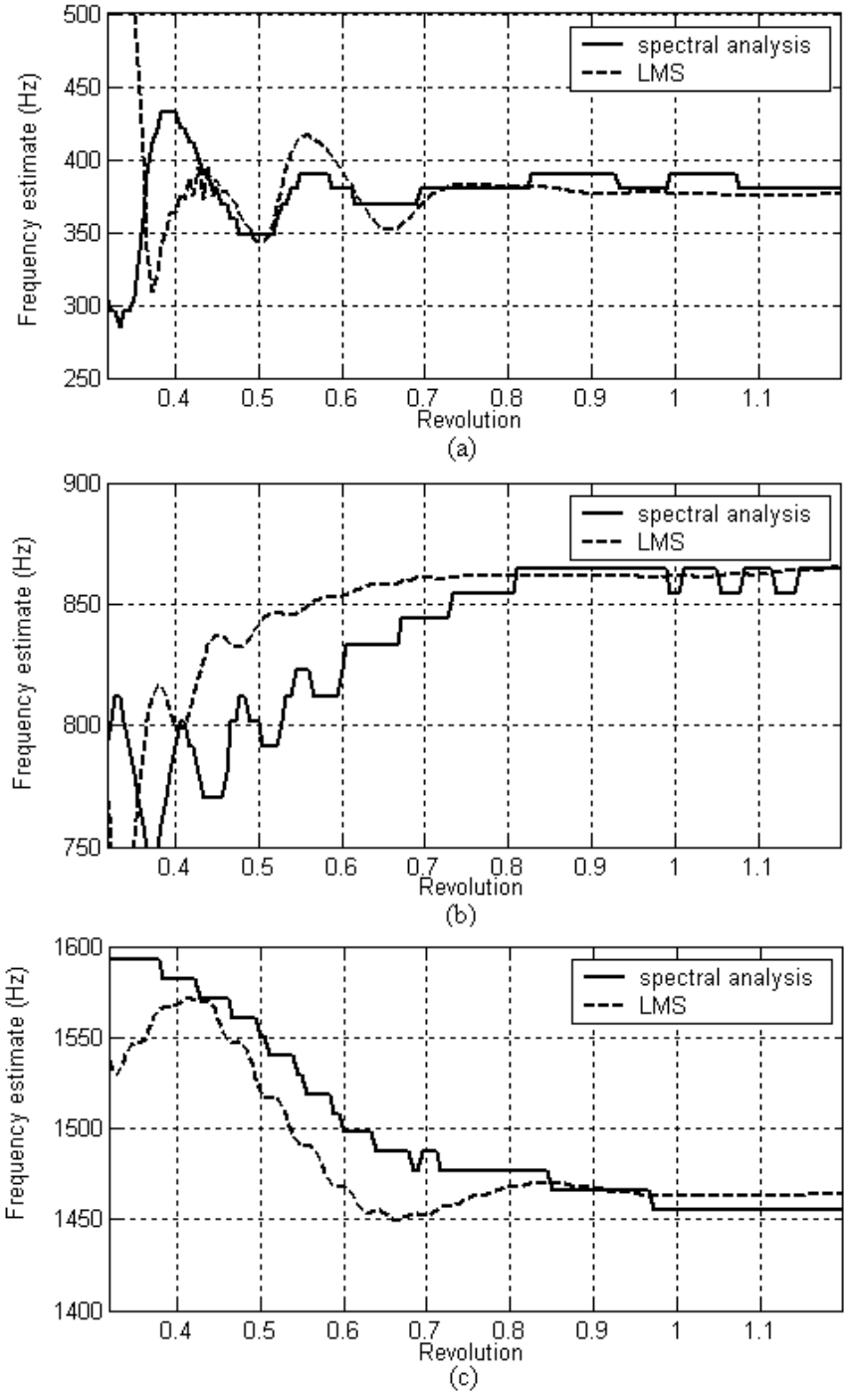

Figure 4.15: Frequency identification for (a) Component No.1; (b) Component No.2; (c) Component No.3, by spectral analysis and by LMS.

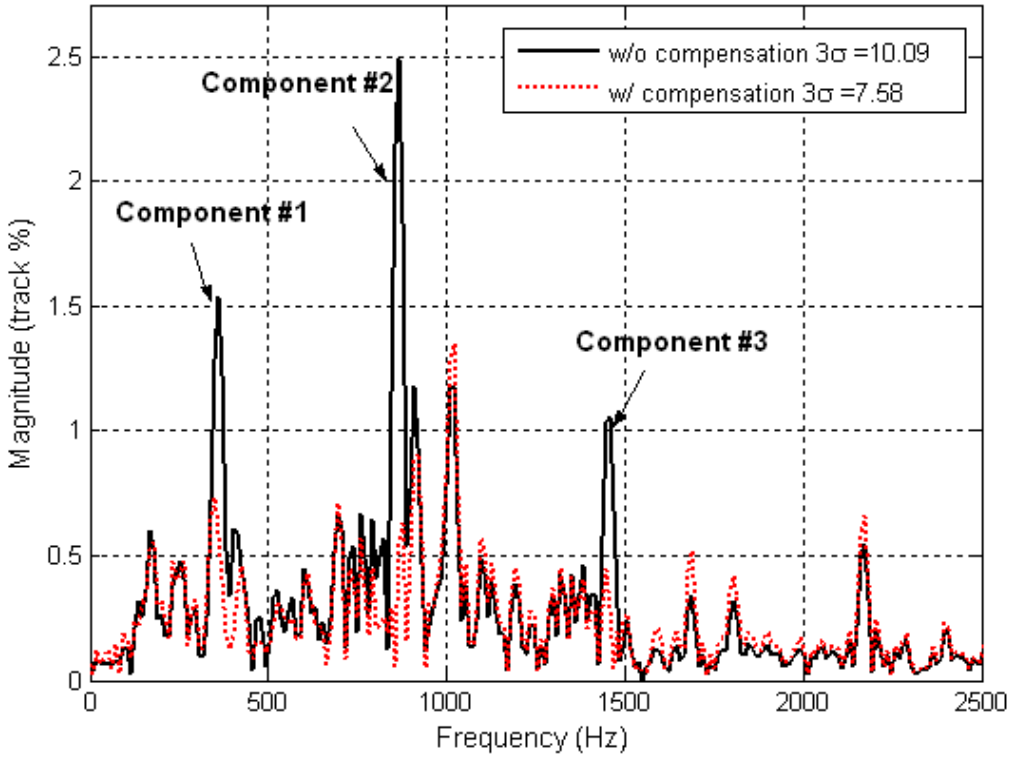

Figure 4.16: PES spectrum with and without multiple component compensation based on basis function algorithm.

4.4 Adaptive Narrow Band Disturbance Observer

The method of computing the filtered disturbance estimate $\hat{d}'(k-m)$ described in the previous section can be put into the block diagram shown in Fig. 4.17, which resembles the structure of a disturbance observer (DOB) with $G_{bpf}(z^{-1})$ representing a Q filter.

Ohnishi ([65], [62]) introduced the DOB to handle disturbances in motion control, which was later refined by Umeno and Hori ([84]). The DOB has been widely used for high-accuracy motion control systems ([53], [94]). For HDD servo systems, the DOB has been applied to improve the access time or settling performance ([25], [33]), reject shock disturbance ([74]), and design track following controller ([52], [78], [86]). In this section, we will introduce a narrow-band DOB that differs from the traditional DOB.

4.4.1 Narrow Bandpass Q Filter

The biggest difference between the DOB used here and the traditional DOB is the bandpass Q filter $G_{bpf}(z^{-1})$. The reason for using a bandpass Q filter instead of a low pass one is to limit the frequency range of the waterbed effect as will be discussed later in this section.

The output of this DOB, $\hat{d}'(k-m)$, is approximately equal to $x'(k-m)$, the dominant component delayed by *m* samples. Since in the HDD system the plant delay *m* is often small (*m* = 1 in our case), most part of the dominant component can be rejected by using $-\hat{d}'(k-m)$ as the compensation signal *v*(*k*) in Fig. 4.1.

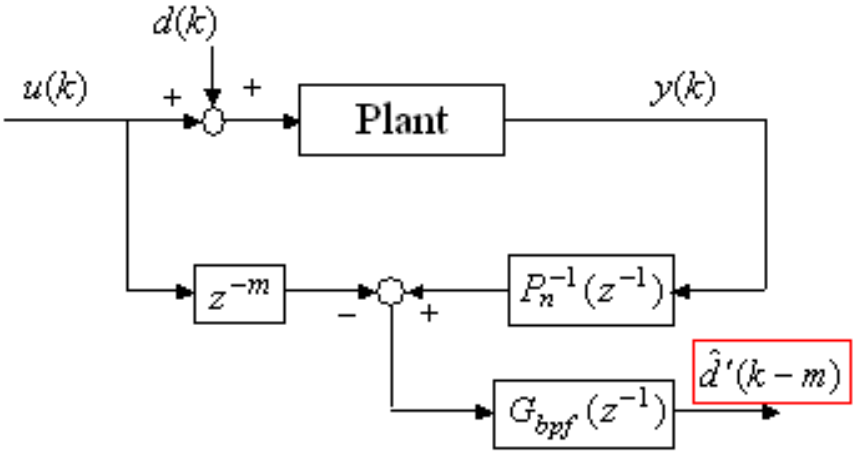

Figure 4.17: Structure of a disturbance observer with $G_{bpf}(z^{-1})$ as the Q filter.

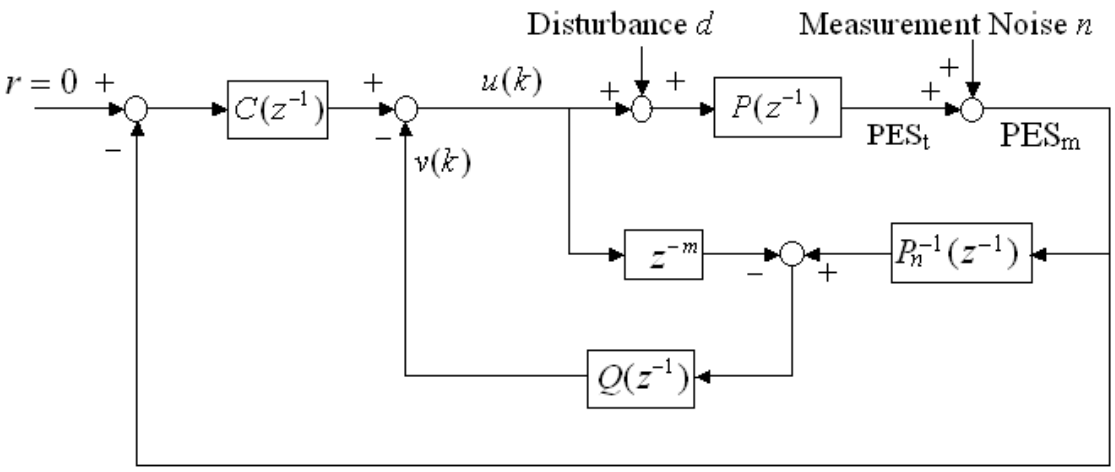

Figure 4.18: Closed loop block diagram of a DOB.

Figure 4.18 shows the block diagram of the resulting closed loop HDD system with the compensation signal, $v(k)$, injected to the loop and with $G_{bpf}(z^{-1})$ denoted by $Q(z^{-1})$, which is a bandpass filter with a narrow pass band centered at the estimated frequency. The servo system is affected by disturbance on the plant input and measurement noise on the plant output. The real head position is denoted by PES_t and the PES measurement that has been contaminated by measurement noise is denoted by PES_m. In HDD track following control, PES_t is the actual quantity to keep small. But since the effect of measurement noise is usually not significant, PES_m and PES_t are often both referred to as PES.

The transfer function of $Q(z^{-1})$ is given in Eq. (4.35) and repeated here:

$$Q(z^{-1}) = (1-\eta)\frac{1-\eta z^{-2}}{1-2\eta\cos(\hat{\omega}T_s)z^{-1}+\eta^2 z^{-2}}. \tag{4.43}$$

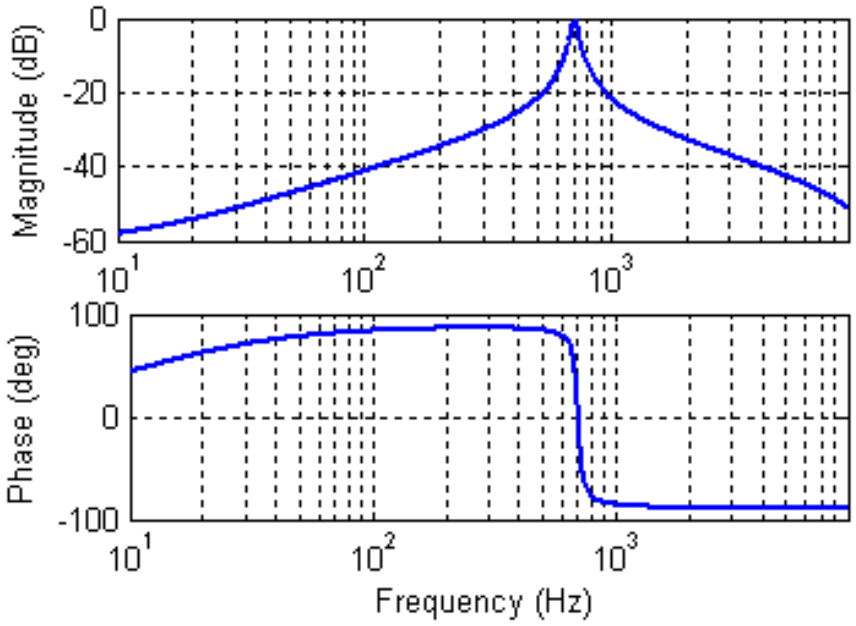

Figure 4.19: Frequency response of a narrow bandpass Q filter.

The closed-loop system is a DOB that differs from the traditional DOB in the nature of the Q filter: bandpass with a narrow pass band instead of low pass. The frequency response of the Q filter with $\hat{\omega} = 2\pi T_s \times 700$ and $\eta = 0.995$ is shown in Fig. 4.19. The narrow pass band is achieved by making η close to and less than 1 (0.995 is used in this Section). The reason for choosing a narrow bandpass Q filter over a low pass filter is to avoid the large waterbed effect of the traditional DOB. This point can be seen from the closed-loop analysis below.

4.4.2 Closed-Loop Analysis

The signals in Fig. 4.18 satisfy the following equations:

$$\mathrm{PES}_{\mathrm{t}}(k) = P(z^{-1})[u(k) + d(k)], \tag{4.44}$$

$$\mathrm{PES}_{\mathrm{m}}(k) = \mathrm{PES}_{\mathrm{t}}(k) + n(k), \tag{4.45}$$

$$u(k) = -C(z^{-1})\mathrm{PES}_{\mathrm{m}}(k) - v(k), \tag{4.46}$$

$$v(k) = Q(z^{-1})[P_n^{-1}(z^{-1})\mathrm{PES}_{\mathrm{m}}(k) - z^{-m}u(k)]. \tag{4.47}$$

From Eq. (4.44), (4.45), and (4.46), we can write u as

$$u(k) = \frac{-C(z^{-1}) - Q(z^{-1})P_n^{-1}(z^{-1})}{1 - z^{-m}Q(z^{-1})}[\mathrm{PES}_\mathrm{t}(k) + n(k)]. \tag{4.48}$$

Substituting (4.48) into (4.44) yields

$$\begin{aligned}\mathrm{PES}_\mathrm{t}(k) = {} & \frac{P(z^{-1})[1 - z^{-m}Q(z^{-1})]}{H(z^{-1})}d(k) \\ & - \frac{P(z^{-1})C(z^{-1}) + Q(z^{-1})P_n^{-1}(z^{-1})P(z^{-1})}{H(z^{-1})}n(k),\end{aligned} \tag{4.49}$$

where

$$H(z^{-1}) = 1 + P(z^{-1})C(z^{-1}) + Q(z^{-1})[P_n^{-1}(z^{-1})P(z^{-1}) - z^{-m}] \tag{4.50}$$

Thus, the transfer function from d to PES_t and the transfer function from n to PES_t with the proposed narrow-band DOB are given by

$$S_d'(z^{-1}) = \frac{P(z^{-1})[1 - z^{-m}Q(z^{-1})]}{H(z^{-1})}, \tag{4.51}$$

$$S_n'(z^{-1}) = -\frac{P(z^{-1})C(z^{-1}) + Q(z^{-1})P_n^{-1}(z^{-1})P(z^{-1})}{H(z^{-1})}. \tag{4.52}$$

These two error rejection functions for the baseline servo system (without DOB) are given by

$$S_d(z^{-1}) = \frac{P(z^{-1})}{1 + P(z^{-1})C(z^{-1})}, \tag{4.53}$$

$$S_n(z^{-1}) = -\frac{P(z^{-1})C(z^{-1})}{1 + P(z^{-1})C(z^{-1})}. \tag{4.54}$$

Notice that if $Q(z^{-1}) = 0$, we have

$$H(z^{-1}) = 1 + P(z^{-1})C(z^{-1}), \tag{4.55}$$

$$S'_d(z^{-1}) = S_d(z^{-1}), \tag{4.56}$$

and

$$S'_n(z^{-1}) = S_n(z^{-1}), \tag{4.57}$$

which means that the add-on narrow-band DOB does not affect the closed loop performance for rejecting disturbance and measurement noise at those frequencies where the magnitude of the Q filter is small. On the other hand, when $Q(z^{-1}) = 1$ at the center frequency $\hat{\omega}$ where the plant model matches the plant or $P(z^{-1}) = z^{-m}P_n(z^{-1})$ for $z = e^{j\hat{\omega}T_s}$, (4.55) still holds and the two error rejection functions become

$$S'_d(z^{-1}) = \frac{P(z^{-1})[1 - z^{-m}]}{1 + P(z^{-1})C(z^{-1})}, \tag{4.58}$$

$$S'_n(z^{-1}) = -\frac{P(z^{-1})C(z^{-1}) + z^{-m}}{1 + P(z^{-1})C(z^{-1})}, \tag{4.59}$$

Since the delay is small (m = 1 in our case), we have $1 - z^{-m} \approx 0$. Thus, the disturbance is greatly attenuated at the center frequency $\hat{\omega}$ ($S'_d(z^{-1}) \approx 0$) and the measurement noise is unattenuated at $\hat{\omega}$ ($S'_n(z^{-1}) \approx -1$). If the frequency estimation is accurate ($\hat{\omega} = \omega_0$), the dominant frequency component is canceled by the proposed scheme. This point can also be seen from the frequency response of $S'_d(z^{-1})$ plotted in Fig. 4.20.

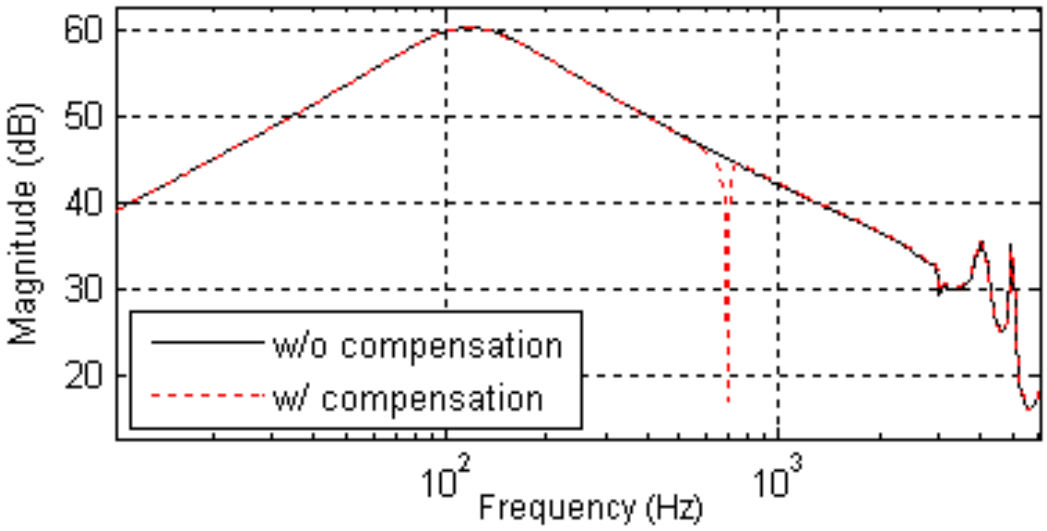

Figure 4.20: Frequency responses of the transfer function from *d* to PES_t without and with compensation.

Since the resulting servo controller with the narrow band DOB is a linear time-invariant system, the frequency domain stability criteria can be applied to analyse the stability of the closed loop HDD system. It is more preferable to give the stability margins for the resulting system than just to show its stability.

A common mistake of evaluating the stability margins for the system with an inner DOB loop is to measure the margins based on the open loop (open the outer feedback loop) transfer function from the reference to PES_m, which is given by

$$L_w(z^{-1}) = \frac{P(z^{-1})C(z^{-1})}{1+Q(z^{-1})[P(z^{-1})P_n^{-1}(z^{-1}) - z^{-m}]}. \tag{4.60}$$

It is known that the major modeling uncertainty for a HDD system takes place in $P(z^{-1})$. The gain (phase) margin of $L_w(z^{-1})$ does not reflect the maximum admissible increase (decrease) of the gain (phase) of $P(z^{-1})$, since $P(z^{-1})$ appears on both the numerator and the denominator of $L_w(z^{-1})$. So the margins of $L_w(z^{-1})$ are not of our interest.

Notice that the reference input in Fig. 4.18 is equal to zero. The closed loop HDD system with the narrow-band DOB is equivalent to the system shown in Fig. 4.21. The loop transfer function for this equivalent system is given by

$$L(z^{-1}) = P(z^{-1})\frac{Q(z^{-1})P_n^{-1}(z^{-1}) + C(z^{-1})}{1 - z^{-m}Q(z^{-1})}, \tag{4.61}$$

which can be used to evaluate the stability margins. $L(z^{-1})$ has no unstable poles. Then the resulting system is stable, if the Nyquist plot of $L(z^{-1})$ has no encirclement of the critical point (-1, 0) in the complex plane. This condition is satisfied for all possible loop transfer functions with the center frequency of $Q(z^{-1})$ varying from 200 Hz to 800 Hz. We constrain the frequency estimate $\hat{\omega}$ to lie in [200 Hz, 800 Hz] under the assumption of the narrow-band disturbance of interest. Therefore, the HDD system with the proposed scheme is stable. The stability margins of the resulting system are also measured from the Bode plot of $L(z^{-1})$ as shown in Fig. 4.22 and the smallest gain/phase margin is 5.57 dB/47.3° corresponding to the 800 Hz center frequency of $Q(z^{-1})$.

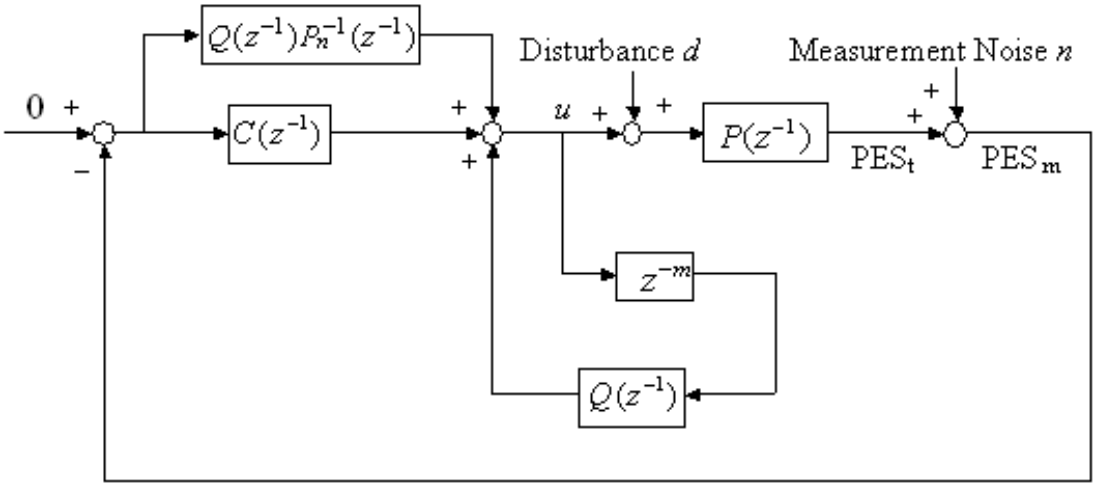

Figure 4.21: An equivalent block diagram of the HDD closed loop system with the narrow band DOB.

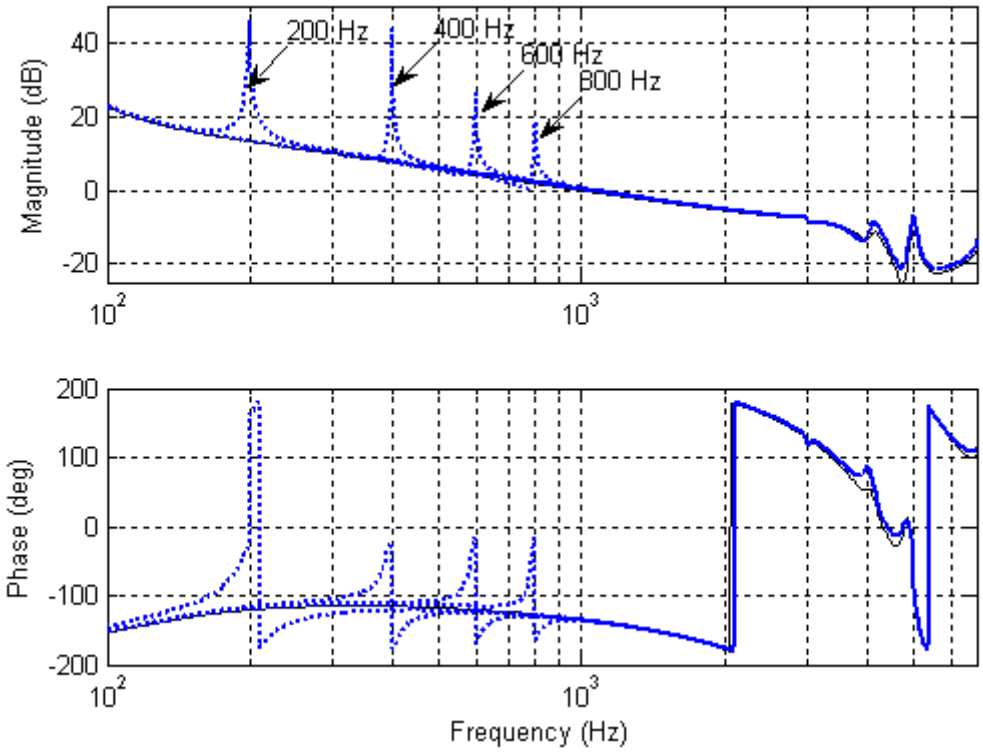

Figure 4.22: Bode plots. Solid thin line: baseline; Dotted thick line: $L(z^{-1})$ for different Q filter center frequencies.

4.4.3 Disturbance Detection

As introduced in Chapter 2, the dominant component may not always exist in a HDD system. Thus, to make the compensation scheme practical, a DOB structure called disturbance detector with a Q filter different from $Q(z^{-1})$ is applied to estimate the disturbance to determine whether a large dominant component occurs. The estimate ($\hat{d}(k-m)$ in Eq. (4.34)) is obtained by comparing the output of the inverted plant model $P_n^{-1}(z^{-1})$ with the control signal delayed by m samples. Since the narrow-band disturbance resides only in the frequency range [200 Hz, 800 Hz] and is the only possible dominant frequency component in this frequency range, a band-pass filter $F(z^{-1})$ similar to the one in Fig. 4.2 with a pass band that contains this frequency range is applied to isolate the narrow-band disturbance from other large frequency components. The structure of the disturbance detector is the same as the block diagram shown in Fig. 4.17 with $G_{bpf}(z^{-1})$ replaced by $F(z^{-1})$.

The output of $F(z^{-1})$ (denoted by $\hat{d}_F(k)$) is a good estimate of the narrow-band

disturbance. To see this point, we express $\hat{d}_F(k)$ by the control signal u and the disturbance d as

$$\hat{d}_F(k) = F(z^{-1})\left\{P_n^{-1}(z^{-1})P(z^{-1})[u(k)+d(k)] - z^{-m}u(k)\right\}, \tag{4.62}$$

where z^{-1} is considered as the one-sample-delay operator. The frequency response of $z^{-m}P_n(z^{-1})$ $(m=1)$ is compared with that of $P(z^{-1})$ in Fig. 4.23. Notice that

$$z^{-m}P_n(z^{-1}) \approx P(z^{-1}), \tag{4.63}$$

for $z = \exp(j2\pi T_s f)$, $f \in [200\,\text{Hz}, 800\,\text{Hz}]$, which implies

$$F(z^{-1})(P_n^{-1}(z^{-1})P(z^{-1}) - z^{-m}) \approx 0. \tag{4.64}$$

Thus, we have $\hat{d}_F(k) \approx F(z^{-1})d(k-m)$. Since the narrow-band disturbance is the only dominant frequency component in the pass band of $F(z^{-1})$, $\hat{d}_F(k)$ consists of the narrow-band disturbance delayed by m samples and other small frequency components that pass through $F(z^{-1})$. Therefore, $\hat{d}_F(k)$ is used to detect the narrow-band disturbance and to estimate the frequency of the disturbance.

When the variance of half revolution (110 sample) $\hat{d}_F(k)$ is larger than a pre-specified threshold, we say that a narrow band disturbance is detected, which activates the frequency estimator and closes the add-on compensator loop, the basis function algorithm or the narrow band disturbance, when the estimated frequency is ready. The other function of the disturbance detector is to disable the frequency estimator and to open the compensator loop to avoid false compensation, when the narrow-band disturbance discontinues.

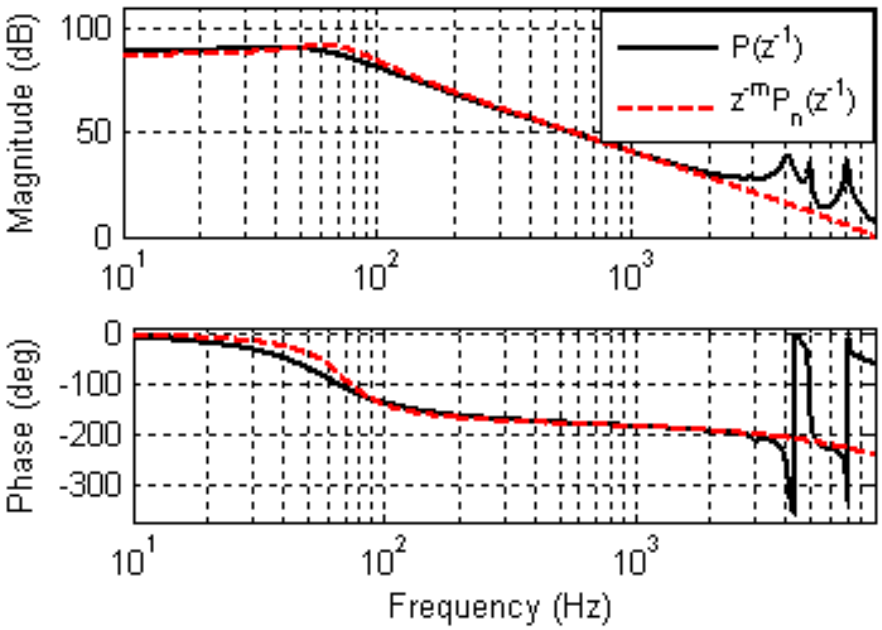

Figure 4.23: Frequency response of the full order plant and the plant model.

4.4.4 Simulation Results

The open-source HDD benchmark problem available at [30] is used with minor modifications to show the efficacy of the proposed narrow band DOB. All realistic disturbances are included in the simulation. In addition, a fictitious sinusoidal signal at 700 Hz is injected to the servo loop near the end of the second revolution (at time *a* as shown in Fig. 4.24) to represent the narrow band disturbance, which then stops at time *b*. Without the proposed compensator, the PES is given by the dashed line in Fig. 4.24 and the TMR (21.0% of the track pitch) is too large for the head to safely perform read/write operation during the presence of the narrow band disturbance.

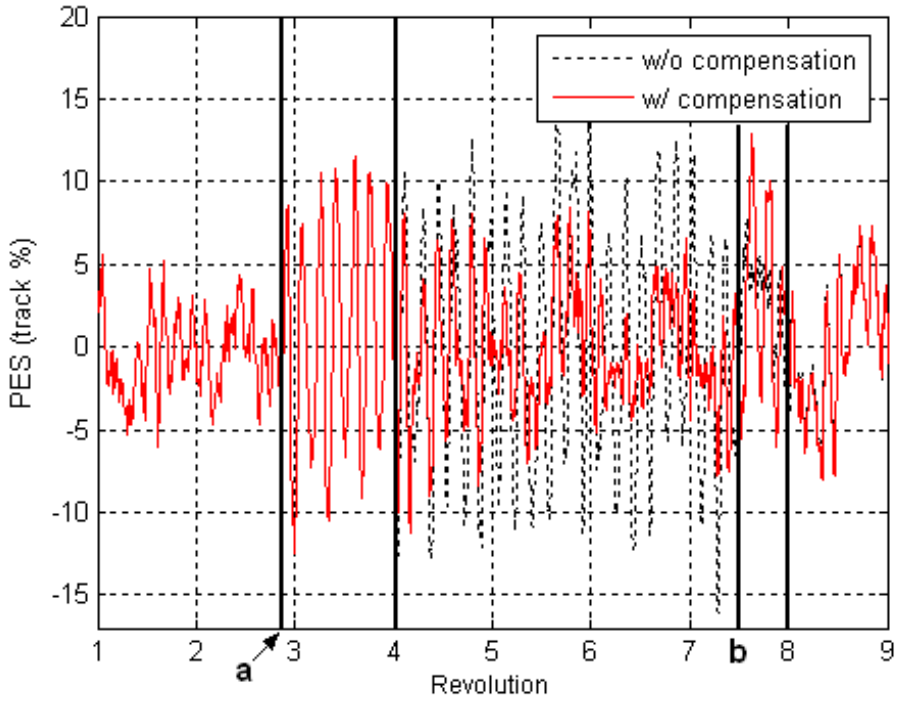

Figure 4.24: Time traces of the PES without and with the proposed scheme. Time a: Beginning of sinusoidal disturbance; b. Ending of sinusoidal disturbance; c. DOB turned on; d. DOB turned off.

The proposed adaptive compensator is applied to improve the track following performance. The whole compensator is controlled by the disturbance detector described in Section 4.4.3. The input to the detector is shown in Fig. 4.25a). The threshold for determining whether a narrow band disturbance occurred is chosen to be 6×10^{-8}, which is exceeded in the middle of the third revolution as shown in Fig. 4.25b). Then the frequency estimation using the LMS method introduced in Section 4.2.3 is activated. The estimated frequency is 701.8 Hz at the end of the third revolution. The narrow band DOB is then switched on with a $Q(z^{-1})$ centered at 701.8 Hz to compensate for the narrow band disturbance. Notice that the disturbance estimate shown in Fig. 4.25a) does not decrease when the narrow band DOB is turned on. The PES with the compensation scheme has smaller peak value in the time window from the beginning of the 4th revolution to time *b* as shown in Fig. 4.24. Figure 4.26 shows the spectral densities of the PES in that time window without and with the proposed compensator. The TMR was improved by 46.7% (11.2% of the track pitch with compensation) due to the big attenuation at the disturbance frequency, which is explained by the deep notch on the frequency response of $S_d'(z^{-1})$ shown in Fig. 4.20. The gain/phase margin of the HDD system with the proposed compensator was 5.58 dB/48.4°.

The disturbance detector is also used to disable the compensator as described in Section

4.4.3. In the simulation, the narrow-band disturbance disappears at time b, but the discontinuation of the disturbance is detected at the end of the 7th revolution and the $Q(z^{-1})$ loop is opened when the variance of $\hat{d}$ dropped below the threshold. Thus, we can see that the PES with compensation is larger than the one without compensation in the time window from b to the end of the 7th revolution due to false compensation and they become the same after the $Q(z^{-1})$ loop is open.

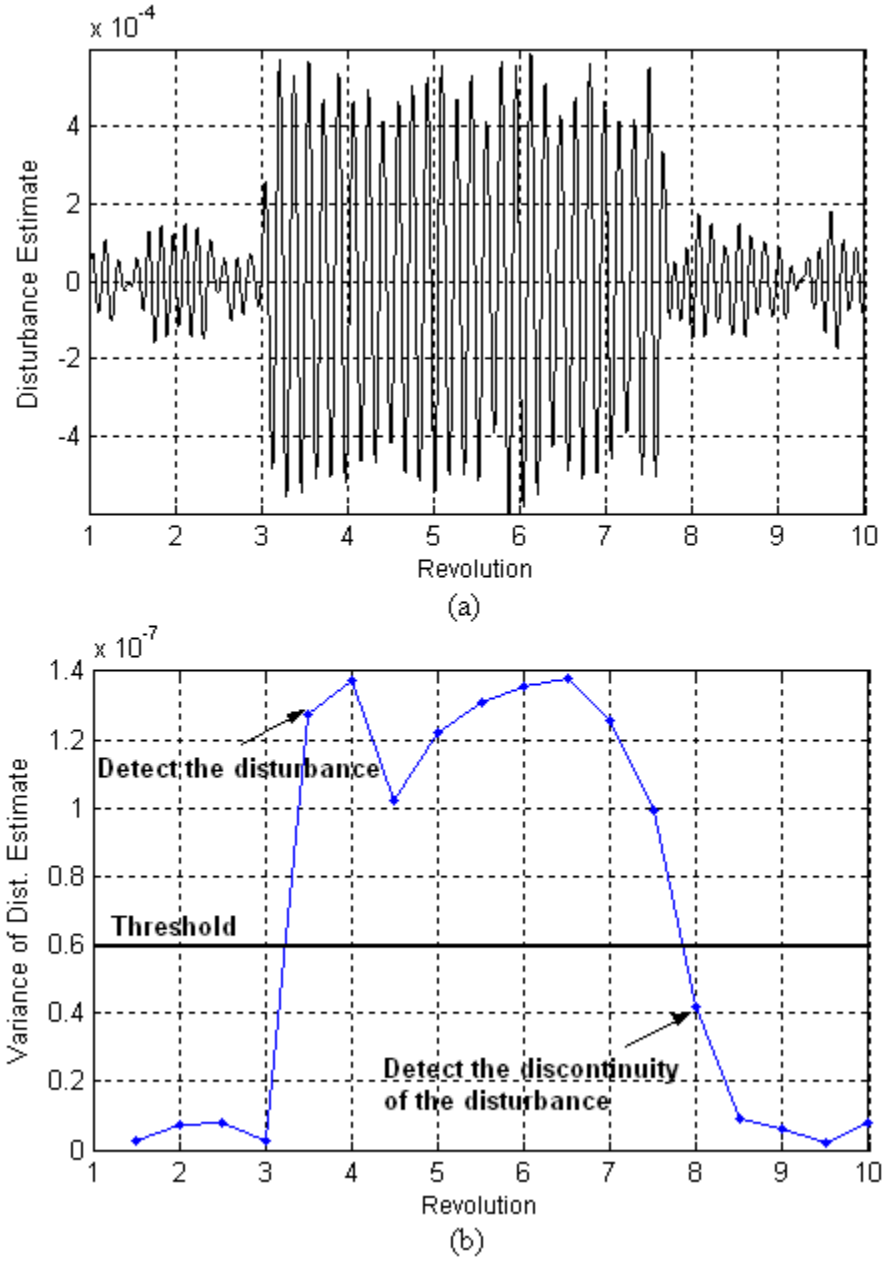

Figure 4.25: (a) Time trace and (b) variance of $\hat{d}$ over every half revolution.

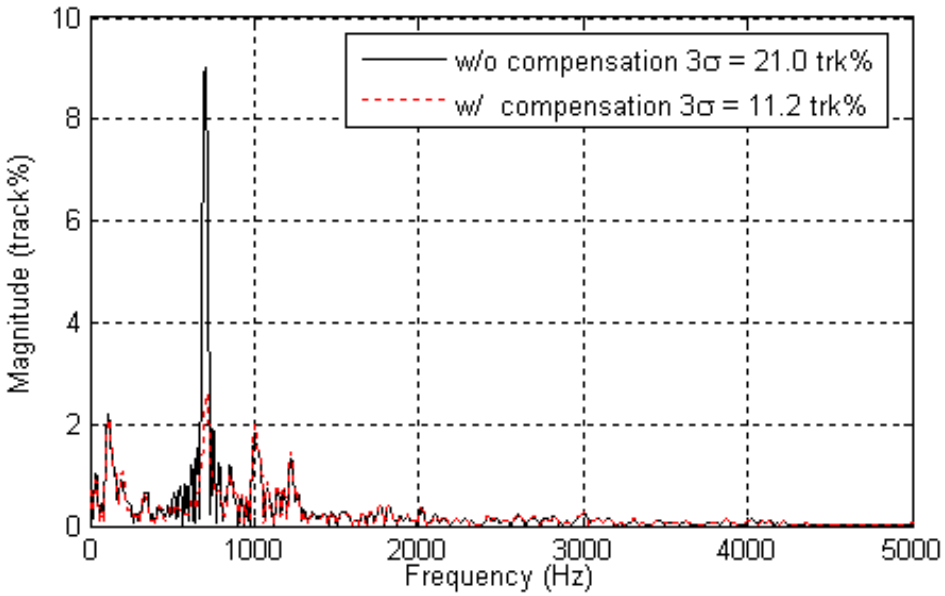

Figure 4.26: Spectral densities of the PES without and with the proposed compensator in the time window from the beginning of the 4th revolution to time *b*.

4.4.5 Transient Compensation

Often times when an add-on compensator is turned on in the servo loop, the abrupt change of feedback controller can excite the slightly damped modes in the system and result in a big transient oscillation. The proposed narrow band DOB scheme also has transient issues. Figure 4.27 shows the PES time traces without and with narrow band DOB compensation. The narrow band disturbance occurs at the time instance a that is different from the simulation in Section 4.4.4. When the narrow band DOB is activated at time b, the PES becomes even larger than the one without compensation. This transient response must be compensated to make the proposed narrow band DOB scheme practical.

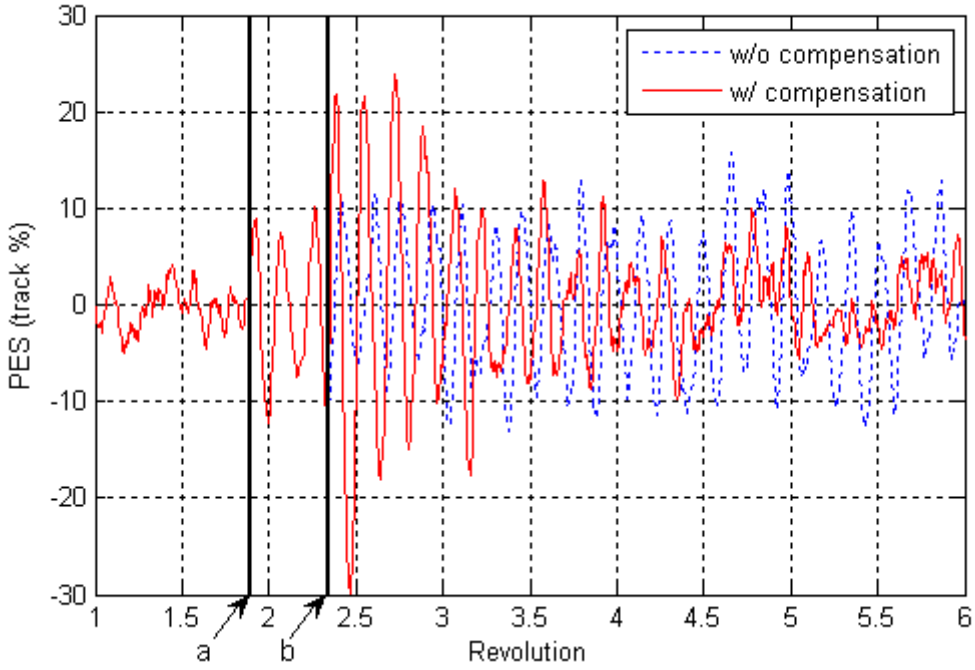

Figure 4.27: Time traces of PES with a big transient oscillation.

The transient issue is also seen in HDD systems during switching from the track seeking mode to the track following mode. The most common treatment for controller induced big transient responses is the initial value compensation ([63], [92], [93]), which assigns the initial value of the controller states at the moment of mode switching based on the plant states, the plant model and a criterion (pole assignment or cost function minimization). However, this method is not suitable for the narrow band DOB scheme, since not all plant states are available and the plant model is not very accurate, this method is not suitable for the narrow band DOB.

It is clear that the oscillation is due to an abrupt switching-on of the narrow band disturbance. So if we gradually exert the compensation signal, the oscillation should be decreased. This idea can be represented by the block diagram in Fig. 4.28. The output of the Q filter $v(k)$ is multiplied by a time-varying gain $K_Q(k)$ gradually increasing from 0 to 1. A simple choice of such a gain is given by

$$K_Q(k) = \begin{cases} 0, & \text{for } k < 0 \\ \dfrac{k}{N}, & \text{for } k = 0,\ldots,N \\ 1, & \text{for } k > N \end{cases} \tag{4.65}$$

where $k = 0$ is when the narrow band DOB is enabled and N is chosen to be a large integer such as the number of servo sectors per revolution. The resulting PES is shown in Fig. 4.29, where the big oscillation does not occur and the PES with compensation is similar to the PES without

compensation in the first revolution after the narrow band DOB is activated. After the first revolution, the PES is greatly reduced by the compensator.

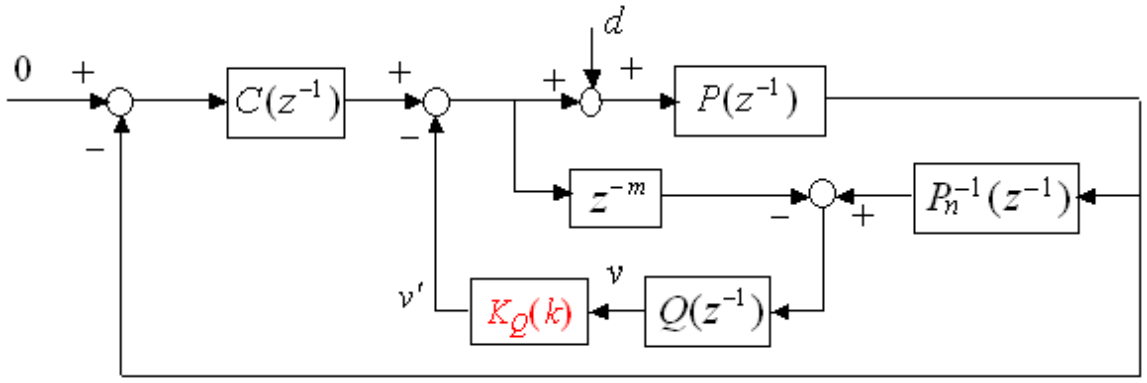

Figure 4.28: Narrow band DOB with a time-varying output gain.

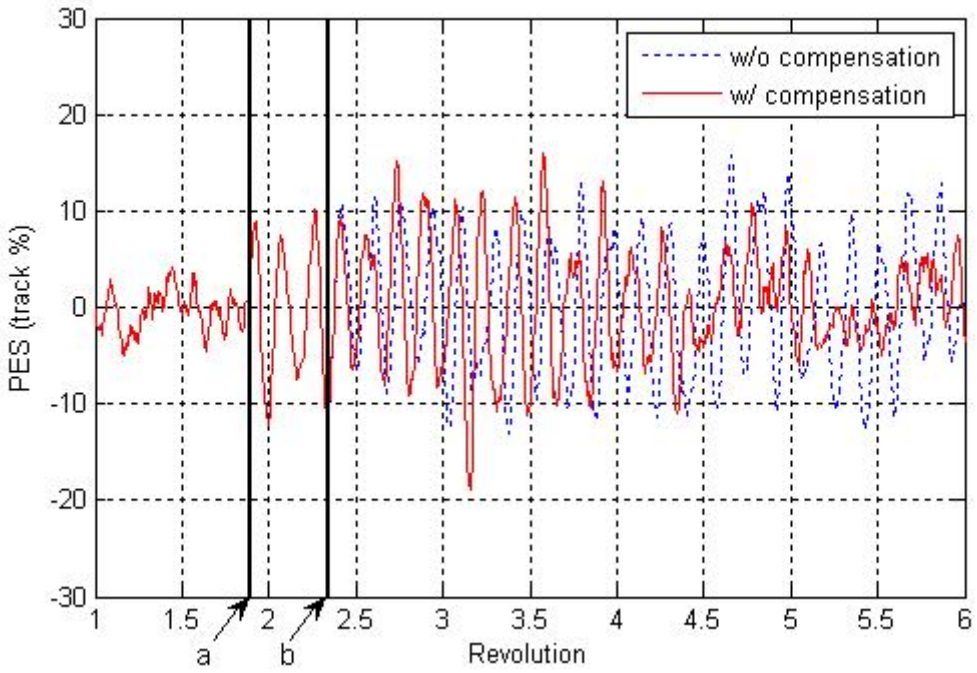

Figure 4.29: Time traces of PES with time-varying output gain of Q filter.

The reason that the gradually increasing gain improves transient response can also be explained in the frequency domain. From Fig. 4.27, it is clear that the frequency of the transient oscillation is same as the center frequency of the Q filter, which means that when the narrow DOB is activated there is a large peak at the center frequency in the spectrum of the signal v. Suppose the DTFT of v is $V(e^{j\omega})$. Then the DTFT of signal $v'(k) = K_Q(k)v(k)$ can be expressed as

$$V'(e^{j\omega}) = \frac{1}{2\pi} K_Q(e^{j\omega}) * V(e^{j\omega}), \tag{4.66}$$

where $K_Q(e^{j\omega})$ is the DTFT of the gain $K_Q(k)$. The sampled magnitudes of $K_Q(e^{j\omega})$ for $K_Q(k) \equiv 1$ and the ramping $K_Q(k)$ given by Eq. (4.65) are compared in Fig. 4.30, which shows that any large peak in the magnitude of $V(e^{j\omega})$ is smoothed out by the ramping $K_Q(k)$.

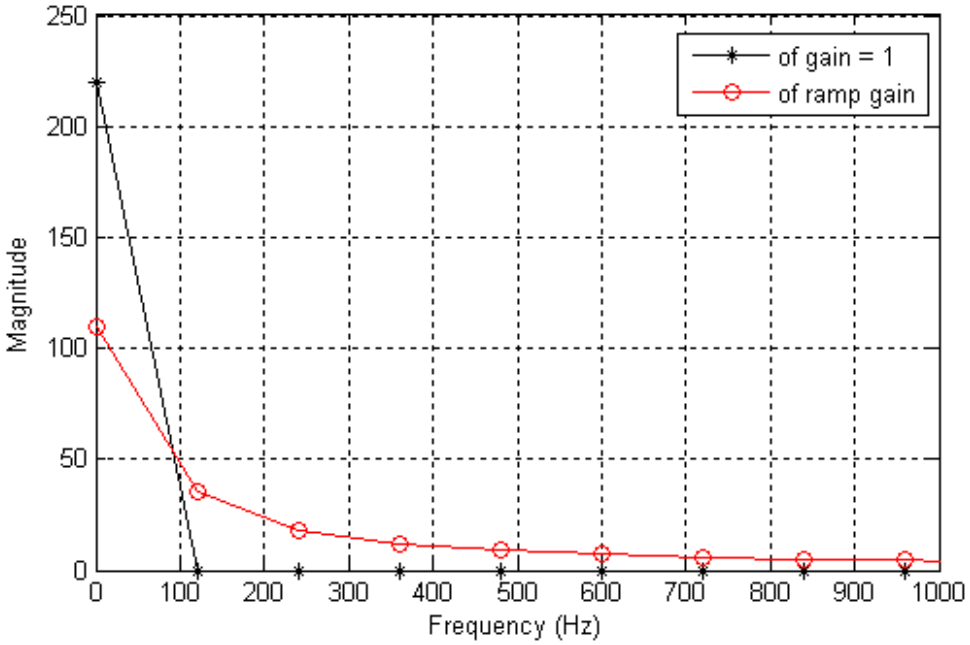

Figure 4.30: Magnitude of the 220-point DFT of $K_Q(k)$.

When the $K_Q(k)$ given in Eq. (4.65) is used in the narrow band DOB loop, the closed-loop system shown in Fig. 4.28 becomes time varying. It is important that the stability of the system is guaranteed. If we remove d from the system and consider v' as the only input to the loop, we can get the following relationship between v and v'

$$v = \frac{P(z^{-1})P_n^{-1}(z^{-1}) - z^{-m}}{1 + P(z^{-1})C(z^{-1})}(-v'). \tag{4.67}$$

Then the closed-loop system can be represented by an equivalent system shown in Fig. 4.31 with

$$S_Q(z^{-1}) = Q(z^{-1})\frac{P(z^{-1})P_n^{-1}(z^{-1}) - z^{-m}}{1 + P(z^{-1})C(z^{-1})}, \tag{4.68}$$

and

$$v'(k) = \Phi(v(k)) = K_Q(k)v(k). \tag{4.69}$$

The stability of this system can be proven by the small gain theorem, which states that the interconnected system in Fig. 4.31 is stable, if $\|\Phi\|_\infty \le 1$ and $\left\|S_Q(z^{-1})\right\|_\infty < 1$. $\|\Phi\|_\infty \le 1$ holds since $0 \le K_Q(k) \le 1$. The condition $\left\|S_Q(z^{-1})\right\|_\infty < 1$ is also satisfied as can be seen in Fig. 4.32 that the magnitude of $S_Q(z^{-1})$ is always below 0 dB. Therefore, the resulting linear time-varying closed-loop system is stable.

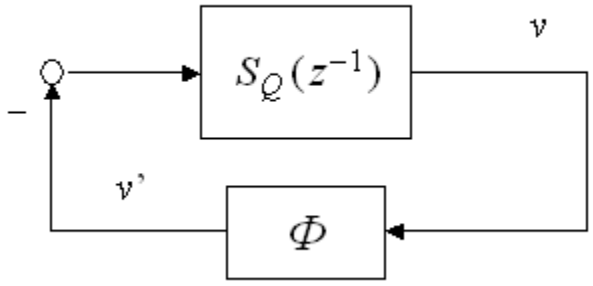

Figure 4.31: An equivalent block diagram for the narrow band DOB with time-varying gain.

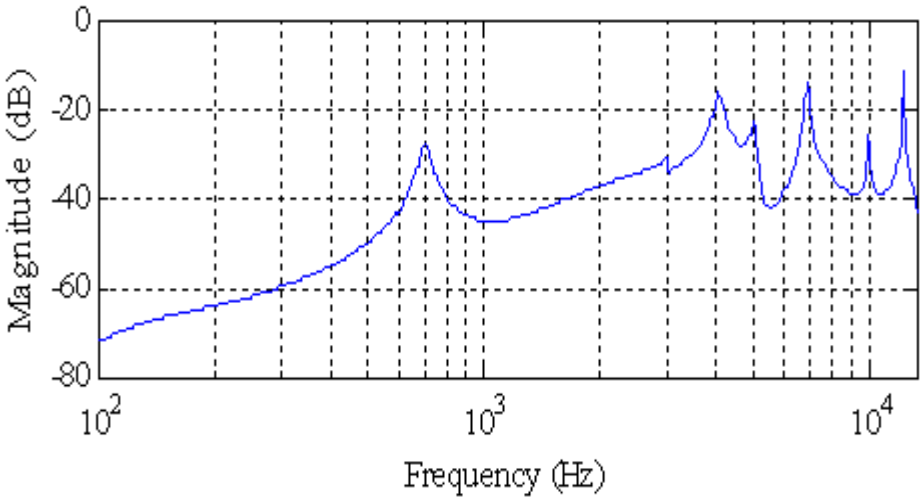

Figure 4.32: Magnitude of $S_Q(z^{-1})$.

4.5 Summary and Concluding Remarks

This chapter presented indirect adaptive control schemes to reject narrow band disturbance. The two steps of the indirect adaptive control can be designed separately and thus were introduced separately in this chapter.

Step one was the disturbance model identification, in particular, the identification of the narrow band disturbance frequency. With prior knowledge about the disturbance, the measurement used for frequency identification, the PES, was filtered by a bandpass filter to isolate the frequency band of the dominant component from other components. Two algorithms have been introduced for frequency identification in this chapter. The frequency identification by the DFT was based on the frequency-domain representation of a discrete-time signal. The DFT method resulted in an accurate and fast frequency estimate. However, it was suited only for off-line identification. The LMS method was based on the parametric model of a sinusoidal signal and required a small amount of computational effort, which made it a good on-line frequency identification method.

The second step of the indirect adaptive approach was the compensator design. Two add-on compensators were introduced in this chapter. One was based on the basis function algorithm (Compensator 1) to estimate the magnitude and the phase of the narrow band disturbance and the other was a DOB with a narrow band pass Q filter (Compensator 2). Both compensators had pros and cons. Compensator 1 required more computation than Compensator 2 due to the identification of two parameters. Moreover, it was difficult to analyze the robustness for Compensator 1 as what we did for Compensator 2. However, Compensator 1 yielded more attenuation of the narrow band disturbance than Compensator 2. Furthermore, it was

straightforward to extend Compensator 1 to reject multiple frequency components.

Chapter 5

Direct Adaptive Rejection of Narrow Band Disturbance

In this chapter two direct adaptive compensation schemes will be introduced to rejecting dominant frequency component of the disturbance. Section 5.1 describes the structure of the direct adaptive rejection scheme. The direct adaptive compensation scheme based on Youla-Kucera parameterization with two modifications for HDD system is introduced in Section 5.2. Another direct adaptive controller based on disturbance observer (DOB) is applied to reject the dominant frequency component in Section 5.3.

5.1 Structure of An Adaptive Rejection System

The previous Chapter described several indirect adaptive control schemes to reject the dominant component. The major advantage of this approach is that the frequency identification part and the compensation part are separated and thus can be operated separately. For example, if no big change is observed on the frequency identifier, the compensator parameters can be fixed. On the other hand, if frequency estimate varies a lot, the compensator must be disabled to avoid stability issue. Moreover, for the indirect adaptive DOB approach, with a fixed frequency estimate, the resulting compensator is a linear time-invariant system, which allows us to analyze the robustness of the closed loop system. However, there are some drawbacks for the indirect approach. First of all, the convergence time required for the frequency identification is not short enough for an HDD system. From the simulation result of frequency identification in the last chapter, we can see that the convergence takes about one revolution, which means that no compensation can be achieved within the first revolution after the indirect adaptive controller is activated. Another drawback is that this method is not optimal in the sense of minimizing the TMR caused by the narrow-band disturbances. Since TMR is the most important performance index for HDD track following control, it is more preferable to base the compensation scheme on

minimizing TMR.

In this chapter, we will apply two add-on direct adaptive compensators to reject the dominant frequency component. The proposed schemes can be represented by the closed-loop structure shown in Fig. 5.1. The structure may look similar to the indirect adaptive control structure in Fig. 4.1, but it is fundamentally different in the way that instead of identifying the disturbance frequency as done for the indirect adaptive control, the parameters of the add-on compensators are directly updated by the adaptation algorithm.

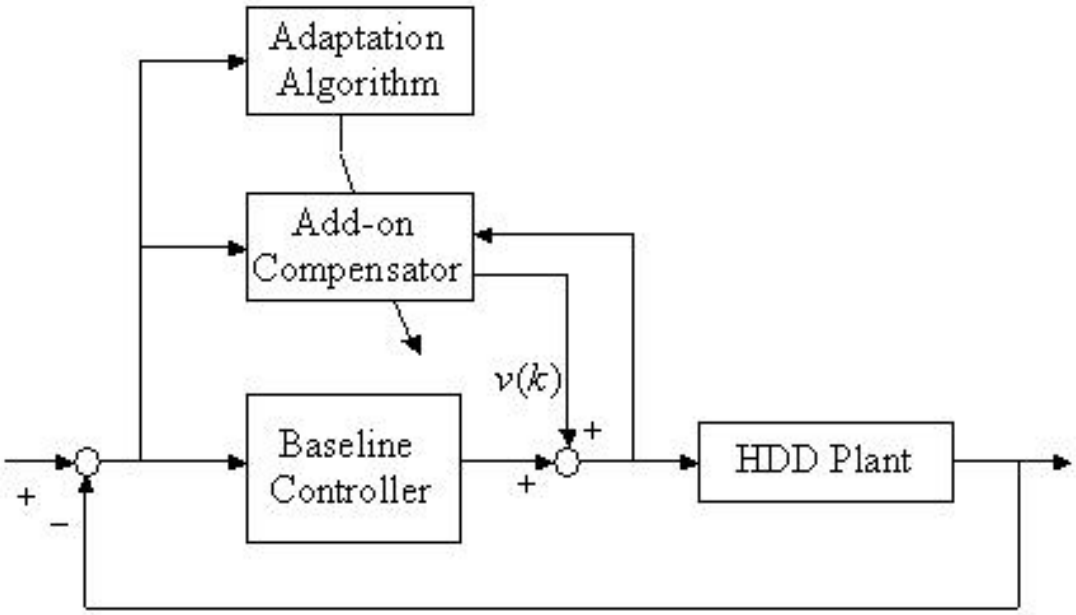

Figure 5.1: Structure of the direct adaptive compensation for narrow band disturbance.

5.2 Adaptive Control Based on Youla-Kucera Parameterization

Landau, Constantinescu, and Rey ([48]) proposed a direct adaptive controller based on Youla-Kucera parameterization to handle narrow band external vibration for an active suspension system and compared it with the indirect adaptive controller. The authors showed by real time experiments that direct adaptive control provided more attenuation than indirect adaptive control. They also reported two problems associated with direct adaptive control: large adaptation transients and influence of inaccurate plant models.

In this section, we introduce the direct adaptive control system based on Youla-Kucera parameterization and represent the HDD track-following baseline servo control system in an equivalent structure suitable for applying the Youla-Kucera parameterization in Section 5.2.1. The adaptive control algorithm based on Youla-Kucera parameterization is described in details in Section 5.2.2. Section 5.2.3 shows simulation results of this adaptive control algorithm. In Section 5.2.3, two modifications are proposed to resolve the two problems with this algorithm to make it applicable for HDD system.

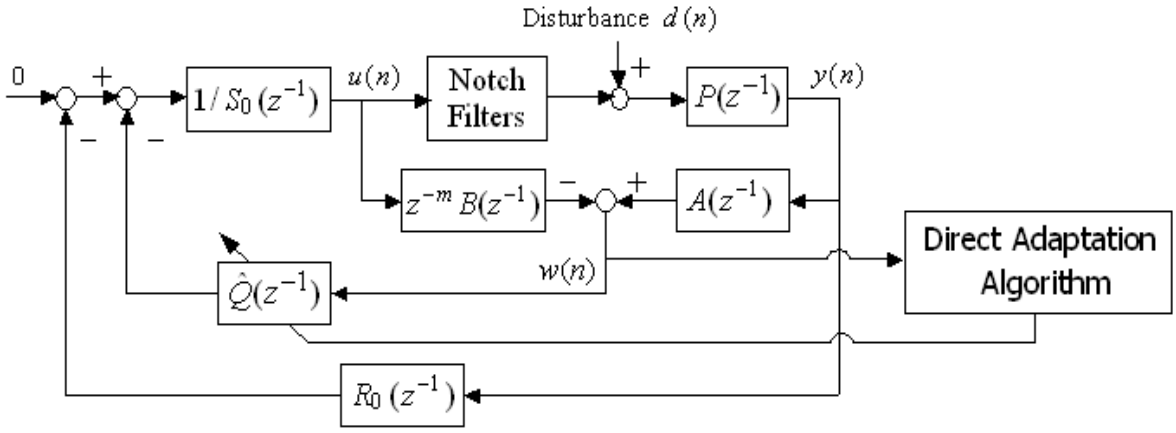

Figure 5.2: Structure of the direct adaptive controller for narrow band disturbance based on Youla-Kucera parameterization.

5.2.1 Overview

The structure of the direct adaptive controller based on Youla-Kucera parameterization is shown in Fig. 5.2. The track-following control for HDD affected by a narrow-band disturbance is considered here, i.e. the reference signal for feedback control is zero. As mentioned in Chapter 1, the power amplifier, the voice coil motor (VCM), the head stack assembly (HSA) are considered as the HDD plant $P(z^{-1})$. The baseline servo controller is a PID controller (given by $R_0(z^{-1})/S_0(z^{-1})$) cascaded with notch filters tuned not to excite the resonant modes. Here the PID controller is implemented as the series connection of $1/S_0(z^{-1})$ and $R_0(z^{-1})$ in order to make use of the Youla-Kucera parameterization. For the simplicity of the adaptive controller design, $P(z^{-1})$ together with the notch filters are considered as the plant of the system, which is denoted by $P_{notch}(z^{-1})$. $z^{-m}B(z^{-1})/A(z^{-1})$ is the discrete-time transfer function of the plant model, $P_m(z^{-1})$, a simplified approximation of $P_{notch}(z^{-1})$. The HDD system is affected by the disturbance d, which includes RRO, sensor noise, disk flutters, external vibration, etc. The numerical values of these polynomials are given by the following equation:

$$R_0(z^{-1}) = 0.0432 - 0.0853z^{-1} + 0.0420z^{-2}, \tag{5.1}$$

$$S_0(z^{-1}) = 1 - z^{-1}, \tag{5.2}$$

$$A(z^{-1}) = 1 - 1.977z^{-1} + 0.9769z^{-2}, \tag{5.3}$$

$$B(z^{-1}) = 3.014 + 2.991z^{-1}, \tag{5.4}$$

$$m = 2. \tag{5.5}$$

Notice that since the plant considered here includes the notch filters, the plant model has 2 sample pure delay steps to match the phase of the plant. The frequency responses of the plant and the plant model are shown in Fig. 5.3. It is clear that the plant model matches well with the plant from 200 Hz to 1000 Hz.

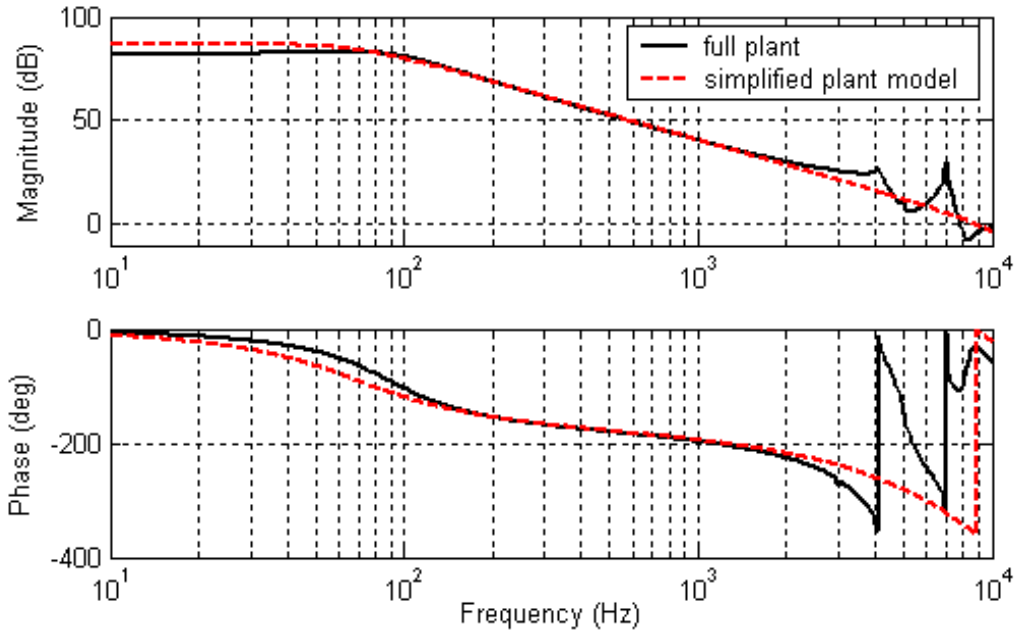

Figure 5.3: Frequency response of the plant and the plant model.

The signal *w* is applied to an adaptation algorithm to adjust the parameters of the finite-impulse-response Q filter, $\hat{Q}(z^{-1})$. The adaptation algorithm is designed based on the internal model principle to achieve asymptotic rejection of narrow-band disturbances.

Suppose that the HDD plant is identical to our plant model. Then, the resulting closed-loop polynomial is

$$H(z^{-1}) = A(z^{-1})S_0(z^{-1}) + z^{-m}B(z^{-1})R_0(z^{-1}). \tag{5.6}$$

Since the closed-loop system with the baseline controller is stable, all the roots of the closed-loop polynomial are stable or inside the unit circle. One useful methodology of designing controllers is the Youla-Kucera parameterization ([6]), which is widely applied to design internal model controller ([60], [98]), two-degrees-of-freedom controller ([59]) and LQG controller ([8]), solve H_∞ problems ([22], [106]) and H_2 problems ([18]), and parameterize the closed-loop system for identification ([27], [73], [79]). The Youla-Kucera parameterization states that all stabilizing controllers for the plant $z^{-m}B(z^{-1})/A(z^{-1})$ have the form $R(z^{-1})/S(z^{-1})$, where

$$R(z^{-1}) = R_0(z^{-1}) + A(z^{-1})Q(z^{-1}), \tag{5.7}$$

$$S(z^{-1}) = S_0(z^{-1}) - z^{-m}B(z^{-1})Q(z^{-1}). \tag{5.8}$$

$Q(z^{-1})$ is a polynomial of z^{-1} with order n_Q:

$$Q(z^{-1}) = q_0 + q_1 z^{-1} + \cdots + q_{n_Q} z^{-n_Q} \tag{5.9}$$

Note that the resulting closed-loop polynomial remains the same for all the stabilizing controllers:

$$\begin{aligned} & A(z^{-1})S(z^{-1}) + z^{-m}B(z^{-1})R(z^{-1}) \\ &= A(z^{-1})S_0(z^{-1}) - z^{-m}A(z^{-1})B(z^{-1})Q(z^{-1}) \\ &\quad + z^{-m}B(z^{-1})R_0(z^{-1}) + z^{-m}A(z^{-1})B(z^{-1})Q(z^{-1}) \\ &= A(z^{-1})S_0(z^{-1}) + z^{-m}B(z^{-1})R_0(z^{-1}) \end{aligned} \tag{5.10}$$

The controller $R(z^{-1})/S(z^{-1})$ can be implemented as shown in Fig. 5.2 without the adaptation algorithm and with the Q filter fixed. The Q filter gives us extra flexibility to tune the controller without sacrificing the stability.

Our focus is the dominant component (a narrow band disturbance) in the disturbance. This component can be modeled as a sinusoidal signal. The Z transform of a sinusoidal signal is given by

$$D(z^{-1}) = \frac{B_d(z^{-1})}{A_d(z^{-1})} \tag{5.11}$$

where

$$A_d(z^{-1}) = 1 - 2\cos(\omega_0)z^{-1} + z^{-2}, \tag{5.12}$$

where ω_0 is the frequency of the dominant component. $B_d(z^{-1})$ depends on the phase and the magnitude of the dominant component. Note that $1/A_d(z^{-1})$ is called the internal model of the signal.

The narrow band disturbance with a model $B_d(z^{-1})/A_d(z^{-1})$ can be asymptotically rejected by using the internal model principle, which says that in order for the feedback control system to achieve regulation ($\lim_{n\to\infty} y(n) = 0$), it is necessary to include the factor $A_d(z^{-1})$ in the denominator of the open loop transfer function. The HDD plant does not contain the factor $A_d(z^{-1})$. So we let

$$S(z^{-1}) = S'(z^{-1})A_d(z^{-1}), \tag{5.13}$$

for some polynomial $S'(z^{-1})$, which means that Q filter must be tuned to satisfy:

$$S'(z^{-1})A_d(z^{-1}) = S_0(z^{-1}) - z^{-m}B(z^{-1})Q(z^{-1}) \tag{5.14}$$

or equivalently,

$$S_0(z^{-1}) = S'(z^{-1})A_d(z^{-1}) + z^{-m}B(z^{-1})Q(z^{-1}) \tag{5.15}$$

This equation has a unique solution for $S'(z^{-1})$ and $Q(z^{-1})$, if polynomials $S_0(z^{-1})$, $A_d(z^{-1})$ and $B(z^{-1})$ are known and orders of these polynomials (n_{S_0}, n_{A_d} and n_B, respectively) satisfy:

$$n_{S_0} \le n_{A_d} + n_B + d - 1 \tag{5.16}$$

The order n_Q of the solution $Q(z^{-1})$ is:

$$n_Q = n_{A_d} - 1 \tag{5.17}$$

For the narrow-band disturbance case, $n_{A_d} = 2$. So $n_Q = 1$. Since the frequency of the narrow-band disturbance (ω_0 in $A_d(z^{-1})$) is unknown, we cannot solve Eq. (5.15). Instead, the coefficients of the polynomial $Q(z^{-1})$, i.e., $q_0, \ldots, q_{n_Q}$, are adaptively tuned to incorporate the internal model of the disturbance in the controller by an adaptation algorithm, which will be described in the next subsection.

5.2.2 Adaptation Algorithm

Throughout this subsection, it is assumed that the narrow band disturbance is the only disturbance and the transfer function of the plant $P(z^{-1})$ cascaded with the notch filters shown in Fig. 5.2 is given by the model $P_m(z^{-1})$ with transfer function

$$P_m(z^{-1}) = \frac{z^{-m}B(z^{-1})}{A(z^{-1})}. \tag{5.18}$$

Under these assumptions the block diagram in Fig. 5.2 is equivalent to the one in Fig. 5.4 with an equivalent disturbance $d'(n)$. The internal model of the disturbance $d'(n)$ is same as that of the original disturbance narrow band disturbance $d(n)$.

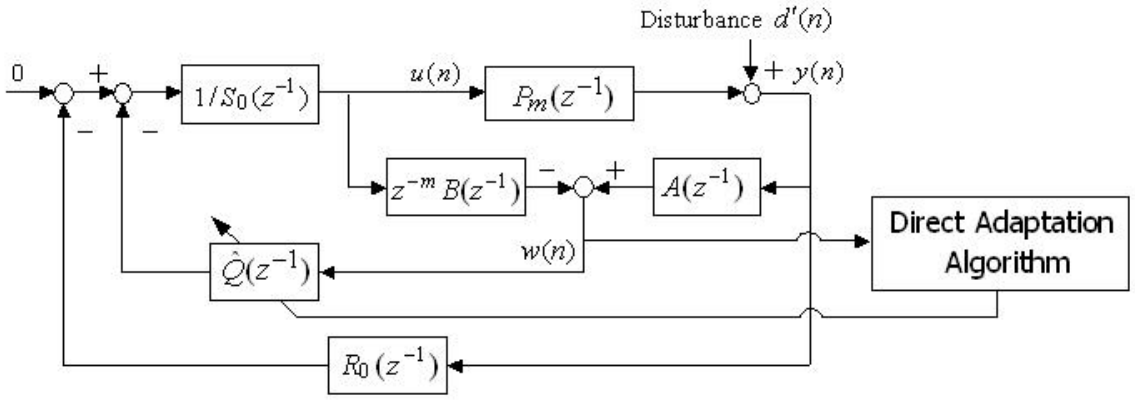

Figure 5.4: Equivalent block diagram of the direct adaptive control system with accurate plant model.

Suppose we have an estimate of the Q filter at the *n*-th sample, denoted as $\hat{Q}(n, z^{-1})$ with order $n_{\hat{Q}}$. Since the objective of the present adaptive controller is to make the plant output go to zero, we define the output ($y(n)$ shown in Fig. 5.4) of the system with $\hat{Q}(n-1, z^{-1})$ in the presence of the disturbance as the *a priori* estimation error $\varepsilon^0(n)$, i.e.

$$\varepsilon^0(n) := y(n) = \frac{A(z^{-1})[S_0(z^{-1}) - z^{-m}B(z^{-1})\hat{Q}(n-1, z^{-1})]}{H(z^{-1})} d'(n), \tag{5.19}$$

where $H(z^{-1})$ is the closed-loop characteristic polynomial given by (5.6) and z^{-1} is interpreted as the unit sample delay operator.

As illustrated in Fig. 5.4, the adaptation algorithm is performed based on the signal $w(n)$, which is given by

$$w(n) = A(z^{-1})y(n) - z^{-d}B(z^{-1})u(n). \tag{5.20}$$

Since

$$y(n) = P_m(z^{-1})u(n) + d'(n) = \frac{z^{-m}B(z^{-1})}{A(z^{-1})}u(n) + d'(n), \tag{5.21}$$

we have

$$w(n) = A(z^{-1})d'(n). \tag{5.22}$$

From (5.19) and (5.22), the *a priori* estimation error is computed by

$$\begin{aligned}\varepsilon^0(n) &= \frac{S_0(z^{-1})}{H(z^{-1})}w(n) - \hat{Q}(n-1,z^{-1})\frac{z^{-m}B(z^{-1})}{H(z^{-1})}w(n) \\ &= w_1(n) - \hat{Q}(n-1,z^{-1})w_2(n)\end{aligned}, \tag{5.23}$$

where

$$w_1(n) = \frac{S_0(z^{-1})}{H(z^{-1})}w(n), \tag{5.24}$$

$$w_2(n) := \frac{z^{-m}B(z^{-1})}{H(z^{-1})}w(n). \tag{5.25}$$

Plugging (5.15) into (5.23), we can rewrite $\varepsilon^0(n)$ as

$$\varepsilon^0(n) = [Q(z^{-1}) - \hat{Q}(n-1,z^{-1})]w_2(n) + v(n), \tag{5.26}$$

where

$$v(n) = \frac{S'(z^{-1})A_d(z^{-1})}{H(z^{-1})}w(n) = \frac{S'(z^{-1})A_d(z^{-1})A(z^{-1})}{H(z^{-1})}d'(n). \tag{5.27}$$

$v(n)$ asymptotically tends to zero, since $A_d(z^{-1})$ is the internal model of $d'(n)$ and $H(z^{-1})$ is stable.

Suppose that we know the order of the Q polynomial (or Q filter), i.e., $n_{\hat{Q}} = n_Q$. Define the estimated polynomial as $\hat{Q}(n,z^{-1}) = \hat{q}_0(n) + \hat{q}_1(n)z^{-1} + \cdots + \hat{q}_{n_Q}(n)z^{-n_Q}$ and the estimated parameter vector as $\hat{\theta}(n) = [\hat{q}_0(n)\ \hat{q}_1(n)\ \cdots\ \hat{q}_{n_Q}(n)]^T$. The true value of the parameter vector is $\theta = [q_0\ \ q_1\ \cdots\ q_{n_Q}]^T$ according to the definition of $Q(z^{-1})$ in (5.9). Also define an observation vector:

$$\phi^T(n-1) = [w_2(n)\ \ w_2(n-1)\ \cdots\ w_2(n-n_Q)]. \tag{5.28}$$

With these definitions, Eq. (5.26) becomes

$$\varepsilon^0(n) = [\theta - \hat{\theta}(n-1)]^T\phi(n-1) + v(n). \tag{5.29}$$

Equation (5.27) shows that $v(n)$ tends to zero. Thus, $\varepsilon^0(n)$ corresponds an adaptation error.

The adaptation algorithm to estimate the parameters of the Q polynomial can be expressed by the following two equations

$$\hat{\theta}(n) = \hat{\theta}(n-1) + \frac{F(n-1)\phi(n-1)\varepsilon^0(n)}{1+\phi^T(n-1)F(n-1)\phi(n-1)}, \tag{5.30}$$

$$F(n) = F(n-1) - \frac{F(n-1)\phi(n-1)\phi^T(n-1)F(n-1)}{1+\phi^T(n-1)F(n-1)\phi(n-1)}. \tag{5.31}$$

Note that the controller parameter vector $\hat{\theta}(n)$ is directly updated by Eq. (5.30). Therefore, the present adaptive controller is a direct adaptive controller.

At each sample of the operation of direct adaptive control, the signals $w_1(n)$ and $w_2(n)$ are first computed from the signal $w(n)$ according to equations (5.24) and (5.25). Then we compute the estimation error $\varepsilon^0(n)$ and update the estimated vector $\hat{\theta}(n)$ according to (5.30) and (5.31). The output of the Q filter is then computed by $\hat{Q}(n, z^{-1})w(n)$ and is applied to the servo loop as illustrated in Fig. 5.4.

It was proven in [48] that $\hat{\theta}(n)$ converges to θ under the following assumptions:

(i) The plant model $P_m(z^{-1}) = \dfrac{z^{-m}B(z^{-1})}{A(z^{-1})}$ is identical to the actual plant;

(ii) The model of the disturbance has poles on the unit circle (which is the case for the narrow-band disturbance);

(iii) The order n_{A_d} of the internal model of the disturbance is known, which means n_Q is known.

5.2.3 Simulation Results

To see the performance of the direct adaptive control scheme described in the previous subsections, the plant model given by (5.18) is used as the actual plant to satisfy the first assumption for the convergence of $\hat{\theta}(n)$. The baseline controller is described in Section 5.2.1. The disturbance source, including disk flutter, RRO, sensor noise, and torque noise, available in [30] is used as the baseline disturbance. A fictitious sinusoidal signal (shown in Fig. 5.5) at 600Hz with fast time-varying magnitude and phase depicted in Fig. 5.6(a) and (b) respectively is injected to the servo loop at the beginning of the third revolution to represent the narrow-band disturbance. The PES ($-y(n)$ in Fig. 5.4) under the influence of both the baseline disturbance and the narrow-band disturbance are shown in Fig. 5.7.

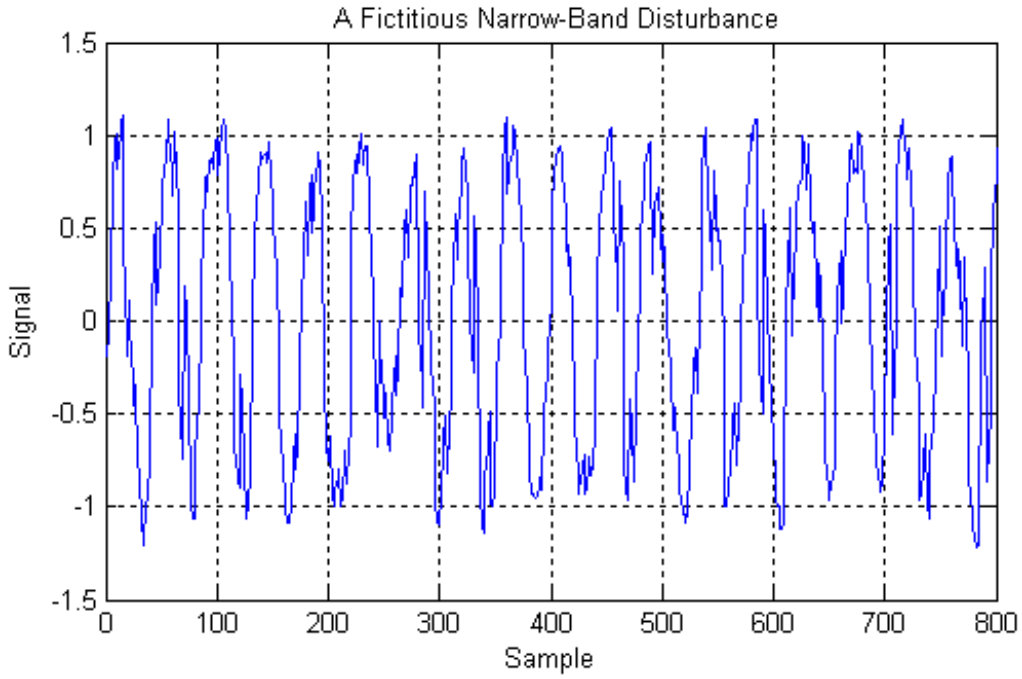

Figure 5.5: Time trace of a fictitious narrow-band disturbance used in the simulation.

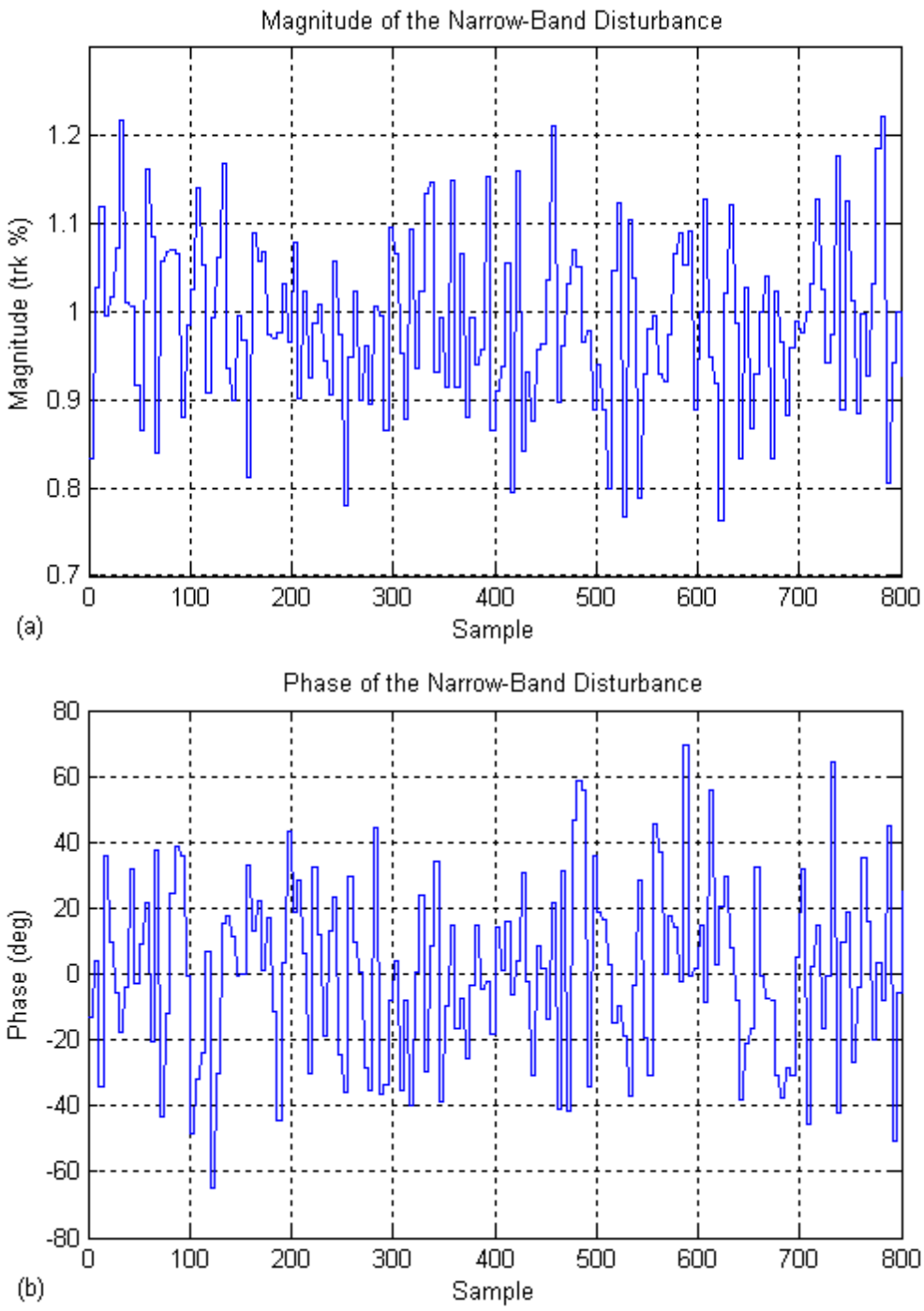

Figure 5.6: Time-varying (a) magnitude and (b) phase of the narrow-band disturbance.

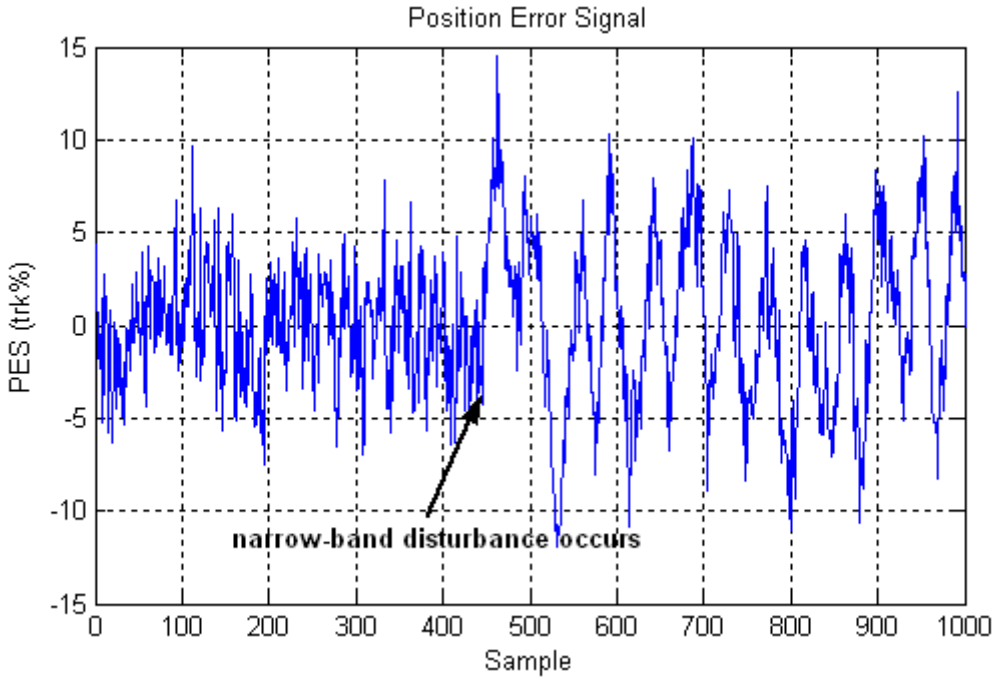

Figure 5.7: Position error signal (PES) under the influence of the disturbances.

Since large narrow-band disturbances do not always occur in HDD systems, the direct adaptive controller is not activated until a large disturbance is detected, which is accomplished by applying the disturbance detection scheme introduced in Section 4.4.3. When a narrow band disturbance in [200Hz, 800Hz] is detected, the adaptation of the parameters of the Q polynomial as described in Section 5.2.2 is initiated and the estimated Q filter is applied to the servo loop shown in Fig. 5.2; otherwise, the baseline controller is used as the servo controller.

In the simulation, the disturbance is detected at the end of the third revolution. Thus, the estimation of the Q polynomial starts at the beginning of the fourth revolution. Since we have one narrow band disturbance, the order of the internal model of this disturbance is two and the order of the Q polynomial is one. So there are two parameters q_0 and q_1 to estimate. Figure 5.8 shows the evolution of the estimates of these two parameters. Note that they converge within 50 samples. The time domain simulation result is shown in Fig. 5.9(a) and (b). The PES is reduced by the proposed compensation scheme (the direct adaptive control scheme) at the steady state as shown in Fig. 5.9(b) compared with the no compensation case (when the baseline controller is used for all the time), but due to the switch of servo controller from the baseline controller to the controller with Q filter, a big oscillation occurs when the direct adaptive controller is activated as shown in Fig. 5.9(a). This oscillation is handled by properly modifying the Q filter as described in the next section.

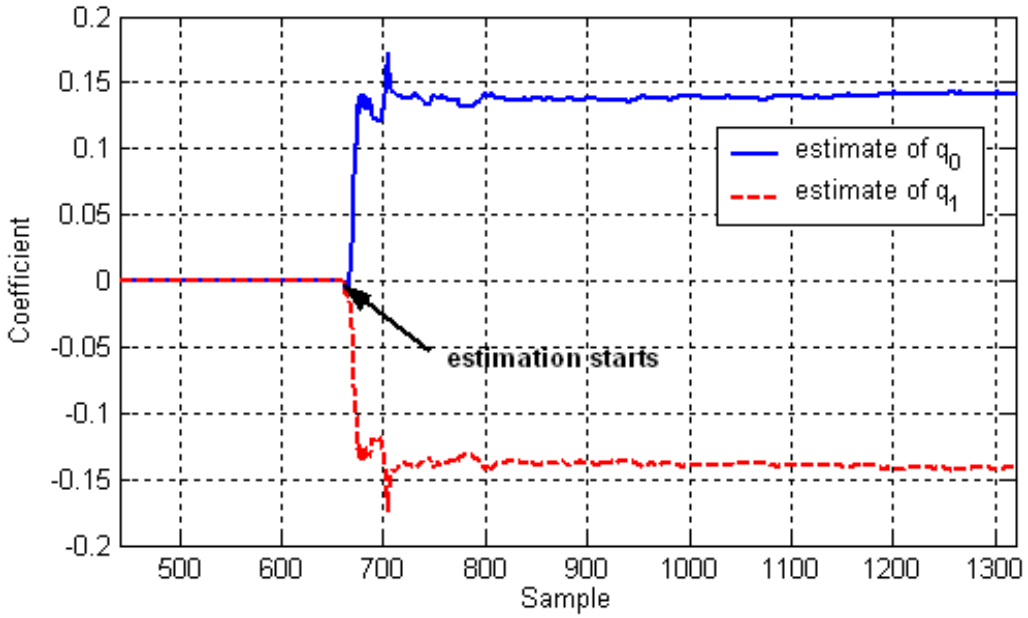

Figure 5.8: Estimation of the parameters of the Q filter

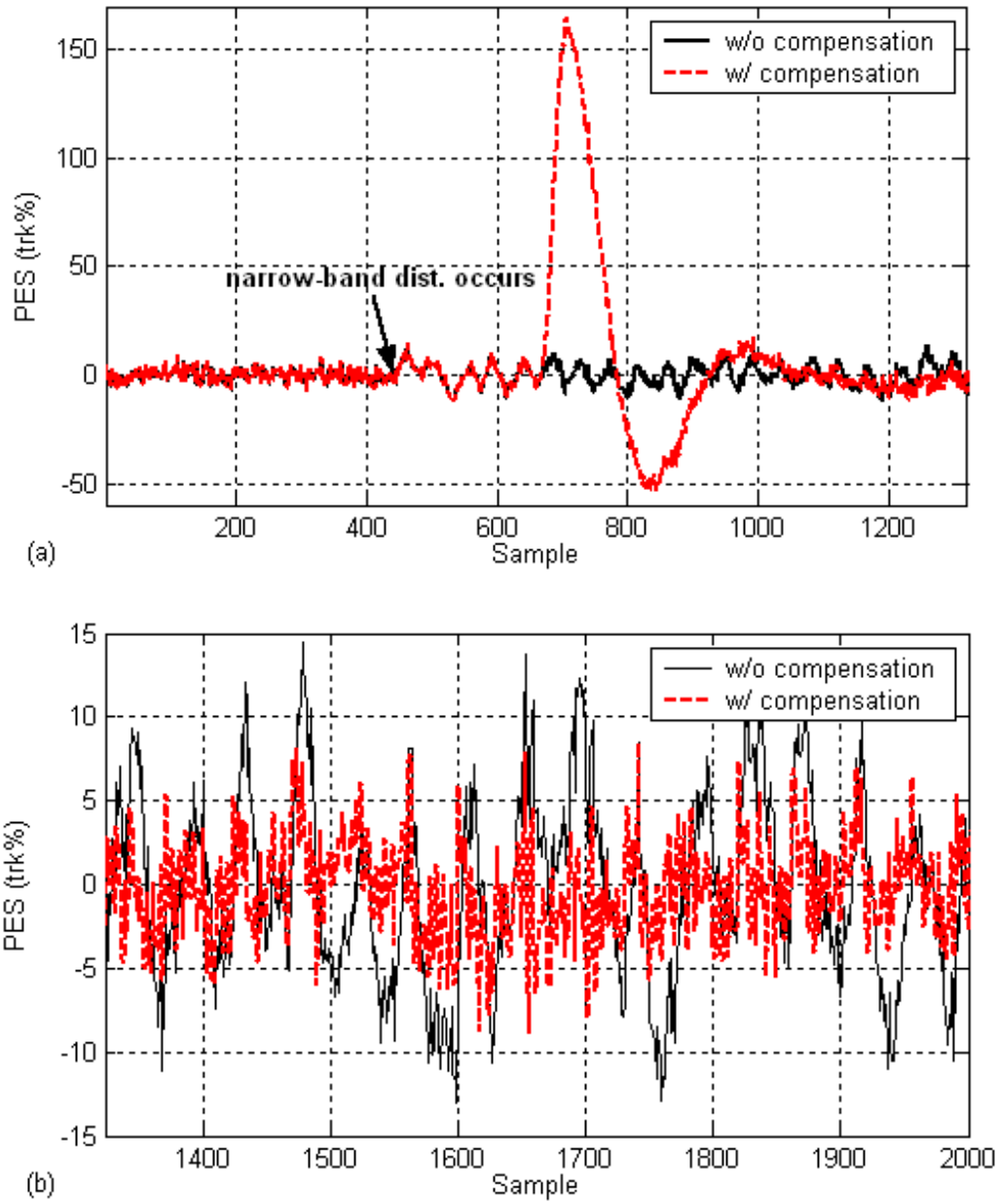

Figure 5.9: Time trace of the PES: (a) in the first 6 revolutions; (b) at the steady state.

5.2.4 Modified Q Filters

The simulation result in Fig. 9(a) shows a large oscillation at low frequency when the adaptive controller is activated. One way of dealing with such big oscillation is using gradually increasing gain as discussed in Section 4.4.5. Instead of applying such ad hoc method, we will introduce a more systematic way that makes use of the structure of the direct adaptive control system.

The baseline PID controller contains the term $1-z^{-1}$ in the denominator $S_0(z^{-1})$, which provides an infinite open-loop gain at 0 Hz to reject low frequency disturbances, but the resulting controller with Q filter no longer contains this term in $S(z^{-1})$. If $Q(z^{-1})$ contains the term $1-z^{-1}$, $S(z^{-1})$ given by Eq. (5.8) will also incorporate this term and it turns out that the transient oscillation may be eliminated. Thus, we let

$$Q(z^{-1}) = H_S(z^{-1})Q'(z^{-1}), \tag{5.32}$$

where $H_S(z^{-1}) := 1-z^{-1}$ is the pre-specified term in $Q(z^{-1})$, and

$$S_0(z^{-1}) = H_S(z^{-1})S_0'(z^{-1}). \tag{5.33}$$

Then the denominator of the resulting controller becomes

$$S(z^{-1}) = H_S(z^{-1})S_0'(z^{-1}) - z^{-m}B(z^{-1})H_S(z^{-1})Q'(z^{-1}), \tag{5.34}$$

and $S(z^{-1})$ contains $H_S(z^{-1})$. $S(z^{-1})$ must also contain $A_d(z^{-1})$ according to the internal model principle. Therefore,

$$S(z^{-1}) = H_S(z^{-1})A_d(z^{-1})S'(z^{-1}). \tag{5.35}$$

Then the equation for computing the Q polynomial becomes

$$S_0'(z^{-1}) = A_d(z^{-1})S'(z^{-1}) + z^{-m}B(z^{-1})Q'(z^{-1}), \tag{5.36}$$

which has the unique solutions for $S'(z^{-1})$ and $Q'(z^{-1})$, if

$$n_{S_0'} \le n_{A_d} + n_B + d - 1, \tag{5.37}$$

where $n_{S_0'}$ is the order of $S_0'(z^{-1})$. This condition is satisfied in the present problem. The solution $Q'(z^{-1})$ has order $n_{Q'} = n_{A_d} - 1$, and the objective of our adaptation algorithm is to

find the coefficients of $Q'(z^{-1})$ ($Q'(z^{-1}) = q'_0 + q'_1 z^{-1} + \cdots + q'_{n_{Q'}} z^{-n_{Q'}}$).

From the procedure similar to the one in Section 5.2.2, the updating equations below for estimating $\theta = [q'_0 \cdots q'_{n_{Q'}}]^T$ follow:

$$\hat{\theta}(n) = \hat{\theta}(n-1) + \frac{F(n-1)\phi(n-1)\varepsilon^0(n)}{1+\phi^T(n-1)F(n-1)\phi(n-1)}, \tag{5.38}$$

$$F(n) = F(n-1) - \frac{F(n-1)\phi(n-1)\phi^T(n-1)F(n-1)}{1+\phi^T(n-1)F(n-1)\phi(n-1)}, \tag{5.39}$$

where

$$\varepsilon^0(n) = w_1(n) - \hat{Q}'(n-1, z^{-1})w_2(n), \tag{5.40}$$

$$\hat{Q}'(n-1, z^{-1}) = \hat{q}'_0(n-1) + \hat{q}'_1(n-1)z^{-1} + \cdots + \hat{q}'_{n_{Q'}}(n-1)z^{-n_{Q'}}, \tag{5.41}$$

$$w_1(n) = \frac{S_0(z^{-1})}{H(z^{-1})}w(n), \tag{5.42}$$

$$w_2(n) = \frac{z^{-m}B(z^{-1})}{H(z^{-1})}H_S(z^{-1})w(n), \tag{5.43}$$

$$\hat{\theta}(n-1) = [\hat{q}'_0(n-1) \ \cdots \ \hat{q}'_{n_{Q'}}(n-1)]^T, \tag{5.44}$$

$$\phi(n-1) = [w_2(n) \ \ w_2(n-1) \ \cdots \ w_2(n-n_{Q'})]^T. \tag{5.45}$$

The signal fed back to the servo loop from the Q filter is $-\hat{Q}'(n, z^{-1})H_S(z^{-1})w(n)$. The direct adaptive control scheme with pre-specified term in Q filter can be implemented as shown Fig. 5.10, after pulling out the $H_S(z^{-1})$ term from the Q filter loop.

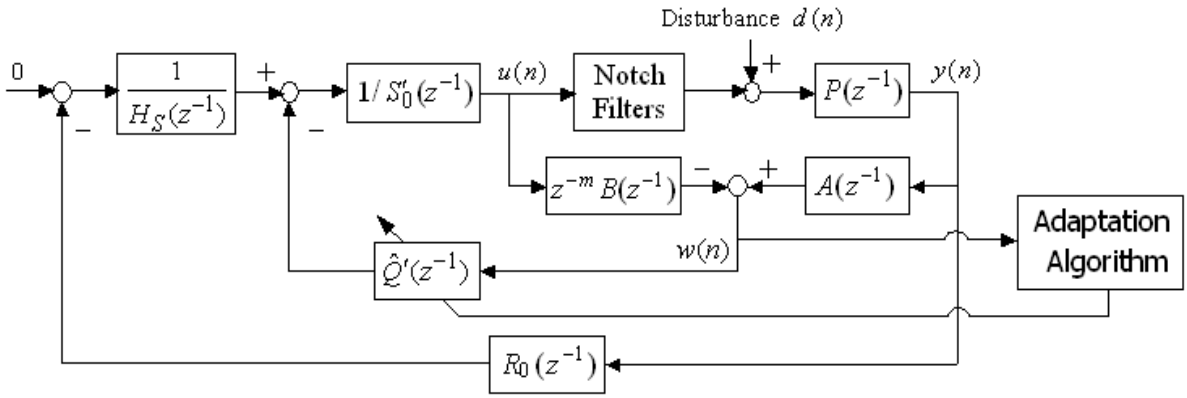

Figure 5.10: Structure of the direct adaptive control with the pre-specified term in Q.

The direct adaptive control scheme with the pre-specified term in the Q filter was simulated under the same condition as in Section 5.2.3. Figure 5.11 shows the time trace of PES with and without compensation. It is clear that the PES is reduced by the proposed control scheme and that the low frequency oscillation does not occur in this case. Figure 5.12 shows the spectrum of PES after the direct adaptive control has been activated and compares it with the one without compensation. As can be seen in the figure, PES is attenuated below 1500Hz, while it is amplified in [3000Hz, 9000Hz] due to the waterbed effect. The attenuation of PES at low frequencies results in a significant reduction of the TMR (15.35% to 8.41% of the track pitch).

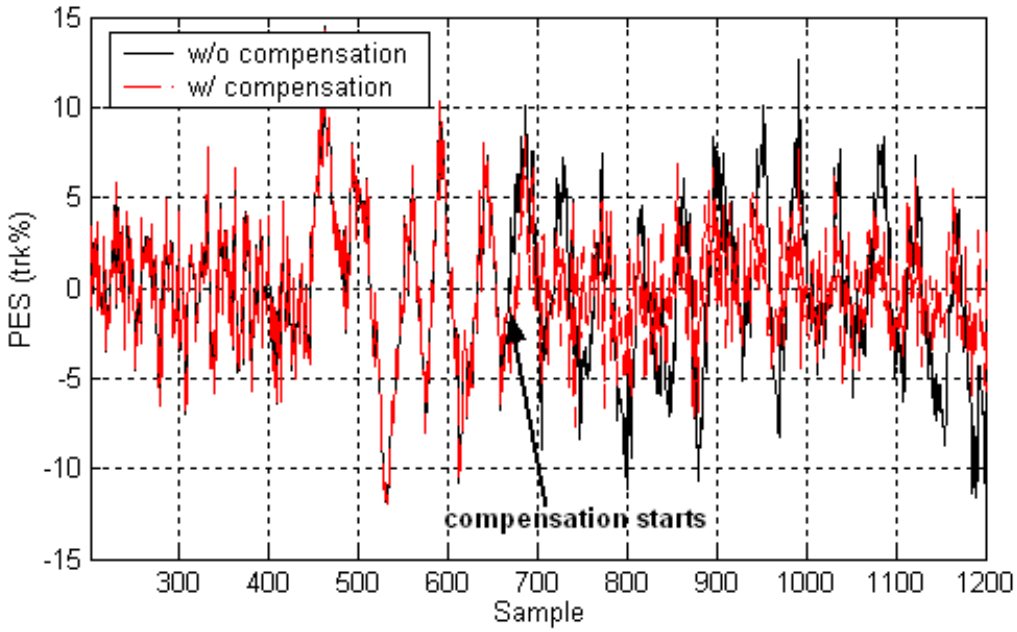

Figure 5.11: Time trace of the PES with and without the direct adaptive control containing the pre-specified term.

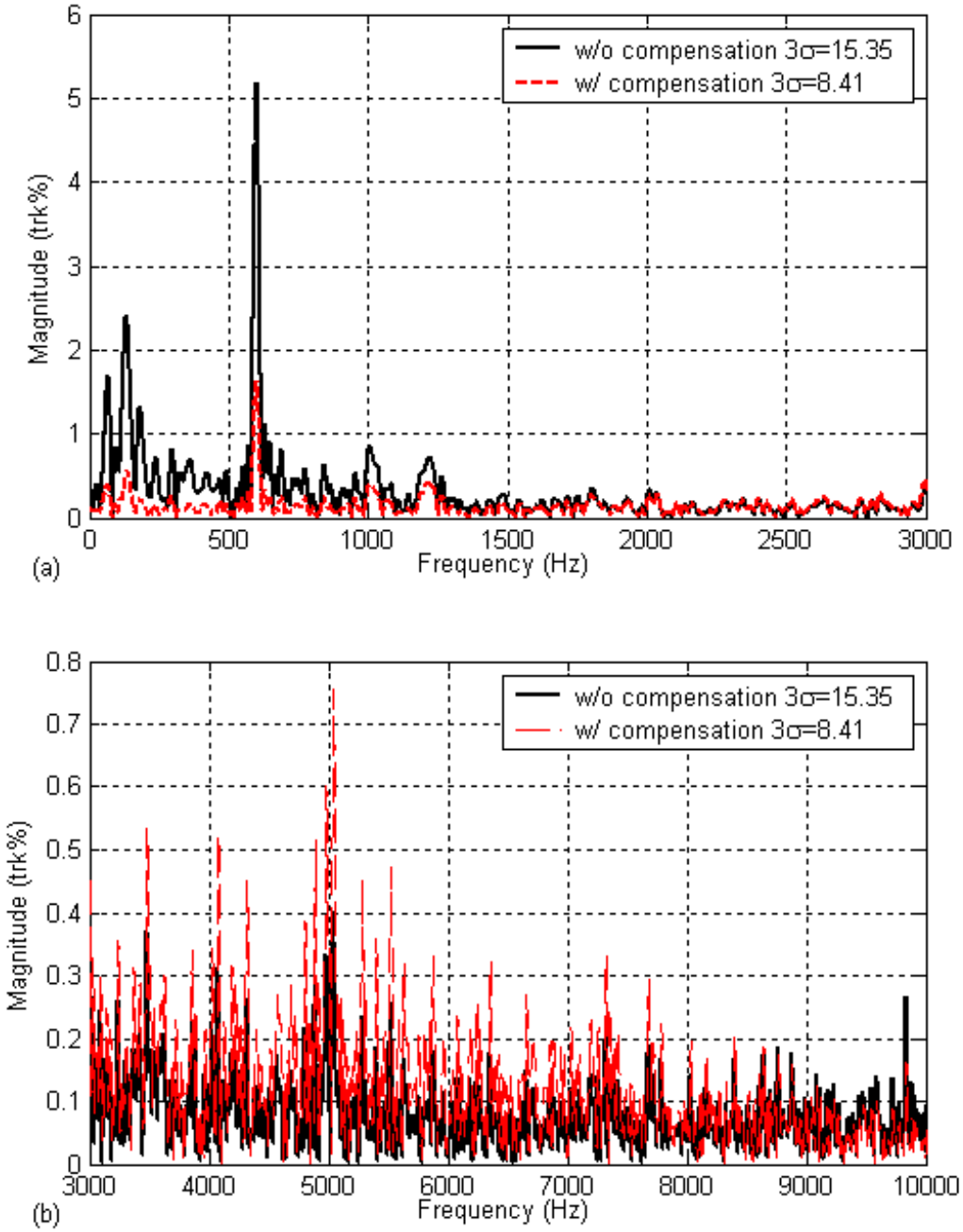

Figure 5.12: Spectrum of the PES with and without compensation (pre-specified term): (a) below 3000Hz; (b) in [3000Hz, 10000Hz].

The adaptive control scheme with or without the pre-specified term in the Q filter does not work if the more realistic full model in Section 5.2.1 is used as the plant. Moreover, it is always desired that the waterbed effect is limited to a certain frequency range when some new dynamics are added to the servo controller. Notice that the frequency response of the plant model is almost the same as the full model in [200Hz, 800Hz] as shown in Fig. 5.3 and it is assumed that the dominant narrow band disturbance only happens in this frequency range. Therefore, a bandpass filter $H_{BPF}(z^{-1})$ with a pass band [200Hz, 800Hz] as depicted in Fig. 5.13 is cascaded to the Q filter, which makes the Q filter become

$$Q(z^{-1}) = H_{BPF}(z^{-1})H_S(z^{-1})Q''(z^{-1}). \tag{5.46}$$

The order of $Q''(z^{-1})$ is $n_{Q''} = n_{A_d} - 1$. $Q(z^{-1}) \approx 0$ at frequencies outside the range [200Hz, 800Hz]. Thus, $R(z^{-1})/S(z^{-1})$ differs from $R_0(z^{-1})/S_0(z^{-1})$ only in [200Hz, 800Hz], which means that the waterbed effect caused by the Q filter containing $H_{BPF}(z^{-1})$ is limited to the pass band of $H_{BPF}(z^{-1})$.

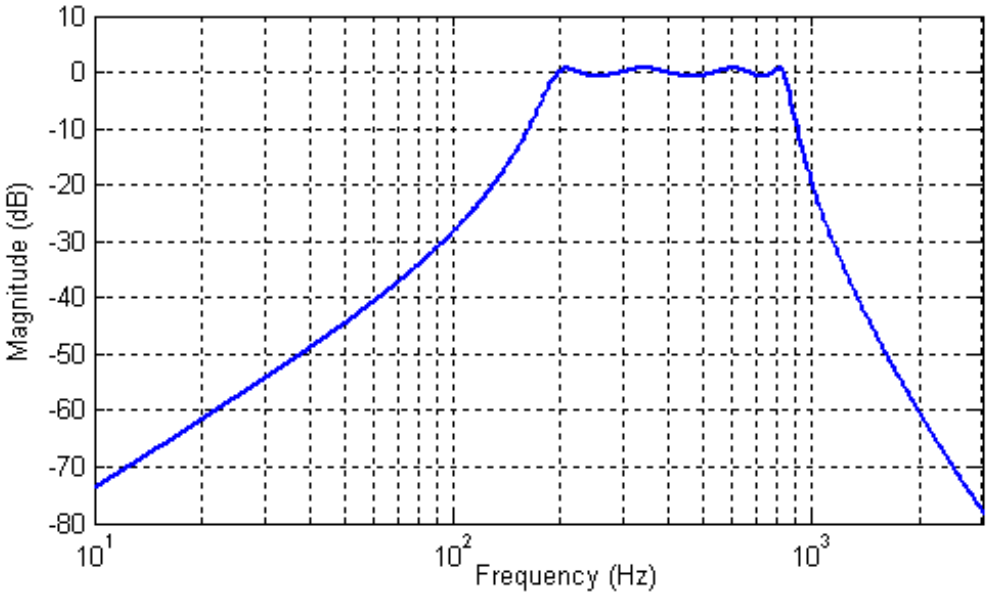

Figure 5.13: Magnitude of the frequency response of the bandpass filter $H_{BPF}(z^{-1})$.

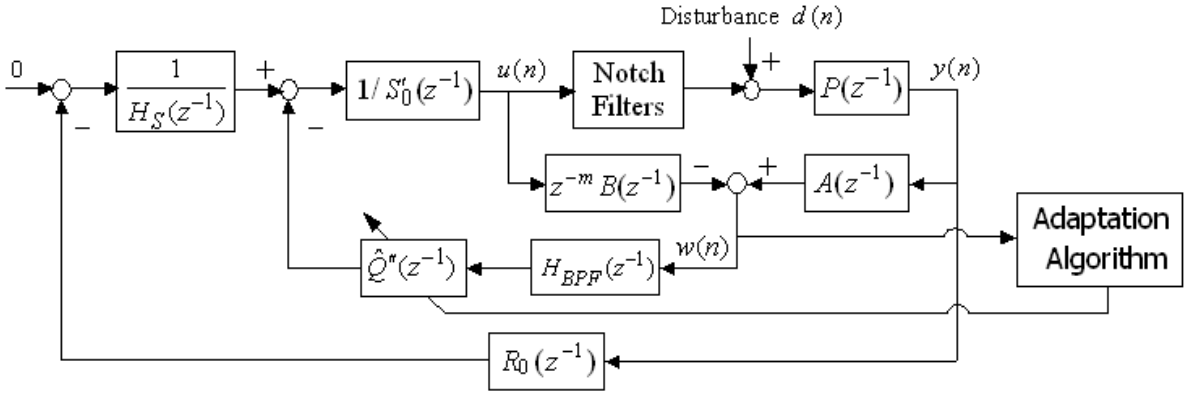

Figure 5.14: Structure of the direct adaptive control with the pre-specified term and the bandpass filter in Q.

The direct adaptive control scheme with this new Q filter is implemented as shown in Fig. 5.14. The same adaptation algorithm described by (5.38)-(5.45) is used for estimating the parameters of $Q''(z^{-1})$ except that $\hat{\theta}(n)$ is a vector of estimated parameters of $Q''(z^{-1})$ and the signal $w_2(n)$ is given by

$$w_2(n) = \frac{z^{-m}B(z^{-1})}{H(z^{-1})} H_S(z^{-1}) H_{BPF}(z^{-1}) w(n). \tag{5.47}$$

The direct adaptive control scheme with the pre-specified term and the bandpass filter in the Q filter works even when the realistic full model is used to represent the HDD dynamics. Figure 5.15 shows the time trace of PES with and without this compensation scheme. Similar to the previous case, no low frequency oscillation occurs when the adaptive controller is activated and the PES is reduced by this compensation scheme. From the spectrum of PES shown in Fig. 5.16, we can see that the narrow-band disturbance at 600Hz is greatly attenuated by the adaptive controller and the waterbed effect happens only in the frequency range [200Hz, 800Hz]. The TMR is reduced from 16.24% of the track pitch to 12.76% by this Youla-Kucera parameterization based direct adaptive controller with modified Q filter.

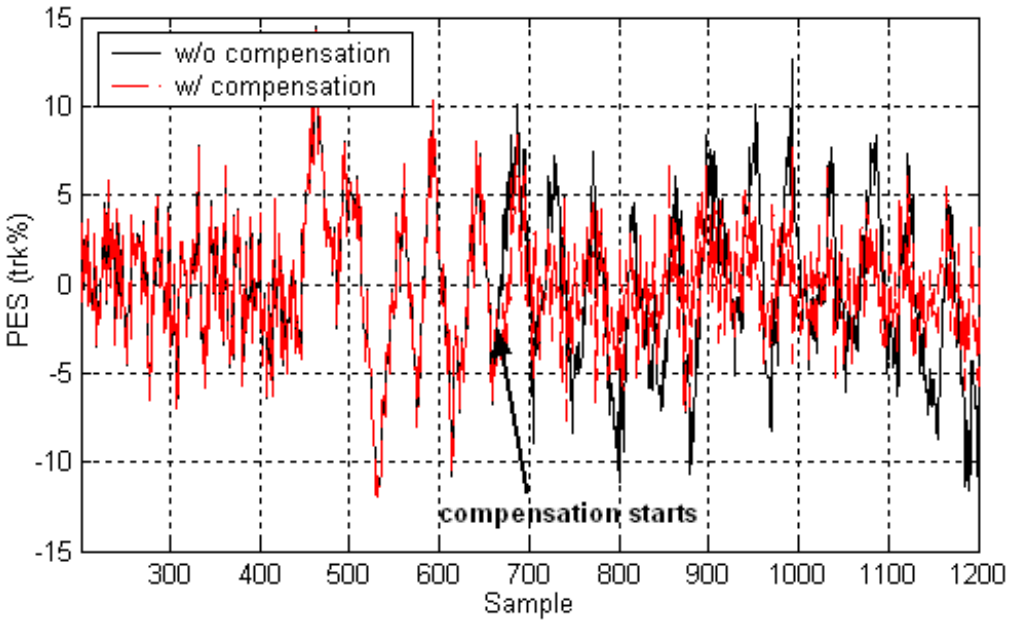

Figure 5.15: Time trace of the PES with and without the direct adaptive control containing the pre-specified term the bandpass filter.

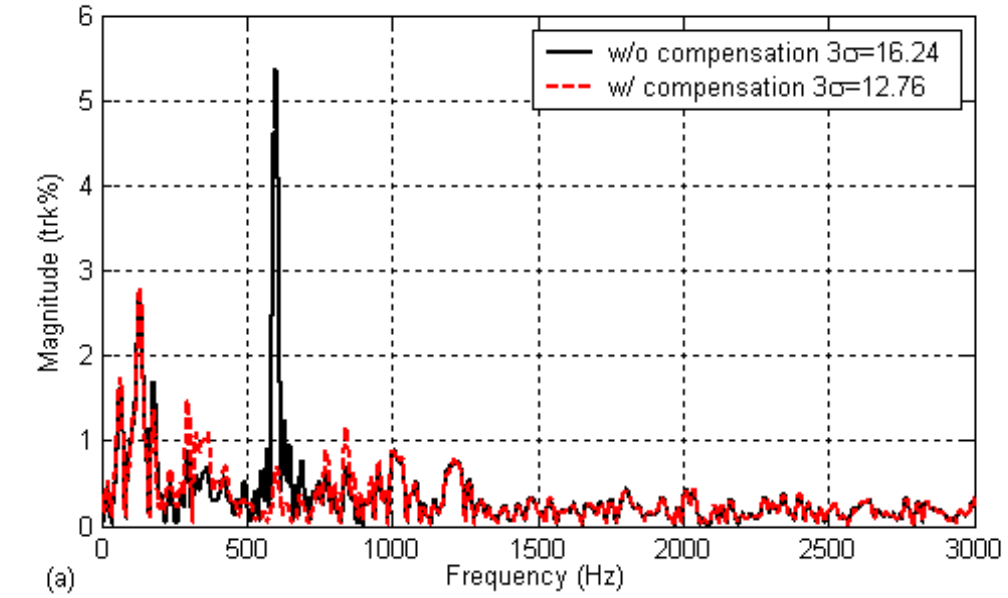

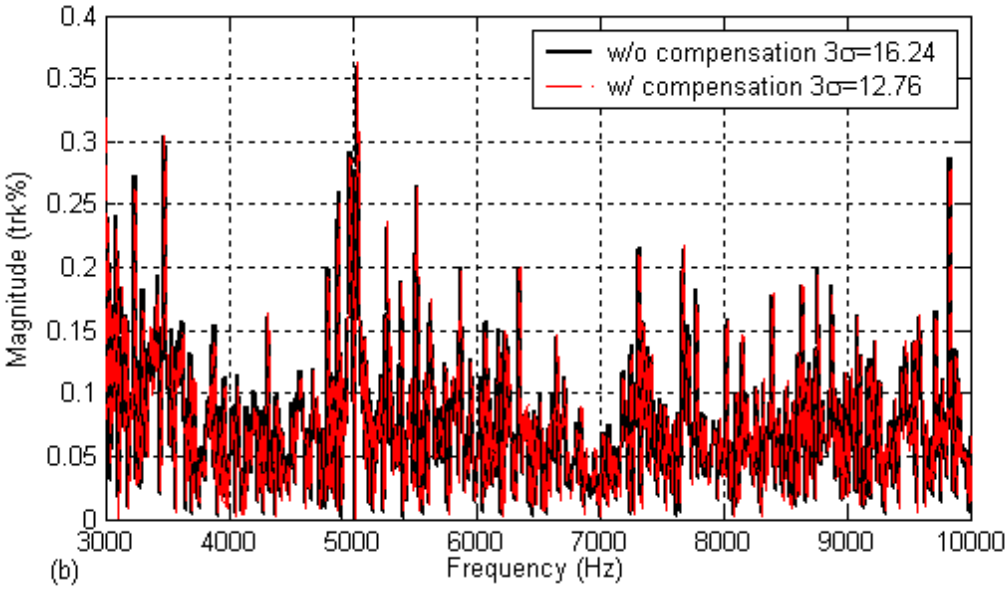

Figure 5.16: Spectrum of the PES with and without compensation (pre-specified term and bandpass filter): (a) below 3000Hz; (b) in [3000Hz, 10000Hz].

5.3 Direct Adaptive Disturbance Observer

It was shown in Section 4.4 that the disturbance observer with a narrow bandpass Q filter is an effective compensator for rejecting narrow band disturbance without causing unwanted amplification in the PES spectrum over a wide range. However, since that method is categorized as an indirect adaptive controller, it has all the drawbacks discussed in Section 5.1, including the dependence on the precise frequency estimation and not taking TMR as an adaptation criterion.

In this section, a direct adaptive narrow band disturbance observer will be introduced to reject the dominant narrow band component in HDD disturbance that resides in [200Hz, 800Hz].

5.3.1 Overview

Figure 5.17 shows the structure of the proposed direct adaptive narrow band disturbance observer. The structure resembles the one depicted in Fig. 4.12 with one main difference that the parameter of the Q filter is directly updated by the adaptation algorithm without estimating the disturbance model. Besides that, the same HDD plant, $P(z^{-1})$, which as before includes the power amplifier, the voice coil motor (VCM), and the head stack assembly (HSA) and the same PID controller with notch filters connected in series is used as the baseline controller $C(z^{-1})$. The reference signal $r(k)$ is zero, since the HDD track following control is considered. The narrow band disturbance together with other disturbances such as RRO, sensor noise, windage, etc. is represented by the signal $d(k)$. The discrete-time transfer function of the plant model is given by $z^{-m}P_n(z^{-1})$, which is a simplified approximation of the plant $P(z^{-1})$ and as seen in Section 1.1 and in Fig. 5.18, the frequency response of $z^{-m}P_n(z^{-1})$ matches that of $P(z^{-1})$ well in [200Hz, 1100Hz].

The inner loop in the block diagram shown in Fig. 5.17 is a disturbance observer with an adaptive Q filter. The signal $x(k)$ is computed by comparing the output of the plant inverse with the control signal delayed by m samples (m=1 for the HDD system considered here). For the implementation purpose, the full order plant cannot be used in the DOB loop. Instead, the 2nd order plant model, $z^{-1}P_n(z^{-1})$, is used. The signal $x(k)$ is applied to an adaptation algorithm to adjust a parameter of the Q filter. The adaptation algorithm is designed based on the minimization of the TMR to achieve asymptotic rejection of the narrow band disturbance.

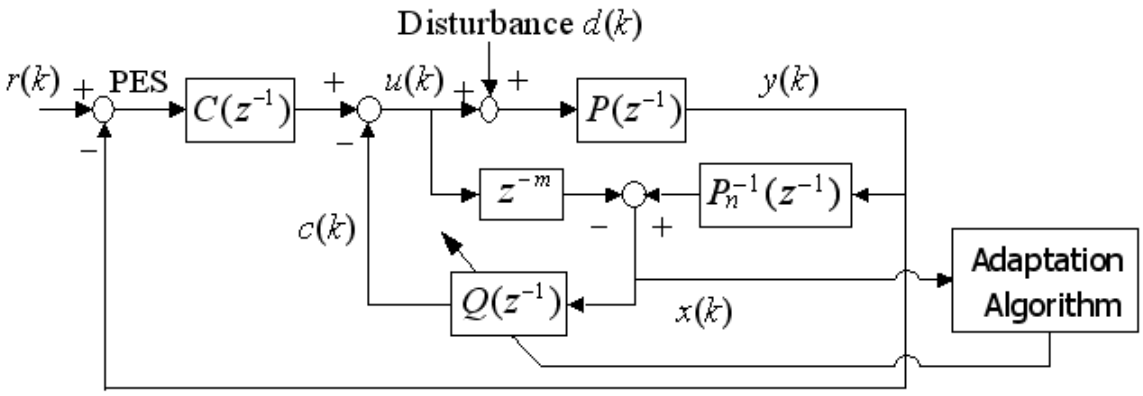

Figure 5.17: Structure of the proposed direct adaptive disturbance observer scheme.

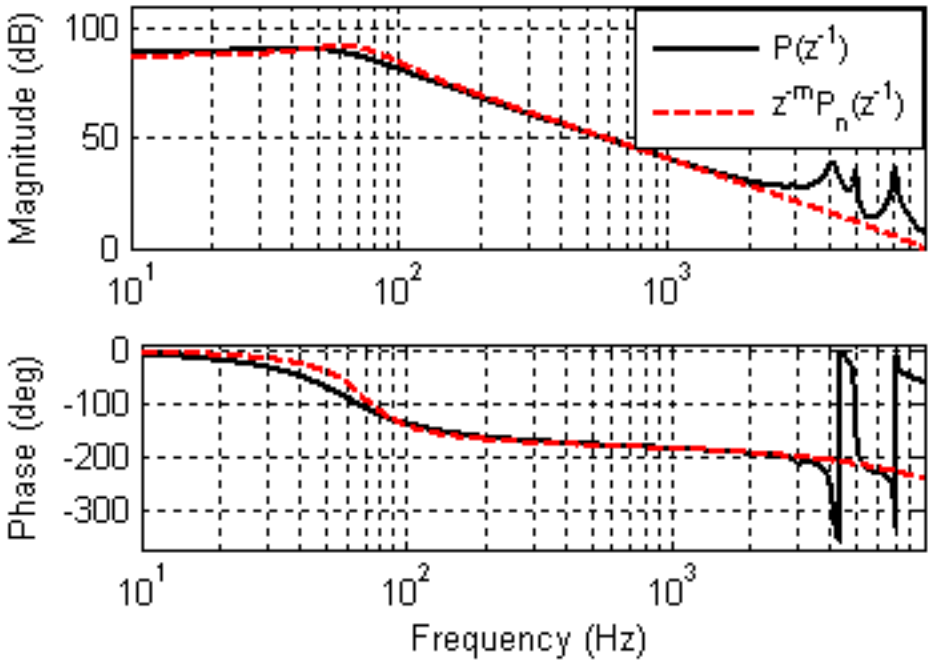

Figure 5.18: Frequency response of the full order plant and the plant model.

The Q filter for the indirect adaptive narrow disturbance observer introduced in Section 4.4.1 is a second order discrete-time filter with transfer function given by

$$Q(z^{-1}) = (1-\eta)\frac{1-\eta z^{-2}}{1-2\eta\cos(\hat{\omega}T_s)z^{-1}+\eta^2 z^{-2}}. \tag{5.48}$$

where $\hat{\omega}$ is the estimated disturbance frequency obtained by a frequency identifier and η is a shaping coefficient, which is close to one and less than one.

The pass band of the Q filter is made narrow (see Fig. 4.13) to limit the waterbed effect. The resulting error rejection function (the transfer function from the disturbance to the PES) with this compensator incorporates a deep notch at the estimated disturbance frequency compared to the error rejection function without this compensator (see Fig. 4.14). The simulation results in Section 4.4.4 demonstrated more than 40% TMR improvement with the DOB based compensator for the track following operation, when a narrow-band disturbance at 700 Hz was present. This indirect adaptive approach has several drawbacks. First of all, the performance highly depends on the frequency identification result. Since a very narrow bandpass Q filter is used, if the estimated frequency differs from the disturbance frequency by more than 30Hz, the compensator cannot achieve enough attenuation of the disturbance. Moreover, the indirect adaptive algorithm in Section 4.4 is not optimal in the sense of minimizing the TMR caused by the narrow band disturbance. In the next section, a direct adaptation algorithm to estimate the parameter $\theta = \cos(\hat{\omega})$ based on minimizing the TMR will be introduced.

5.3.2 Adaptation Algorithm

The purpose of the proposed adaptive compensator is to cancel the influence of a narrow band disturbance on the TMR. The narrow band disturbance is assumed to reside in the frequency range from 200 Hz to 800 Hz, which is the range of large disk modes that cannot be effectively rejected by the baseline servo controller in the HDD system considered here. As shown in Fig. 5.17, an adaptive Q filter is devised as an add-on compensator to handle the disturbance. The transfer function of the Q filter introduced in the previous section is rewritten as

$$Q(z^{-1}) = (1-\eta)\frac{1-\eta\, z^{-2}}{1-2\eta\theta z^{-1}+\eta^2 z^{-2}}, \tag{5.49}$$

where the shaping coefficient η is chosen to be 0.97 and $\theta = \cos(2\pi T_s f_c)$ with f_c in the unit of Hz is the frequency coefficient. In order to achieve the best result using the compensator, instead of choosing the parameter θ of the Q filter from a frequency estimation, θ is directly adapted based on the minimization of the TMR caused by the narrow band disturbance.

The TMR can be expressed as

$$\text{TMR} = 3\sqrt{\frac{1}{N}\sum_{k=1}^{N} PES(k)^2} = \frac{3}{\sqrt{N}}\left\|PES(k)\right\|, \tag{5.50}$$

where $\|\cdot\|$ is the extended l_2-norm of a discrete-time signal.

When there exists a disturbance signal $d(k)$, the PES in Fig. 5.17 with a fixed Q filter, $Q(z^{-1})$, is given by

$$PES(k) = -\frac{P(z^{-1})[1-z^{-1}Q(z^{-1})]}{1+P(z^{-1})C(z^{-1})+Q(z^{-1})[P_n^{-1}(z^{-1})P(z^{-1})-z^{-1}]}d(k). \tag{5.51}$$

Here z^{-1} is considered as the one-step delay operator. As shown in Fig. 5.19, the Q filter here is still a narrow bandpass filter. If the pass band of the Q filter is limited to be contained in [200 Hz, 800 Hz], where the plant model matches the plant very well as can be seen from the frequency response in Fig. 5.18, then approximately,

$$Q(z^{-1})[P_n^{-1}(z^{-1})P(z^{-1})-z^{-1}] = 0, \tag{5.52}$$

which yields

$$PES(k) = -\frac{P(z^{-1})}{1 + P(z^{-1})C(z^{-1})}[1 - z^{-1}Q(z^{-1})]d(k). \tag{5.53}$$

Since the baseline controller $C(z^{-1})$ asymptotically stabilizes the closed loop system for plant $P(z^{-1})$ and the magnitude of $[-P(z^{-1})/(1+P(z^{-1})C(z^{-1}))]|_{z=\exp(j\omega)}$ is finite for any ω and does not depend on $Q(z^{-1})$, minimizing the TMR is equivalent to minimizing the l_2-norm of $[1 - z^{-1}Q(z^{-1})]d(k)$. Thus, the adaptation of the parameter of the Q filter can be based on the minimization of $\left\|(1 - z^{-1}Q(z^{-1}))d(k)\right\|$.

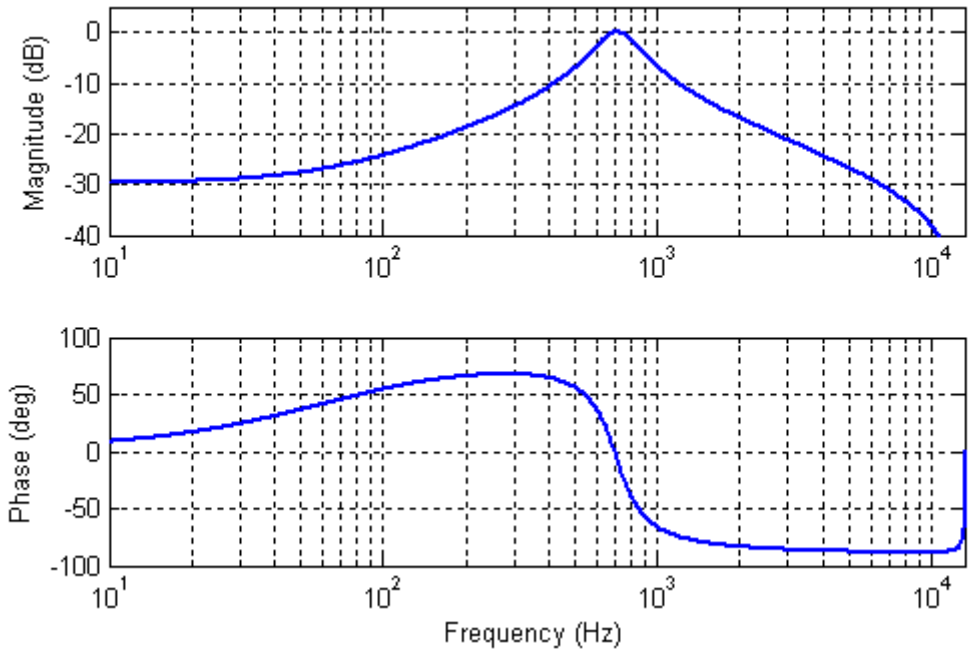

Figure 5.19: Frequency response of a narrow bandpass Q filter with $\eta = 0.97$ and $f_c = 700$ Hz.

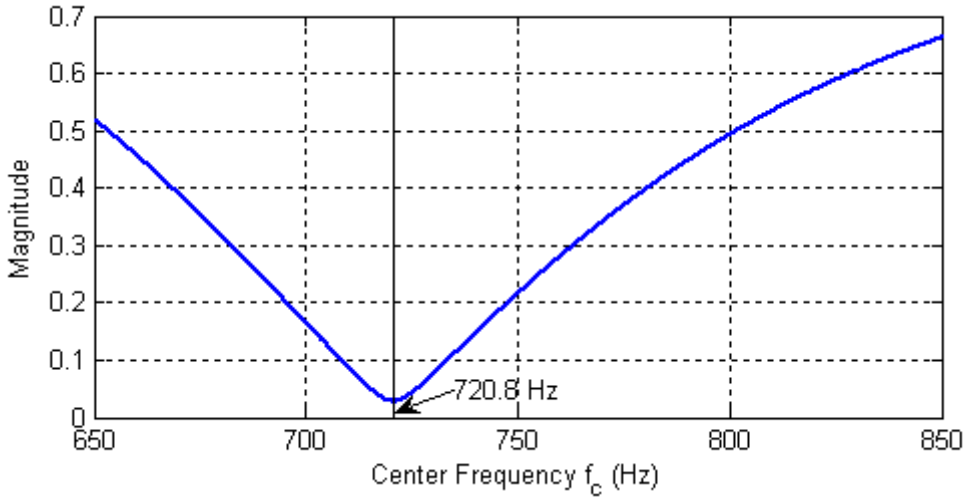

Figure 5.20: $\left|1-e^{-j2\pi T_s f_d}Q(e^{-j2\pi T_s f_d})\right|$ for f_d =700 Hz.

When $d(k)$ is a narrow band signal, minimizing $\left\|(1-z^{-1}Q(z^{-1}))d(k)\right\|$ is equivalent to minimizing $\left|1-e^{-j2\pi T_s f_d}Q(e^{-j2\pi T_s f_d})\right|$ (the magnitude of $1-z^{-1}Q(z^{-1})$ at the disturbance frequency), where T_s is the sampling time and f_d is the frequency of the disturbance in the unit of Hz. Figure 5.20 shows the value of $\left|1-e^{-j2\pi T_s f_d}Q(e^{-j2\pi T_s f_d})\right|$ for $f_d = 700Hz$ and f_c ($\theta = \cos(2\pi T_s f_c)$) varies from 650 Hz to 800 Hz. It can is implied in the plot that the optimal f_c is 720.8 Hz.

Since the frequency of the narrow band disturbance is unknown, the parameter $\theta = \cos(2\pi T_s f_c)$ of the Q filter is adapted to get the best rejection of the disturbance based on the minimization of $\left\|(1-z^{-1}Q(z^{-1}))d(k)\right\|$. In order to derive the adaptation algorithm for estimating θ, the first thing is to obtain a good estimate of the disturbance $d(k)$ that cannot be directly measured. The same idea for detecting the disturbance described in Section 4.4.3 can be applied here to provide an estimate of the narrow band disturbance.

Notice that the information of the disturbance is contained in the signal $x(k)$ in Fig. 5.17,

$$x(k) = [P_n^{-1}(z^{-1})P(z^{-1}) - z^{-1}]u(k) + P_n^{-1}(z^{-1})P(z^{-1})d(k). \tag{5.54}$$

It is assumed that the narrow band disturbance resides only in the frequency range [200 Hz, 800 Hz] and is the only possible dominant frequency component in this frequency range. Then $x(k)$ can be filtered by a bandpass filter $F(z^{-1})$ with a pass band that contains the frequency range

[200 Hz, 800 Hz] to isolate the narrow band disturbance from other frequency components. For this purpose, the bandpass filter $H_{BPF}(z^{-1})$ introduced in Section 5.2.4 is used again as $F(z^{-1})$, the frequency response of which is shown in Fig. 5.21.

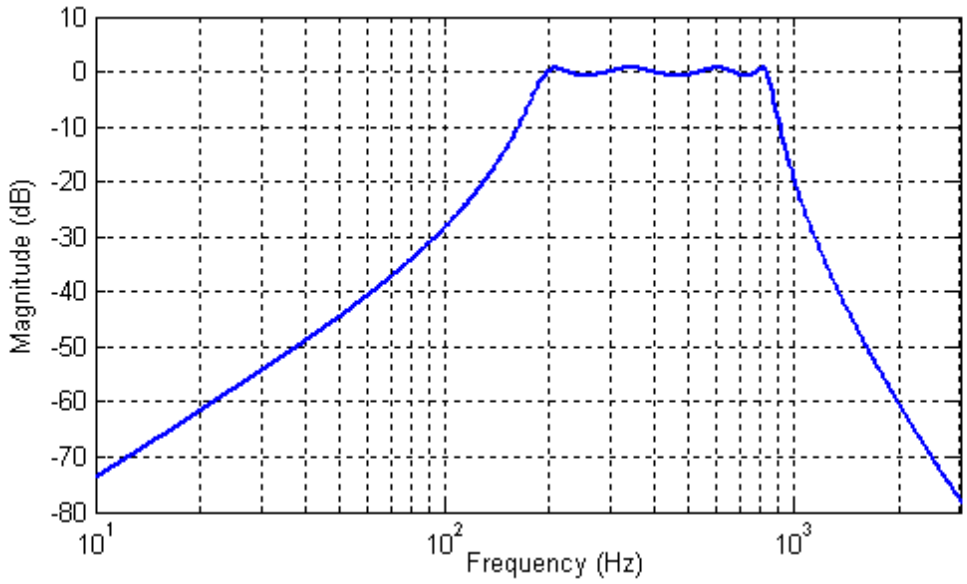

Figure 5.21: Magnitude of the frequency response of the bandpass filter $F(z^{-1})$.

The output of $F(z^{-1})$, denoted by $w(k)$, can be computed and is a good estimate of the narrow band disturbance. To see this point, $w(k)$ is put into the expression:

$$\begin{aligned} w(k) = F(z^{-1})[P_n^{-1}(z^{-1})P(z^{-1}) - z^{-1}]u(k) \\ + F(z^{-1})P_n^{-1}(z^{-1})P(z^{-1})d(k). \end{aligned} \tag{5.55}$$

From Fig. 5.18, it is clear that $z^{-1}P_n(z^{-1})$ is approximately equal to $P(z^{-1})$ in the pass band of $F(z^{-1})$. So it follows that

$$F(z^{-1})[P_n^{-1}(z^{-1})P(z^{-1}) - z^{-1}] = 0. \tag{5.56}$$

Then $w(k)$ can be expressed as

$$w(k) = z^{-1}F(z^{-1})d(k). \tag{5.57}$$

Moreover, from the nature of a bandpass filter,

$$\left|F(e^{-j2\pi T_s f_d})\right| \approx 1, \tag{5.58}$$

for $f_d \in$ [200 Hz, 800 Hz], which means that $w(k)$ and $d(k)$ have the similar amplitude, if $d(k)$ is a narrow band signal in [200 Hz, 800 Hz]. So the l_2-norm of $[1-z^{-1}Q(z^{-1})]d(k)$ is approximately equal to the l_2-norm of $[1-z^{-1}Q(z^{-1})]w(k)$. Thus, θ can be adapted based on the minimization of $\left\|(1-z^{-1}Q(z^{-1}))w(k)\right\|$.

Denote $e(k) = [1-z^{-1}Q(z^{-1},\theta^{opt})]w(k)$ with

$$Q(z^{-1},\theta^{opt}) = (1-\eta)\frac{1-\eta\, z^{-2}}{1-2\eta\theta^{opt}z^{-1}+\eta^2 z^{-2}}, \tag{5.59}$$

where θ^{opt} is the optimal value of the parameter θ in the sense of minimizing $\left|1-z^{-1}Q(z^{-1},\theta)\right|$ for $z = e^{j2\pi T_s f_d}$ and f_d is the frequency of the narrow band disturbance. The difference equation for $e(k)$ is given by

$$\begin{aligned} e(k+1) = {} & w(k+1) - 2\eta[w(k)-e(k)]\theta^{opt} + \eta^2 w(k-1) \\ & -(1-\eta)w(k) + \eta(1-\eta)w(k-2) - \eta^2 e(k-1). \end{aligned} \tag{5.60}$$

Define $Q(z^{-1},\hat{\theta}(k))$ as the transfer function of the Q filter with the parameter estimate $\hat{\theta}(k)$ at time k. Then the *a posteriori* prediction error $\varepsilon(k+1)$ is defined as

$$\varepsilon(k+1) = [1-z^{-1}Q(z^{-1},\hat{\theta}(k+1))]w(k+1), \tag{5.61}$$

which can also be written as a difference equation:

$$\begin{aligned} \varepsilon(k+1) = {} & w(k+1) - 2\eta[w(k)-\varepsilon(k)]\hat{\theta}(k+1) + \eta^2 w(k-1) \\ & -(1-\eta)w(k) + \eta(1-\eta)w(k-2) - \eta^2 \varepsilon(k-1). \end{aligned} \tag{5.62}$$

Similarly, the *a priori* prediction error $\varepsilon^0(k+1)$ is defined by

$$\begin{aligned} \varepsilon^0(k+1) = {} & w(k+1) - 2\eta[w(k)-\varepsilon(k)]\hat{\theta}(k) + \eta^2 w(k-1) \\ & -(1-\eta)w(k) + \eta(1-\eta)w(k-2) - \eta^2 \varepsilon(k-1), \end{aligned} \tag{5.63}$$

which only depends on the signals that can be measured or computed at time k+1.

The adaptation algorithm is designed to recursively update $\hat{\theta}(k+1)$ to minimize the cost function

$$J(k,\hat{\theta}(k+1)) = \sum_{i=0}^{k}[\varepsilon(i+1)]^2 . \tag{5.64}$$

The parameter adaptation algorithm (PAA) used here is the recursive least squares (RLS) method with a fixed compensator ([47], [49], [55], [56]). The parameter estimate is updated using the following equations:

$$\hat{\theta}(k+1) = \hat{\theta}(k) + \frac{F(k)\phi(k)\nu^0(k+1)}{1+F(k)\phi(k)^2} \tag{5.65}$$

$$\nu^0(k+1) = \varepsilon^0(k+1) - \eta\varepsilon(k) \tag{5.66}$$

$$F(k+1) = F(k) - \frac{F(k)^2\phi(k)^2}{1+F(k)\phi(k)^2} \tag{5.67}$$

$$\phi(k) = 2\eta[w(k) - \varepsilon(k)] . \tag{5.68}$$

$\varepsilon^0(k+1)$ and $\varepsilon(k+1)$ are given by equations (5.62) and (5.63), respectively. $\nu^0(k+1)$ is called the *a priori* adaptation error. We can also define the *a posteriori* adaptation error, $\nu(k+1)$, for the stability analysis by

$$\nu(k+1) = \varepsilon(k+1) - \eta\varepsilon(k) , \tag{5.69}$$

which means that the prediction error $\varepsilon(k+1)$ is filtered by a fixed compensator $D(z^{-1}) = 1-\eta z^{-1}$ to generate the adaptation error $\nu(k+1)$:

$$\nu(k+1) = D(z^{-1})\varepsilon(k+1) . \tag{5.70}$$

On the other hand, from the definitions and the relationship between $\varepsilon^0(k+1)$ and $\varepsilon(k+1)$, it follows that

$$\nu(k+1) = \frac{\nu^0(k+1)}{1+F(k)\phi(k)^2} . \tag{5.71}$$

With the estimated parameter, the compensation signal $c(k)$ in Fig. 5.17 is computed by $c(k) = Q(z^{-1},\hat{\theta}(k))x(k)$, i.e.

$$c(k) = (1-\eta)x(k) - \eta(1-\eta)x(k-2) + 2\eta\hat{\theta}(k)c(k-1) - \eta^2 c(k-2). \tag{5.72}$$

This signal is removed from the output of the baseline controller to generate the control signal for the VCM actuator.

5.3.3 Stability Analysis

The stability of the PAA can be proved by the equivalent feedback structure and the passivity concepts ([7], [45], [71], [99]). First of all, we need to find the equivalent feedback system for our PAA. From equations (5.60) and (5.62), the following relationship between $\varepsilon(k)$ and $e(k)$ holds:

$$\varepsilon(k+1) = e(k+1) - \frac{1}{H(z^{-1})}\phi(k)\tilde{\theta}(k+1), \tag{5.73}$$

where $\tilde{\theta}(k+1) = \hat{\theta}(k+1) - \theta^{opt}$ is the parameter estimation error and

$$H(z^{-1}) = 1 - 2\eta\theta^{opt}z^{-1} + \eta^2 z^{-2} \tag{5.74}$$

with z^{-1} considered as the one-step delay operator. Then Eq. (5.70) becomes

$$v(k+1) = D(z^{-1})e(k+1) - \frac{D(z^{-1})}{H(z^{-1})}\phi(k)\tilde{\theta}(k+1). \tag{5.75}$$

From the definition of $\tilde{\theta}(k+1)$ and equations (5.65) and (5.71), we obtain

$$\phi(k)\tilde{\theta}(k+1) = \phi(k)\tilde{\theta}(k) + F(k)\phi(k)^2 v(k+1). \tag{5.76}$$

Then the PAA can be described by an equivalent feedback system shown in Fig. 5.22. In the feedforward path, we have a linear time invariant system defined by a transfer function

$$G_{ff}(z^{-1}) = \frac{D(z^{-1})}{H(z^{-1})} = \frac{1-\eta z^{-1}}{1-2\eta\theta^{opt}z^{-1}+\eta^2 z^{-2}}. \tag{5.77}$$

The feedback block is a nonlinear time varying system described by Eq. (5.76). $e'(k) = D(z^{-1})e(k+1)$ is considered as a disturbance signal for the PAA. After applying "add and subtract operations", we obtain an equivalent block diagram representation as shown in Fig. 5.23.

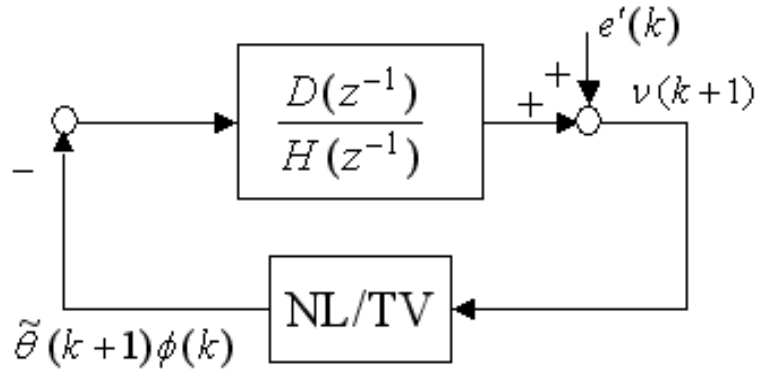

Figure 5.22: The equivalent feedback representation of the PAA for adapting narrow band disturbance observer.

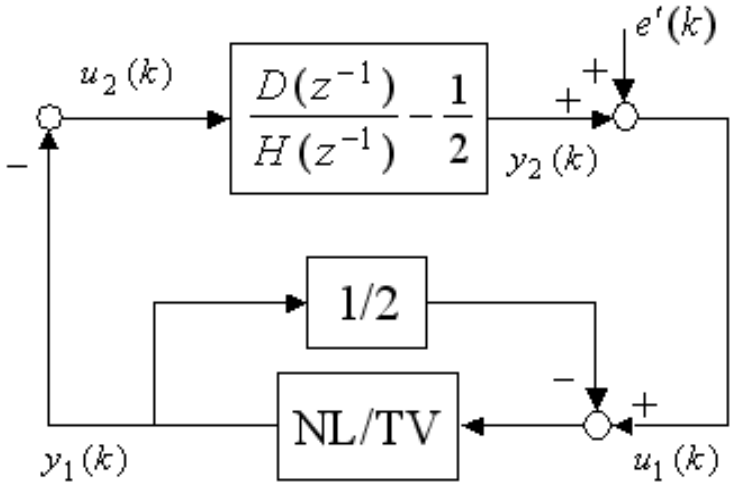

Figure 5.23: Another equivalent feedback representation of the PAA for stability analysis.

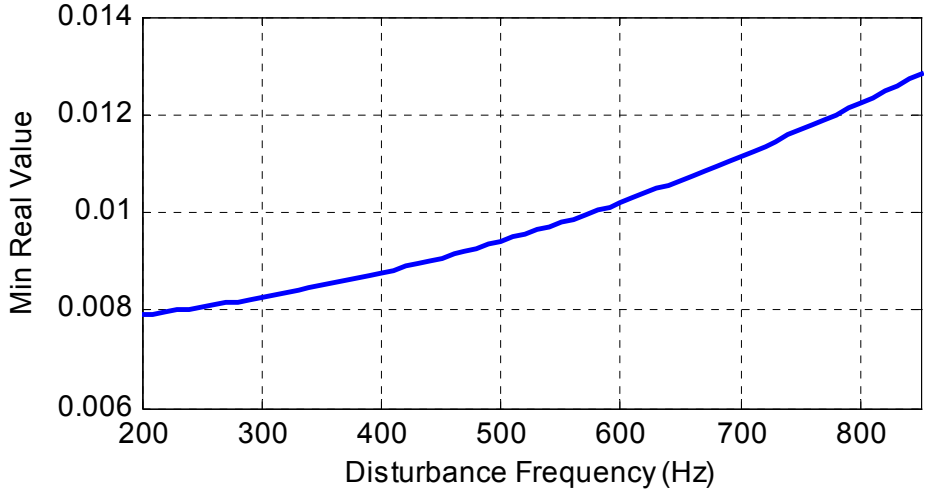

Figure 5.24: Minimum value of the real part of the feedforward block for different θ^{opt}.

It was proved in [49] that the nonlinear block in Fig. 5.23 with input $u_1(k)$ and output $y_1(k)$ is passive and satisfies the Popov's inequality:

$$\sum_{k=0}^{N}[u_1(k)y_1(k)] \geq -\gamma_1^2, \tag{5.78}$$

for some finite γ_1^2 and all $N > 0$. The feedforward linear time invariant block $\frac{D(z^{-1})}{H(z^{-1})} - \frac{1}{2}$ is asymptotically stable. Moreover, as shown in Fig. 5.24, the minimum value of the real part of $\frac{D(e^{-j\omega})}{H(e^{-j\omega})} - \frac{1}{2}$, $0 \leq \omega \leq \pi$, is positive for all possible θ^{opt}'s, when the disturbance frequency lies in [200 Hz, 800 Hz] and $\eta = 0.97$. So the feedforward block is strictly positive real and input strictly passive, i.e.

$$\sum_{k=0}^{N}[u_2(k)y_2(k)] \geq -\gamma_2^2 + \kappa\|u_2\|^2, \tag{5.79}$$

for some finite γ_2^2, positive κ and all $N > 0$. The squared extended l_2-norm of u_2 is defined by

$$\|u_2\|^2 = \sum_{k=0}^{N} [u_2(k)]^2 . \tag{5.80}$$

Notice that $y_2(k) = u_1(k) - e'(k)$ and $u_2(k) = -y_1(k)$. Then from inequality (5.79), we get the following inequality:

$$\sum_{k=0}^{N} [e'(k) y_1(k)] - \sum_{k=0}^{N} [u_1(k) y_1(k)] \geq -\gamma_2^2 + \kappa \|u_2\|^2 , \tag{5.81}$$

which implies that

$$\begin{aligned} -\sum_{k=0}^{N} [e'(k) u_2(k)] &= \sum_{k=0}^{N} [e'(k) y_1(k)] \\ &\geq \sum_{k=0}^{N} [u_1(k) y_1(k)] - \gamma_2^2 + \kappa \|u_2\|^2 \\ &= -\gamma_1^2 - \gamma_2^2 + \kappa \|u_2\|^2 . \end{aligned} \tag{5.82}$$

On the other hand,

$$\begin{aligned} -\sum_{k=0}^{N} [e'(k) u_2(k)] &\leq \frac{\beta}{2} \sum_{k=0}^{N} [u_2(k)]^2 + \frac{1}{2\beta} \sum_{k=0}^{N} [e'(k)]^2 \\ &= \frac{\beta}{2} \|u_2\|^2 + \frac{1}{2\beta} \|e'\|^2 \end{aligned} \tag{5.83}$$

by using the fact that $\sum_{k=0}^{N} \left[\sqrt{\frac{1}{2\beta}} e'(k) + \sqrt{\frac{\beta}{2}} u_2(k) \right]^2 \geq 0$, for any positive real number β. Thus,

$$\left(\kappa - \frac{\beta}{2} \right) \|u_2\|^2 \leq \frac{1}{2\beta} \|e'\|^2 + \gamma_1^2 + \gamma_2^2 . \tag{5.84}$$

Therefore, with a choice of $\beta < 2\kappa$, it follows that

$$\|u_2\|^2 \leq c_1 \|e'\|^2 + c_2 , \tag{5.85}$$

for some $0 < c_1 < \infty$ and $0 \le c_2 < \infty$. The l_2-norm of the signal $w(k)$ given in Eq. (5.55) that drives the adaptation is bounded. $e'(k)$ is related to $w(k)$ by

$$e'(k) = D(z^{-1})e(k+1) = D(z^{-1})\left[1 - z^{-1}Q\left(z^{-1}, \theta^{opt}\right)\right]w(k+1), \tag{5.86}$$

and $D(z^{-1})\left[1 - z^{-1}Q\left(z^{-1}, \theta^{opt}\right)\right]$ has finite magnitude at all frequencies. So $\|e'\|^2$ is bounded and it is concluded that $\|u_2\|^2$, $\|y_2\|^2$, $\|u_1\|^2$ and $\|y_1\|^2$ are all bounded, which proves that the PAA is stable.

5.3.4 Simulation Results

The proposed direct adaptive narrow band DOB scheme described in previous sections is applied to the open-source HDD benchmark problem available at [30] to show its performance. As usual, the baseline disturbance includes the disk flutter, the RRO, the measurement noise, and the torque noise. In addition, a fictitious sinusoidal signal at 700 Hz with time-varying magnitude and phase similar to the one described in Section 5.2.3 is injected to the servo loop at the beginning of the 2nd revolution to represent the narrow-band disturbance, which then stops at the end of the 7th revolution. Figure 5.25 shows the time trace of this narrow band disturbance by the solid line. The dashed line in Fig. 5.26 represents the PES due to all the disturbance and noise with the baseline controller only. We can see that the peak of the PES was larger than 15% track pitch and the resulting TMR was 19.92% track pitch, which is too large for the head to safely perform read/write operation.

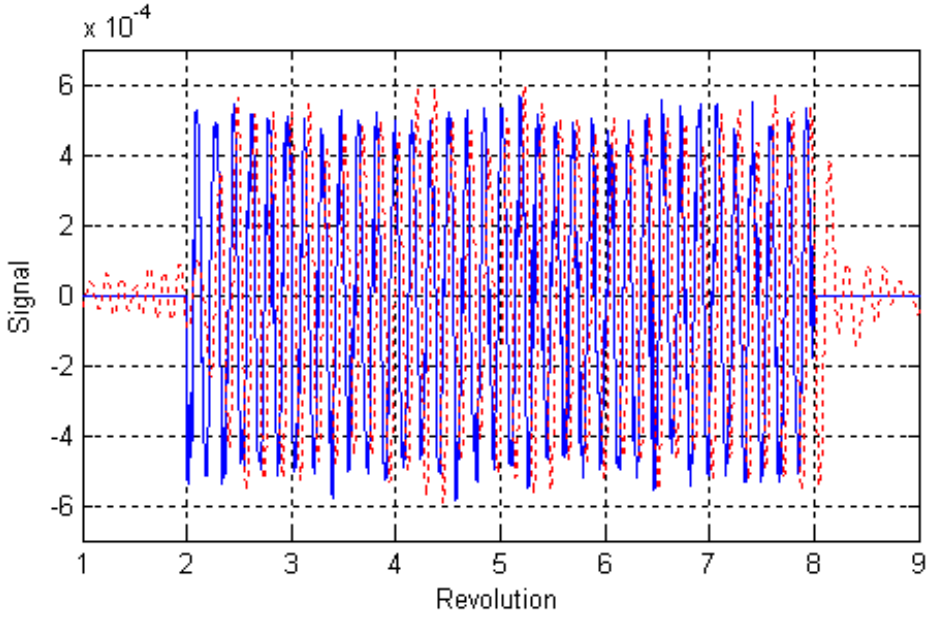

Figure 5.25: Narrow band disturbance (solid line) and disturbance estimate (dotted line).

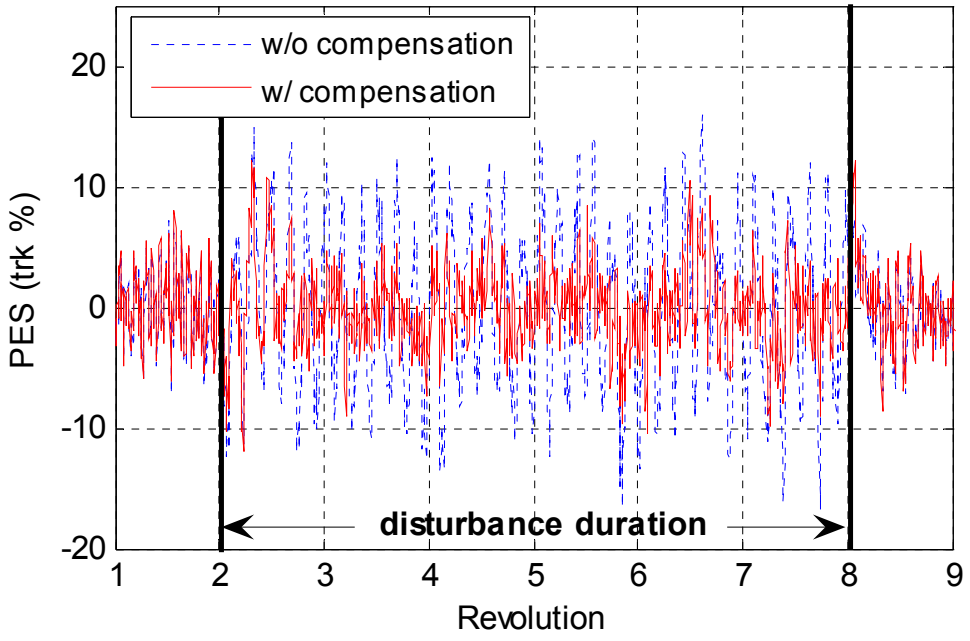

Figure 5.26: Time trace of PES without and with the proposed adaptive compensator.

The adaptation algorithm is driven by the filtered disturbance estimate, $w(k)$, which is represented by the dotted line in Fig. 5.25. Notice that the disturbance estimate has same frequency and similar magnitude as the injected narrow band disturbance. The proposed compensator is turned on at the beginning of the simulation. The initial value of the adaptation gain is set to 10,000 ($F(0)$ = 10,000) and the initial guess of the parameter estimate is $\theta(0) = \cos(2\pi T_S \times 500)$, the middle point of the frequency range of interest. Figure 5.27 shows the convergence of the parameter estimate. We can see that the estimate converges to the neighbourhood of the optimal value $\cos(2\pi T_S \times 720.8)$ within one revolution and the variation after convergence was small. The resulting PES with the proposed compensator had smaller peak value than the one without compensation in the time window from the beginning of the 2nd revolution to the end of the 7th revolution as shown in Fig. 5.26. Figure 5.28 compares the spectral densities of the PES in that time window without and with the proposed compensator. The TMR is improved by 50.2% (9.91% track pitch with compensation) due to the big attenuation at the disturbance frequency. We can also notice that when no narrow-band disturbance is present, the PES is similar with or without the proposed compensator.

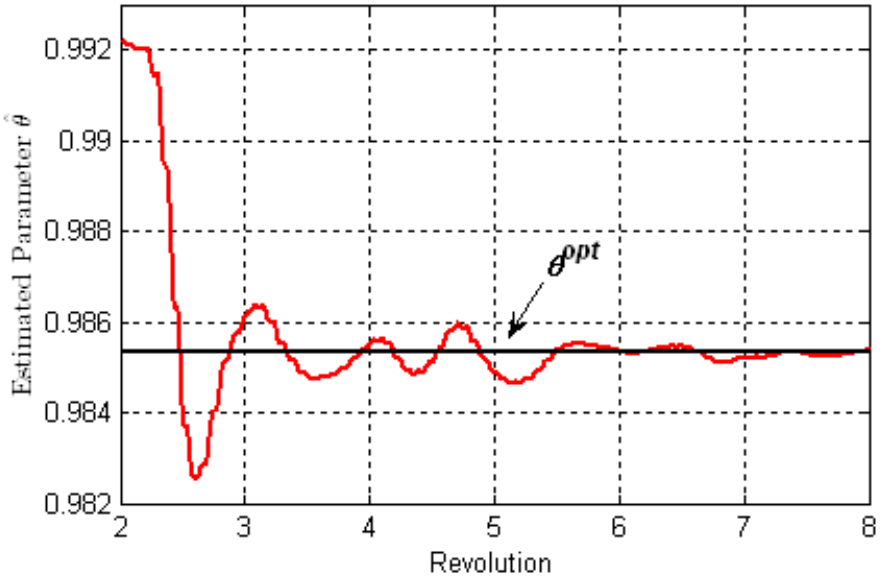

Figure 5.27: Simulation result of Q filter parameter estimation for the narrow band DOB.

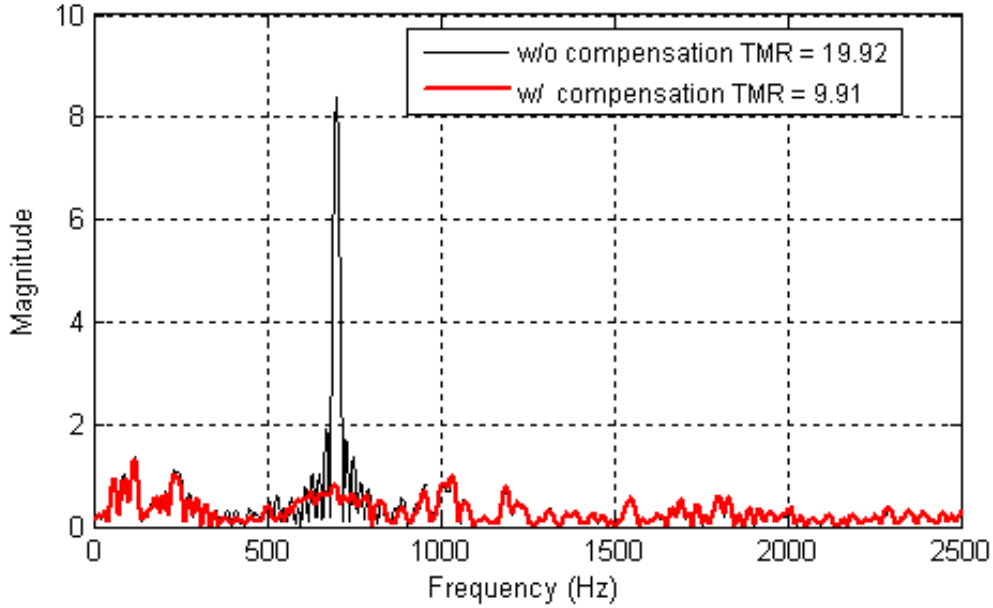

Figure 5.28: Spectral densities of PES without and with direct adaptive narrow band DOB.

5.4 Summary and Concluding Remarks

This chapter has been concerned with direct adaptive rejection schemes for narrow band disturbance rejection. Two schemes have been described. One is based on Youla-Kucera parameterization (Method 1) and the other is direct adaptive narrow band disturbance (Method 2). Each method has both advantages and disadvantages, which will be discussed in this section.

When the plant model is accurate and a sinusoidal disturbance is the only disturbance (the ideal case), Method 1 can completely reject the disturbance according to the internal model principal and outperforms Method 2 that can only reduce the disturbance by around 97%. Since for the HDD system, the accurate plant model is never available and there are many other kinds of disturbances, Method 1 and Method 2 give similar attenuation of the narrow band disturbance.

By the nature of the internal model principal, Method 1 can be easily extended to handle multiple narrow band disturbances by increasing the order of the FIR Q filter such that Eq. (5.15) has a unique solution ([48], [50]). But for Method 2, there is not straightforward way of devising a Q filter for multiple narrow band disturbance.

Computational complexity must be taken into consideration when choosing a control algorithm. Method 1 requires a lot of computational effort, since there are two parameters to estimate, compared to one parameter to estimate for Method 2. At each control sample, the amount of multiplication and addition operations required to calculate parameter estimate and adaptation for Method 1 is more than twice as large as that for Method 2. Although the computation power keeps growing on the modern controller chips, computationally simple algorithm is always more preferable in HDD systems to reduce computational delay that can severely degrade stability margins of the closed loop system. Another benefit of using Method 2 is that it can be kept on all the time whether narrow band disturbance occurs or not to avoid transient oscillation without wasting too much computational effort.

The convergence of the parameter estimate for Method 1 is guaranteed in the ideal case. But in the practical case where the plant model is inaccurate, there is no existing convergence proof for Method 1, while for Method 2 the stability proof shows that the parameter estimate does not go unbounded.

In this chapter, the performance of Method 1 and Method 2 is shown by applying each method to reject a narrow band disturbance in the frequency range [200 Hz, 800 Hz]. Both methods will work for a wider frequency range as long as the plant model in the range is good. When the frequency range is wider, however, performance of the disturbance rejection may be poorer. The reason for the performance degradation is that the parameter estimates become less accurate because more noise may be involved during estimation. In contrast, if we have better prior knowledge about the narrow band disturbance so that the frequency range may be tighter, then the performance will be better.

Chapter 6

Conclusions and Future Research

6.1 Conclusions

This dissertation has introduced several adaptive control schemes to reject the narrow band disturbance in HDD systems to improve the performance of the track-following servo control for higher achievable areal densities.

The HDD plant for servo control system consists of the power amplifier, the voice coil motor (VCM), and the head stack assembly (HSA). The head position is controlled by the servo system in either of the two operation modes: track-following and track-seeking. Several existing HDD servo controllers have been reviewed in Chapter 1.

As discussed in Chapter 2, the sources of track mis-registration (TMR) can be categorized into repeatable runout (RRO) and non-repeatable runout (NRRO), and correspondingly the position error signal (PES) is decomposed into repeatable PES (RPES) and non-repeatable PES (NRPES). The focus of this dissertation was rejecting the dominant frequency components in the NRPES spectrum so that the performance of the track-following servo control system was enhanced by reducing the TMR.

Chapter 3 provided an overview of the adaptive control theory, which is categorized into direct adaptive control and indirect adaptive control depending on the way that the controller parameters are adjusted. Examples of popular direct adaptive control and indirect adaptive control schemes were introduced. Several applications of the adaptive control theory to HDD servo systems were also discussed in Chapter 3.

Chapter 4 was concerned with the indirect adaptive control for rejecting narrow band disturbance, involving frequency identification and add-on compensation. Two frequency identification algorithms were described: the discrete Fourier transform which is the frequency-

domain representation of the PES and the least mean squares (LMS) algorithm which is based on the parametric model of a sinusoidal signal. With the frequency estimate of the narrow band disturbance, an add-on compensator was applied to reject it. One compensator design estimated the magnitude and the phase of the narrow band disturbance using the basis function algorithm. An alternative compensator is the disturbance observer (DOB) with a narrow bandpass Q filter. Conclusions of this study are

- The DFT method is suitable for accurate off-line frequency identification, while the LMS method is a computationally simple on-line approach.

- The basis function algorithm based compensator provides a near perfect rejection of the disturbance, while the DOB based compensator results in about 30 dB attenuation in the frequency response of the error rejection function at the disturbance frequency.

- The compensator using the basis function algorithm can be extended to reject multiple frequency components, which is difficult for the DOB based approach. If we apply multiple narrow bandpass Q filters to reject multiple frequency components, they will adversely affect one another degrading the overall performance.

- The resulting closed-loop system with the DOB based compensator is a linear time invariant system so that it is possible to show that the robustness of the system is similar to the baseline system.

- The basis function algorithm requires more computational effort to obtain the magnitude and the phase estimates than the DOB based compensator which does not involve any parameter estimation.

Two direct adaptive rejection schemes for the narrow band disturbance were introduced in Chapter 5. One scheme is based on Youla-Kucera (YK) parameterization with a pre-specified term to improve transient responses and a bandpass filter to deal with inaccurate HDD plant models as well as to limit the waterbed effect to a certain frequency range. The other direct adaptive scheme adopts the structure of the DOB with a narrow bandpass Q filter. The frequency coefficient of the Q filter is adapted through the minimization of the TMR caused by the narrow band disturbance. The conclusions of the two direct adaptive rejection schemes are

- Theoretically, the YK parameterization based scheme can completely reject the narrow band disturbance. However, due to the inaccuracy of the plant model and disturbances other than the dominant frequency component, the YK based scheme gives only a similar amount of attenuation of the dominant component as the DOB based scheme.

- The YK based scheme can be easily extended to reject multiple frequency components, while for the DOB based scheme, there is no straightforward way of adapting a Q filter for multiple components.

- One main drawback of the YK parameterization based scheme is its computational

intensity as two parameters need to be estimated for rejecting one frequency component. The computation involved in DOB based scheme is less than half of the YK parameterization approach.

- The hyperstability of the DOB based scheme assures that the parameter estimate does not go unbounded. The convergence of the parameter estimates for the YK parameterization scheme is guaranteed in the ideal case. In the practical cases where the plant model is inaccurate, however, there is no existing convergence proof for the scheme.

All compensation schemes introduced in this dissertation for HDD servo systems can be applied with no or little modification to reject narrow band disturbances in other servo systems, such as optical disk drives, microphones, and active suspension systems.

6.2 Future Research Topics

The disk flutter induced disturbances in HDD systems may show up in PES spectrum as several narrow band peaks only a few hundred hertz apart from one another. Due to the change of boundary conditions of the disk flutter, a real-time method to reject such disturbances is preferred. A multiple component frequency identification algorithm with good resolution is required for any indirect adaptive rejection schemes to work in this case. The direct adaptive control schemes must be improved to handle such clustered narrow band disturbances.

To avoid exciting the resonant modes in HDD systems, notch filters at resonant frequencies are commonly used. When the frequency of a notch filter does not align with the targeted resonant mode due to either the change of environment or parameter perturbation caused by mass production, a big peak shows up in the PES spectrum and the system can even be unstable. Thus, the detection of such resonances is an issue, and properly altering notch parameters on the fly is an important topic for HDD servo control.

The first one or two revolutions after the track seeking operation are usually referred to as settling stage. The PES for the settling stage is called settle PES. Sometimes a seek operation can induce big settle PES oscillation, which can greatly increase seek time and worsen seek consistency. The oscillation can be caused by improper mode switching or sometimes by where the drives are sitting. These causes are unit dependent also. So it is crucial for the HDD servo system to detect the settle oscillation and compensate for it to achieve fast and consistent seeking performance for each HDD unit.

The dual-stage HDD systems use an additional piezoelectric actuator to achieve a higher bandwidth than the traditional single-stage HDD systems discussed in this dissertation, which means that the dominant frequency component may reside in higher frequency range for the dual-stage HDD systems. This may require some modification of the rejection schemes introduced in this dissertation to handle narrow band disturbances in dual-stage HDDs. Moreover, dual actuation may provide more degree of freedom for the narrow disturbance compensator design.

Bibliography

[1] T. J. Abatzoglou. A fast maximum likelihood algorithm for frequency estimation of a sinusoid based on Newton's method. *IEEE Trans. on Acoustics, Speech and Signal Processing*, Vol. ASSP-33, No. 1, Feb. 1985.

[2] D. Abramovitch and G. Franklin. A brief history of disk drive control. *IEEE Control Systems Magazine*, Vol. 22, No. 3, pp. 28-42, Jun. 2002.

[3] D. Abramovitch, T. Hurst, and D. Henze. An overview of the PES Pareto method for decomposing baseline noise sources in hard disk position error signals. *IEEE Transactions on Magnetics*, Vol. 34, No. 1, pp. 17-23, Jan. 1998.

[4] D. Abramovitch, T. Hurst, and D. Henze. Decomposition of baseline noise sources in hard disk position error signals using the PES Pareto method. *Proceedings of the American Control Conference*, pp. 2901-2905, Albuquerque, Jun. 1997.

[5] D. Abramovitch, T. Hurst, and D. Henze. The PES Pareto method: uncovering the strata of position error signals in disk drives. *Proceedings of the American Control Conference*, pp. 2888-2895, Albuquerque, Jun. 1997.

[6] B. D. O. Anderson. From Youla-Kucera to identification, adaptive and nonlinear control. *Automatica*, Vol. 34, No. 12, pp. 1485-1506, 1998.

[7] B. D. O. Anderson and I. D. Landau. Least squares identification and the robust strict positive real property. *IEEE Trans. on Circuits and Systems*, Vol. 49, No. 9, 1994.

[8] B. D. O. Anderson and J. B. Moore. *Optimal Control: Linear Quadratic Methods*. Prentice Hall, Englewood Cliffs, NJ, 1990.

[9] K. Astrom and B. Wittenmark. On self-tuning regulators. *Automatica*, Vol. 9, pp. 185-199.

[10] K. Astrom and B. Wittenmark. Self-tuning regulators based on pole-zero placement. *IEE Proceedings Part D*, 127: 120-130, 1980.

[11] K. Astrom and B. Wittenmark. *Adaptive Control*, second edition. Addison-Wesley Publishing Company, 1995

[12] S. Bittanti, M. Campi and S. M. Savaresi. Unbiased estimation of a sinusoid in colored noise via adapted notch filters. *Automatica,* Vol. 33, No. 2, pp. 209-215, 1997.

[13] S. Bittanti and S. M. Savaresi. Safe estimate of sinusoidal signals for control applications. *Proc. of the 38th Conf. On Decision & Control*, pp. 2827-2832, Phoenix, AZ, Dec. 1999.

[14] M. Bodson, A. Sacks and P. Khosla. Harmonic generation in adaptive feedforward cancellation schemes. *IEEE Trans. on Automatic Control*, Vol. 39, No. 9, pp. 1939-1944, 1994.

[15] M. Bodson and S. Douglas. Adaptive algorithm for the rejection of sinusoidal disturbances with unknown frequency. *Automatica*, Vol. 33, No. 12, pp. 2213-2221, 1997.

[16] J-K. Chang and H. T. Ho. LQG/LTR frequency loop shaping to improve TMR budget. *IEEE Trans. on Magnetics*, Vol. 35, No. 5, pp. 2280-2282, Sep. 1999.
[17] S. Deeyiengyang and K. Ono. Suppressing of resonance amplitude of disk vibrations by squeeze air bearing plate. *IEEE Trans. on Magnetics*, Vol. 37, *No*. 2, pp. 820-825, Mar. 2001.
[18] J. C. Doyle, B. A. Francis and A. Tannenbaum. *Feedback Control Theory*. Macmillan, New York, 1992.
[19] C. Du, S. S. Ge, and F. L. Lewis. H_∞ compensation of external vibration impact on servo performance of hard disk drives in mobile applications. *Int. Journal of Adaptive Control and Signal Processing*, Vol. 22, pp. 374-387, 2008.
[20] C. Du, J. Zhang, and G. Guo. Vibration analysis and control design comparison of HDDs using fluid bearing and ball bearing spindles. *Proc. of the American Control Conf.*, Anchorage, Ak, pp. 1378-1383, May 2002.
[21] P. Gahinet and P. Apkarian. Following control of a hard disk drive by using sampled-data H_∞ control. *Proc. of IEEE Int. Conf. on Control Applications*, Hawaii, USA, pp. 182-186, Aug. 1999.
[22] M. Green and D. J. N. Limebeer. *Linear Robust Control*. Prentice Hall, Englewood, Cliffs, NJ, 1995.
[23] L. Guo and Y. Chen. Disk flutter and its impact on HDD servo performance. *IEEE Trans. on Magnetics*, Vol. 37, No. 2, pp. 866-870, Mar. 2001.
[24] G. Guo and J. Zhang. Feedforward control for reducing disk-flutter-induced track misregistration. *IEEE Transactions on Magnetics*, *Vol*. 39, *No*. 4, pp. 2103-2108, Jul. 2003.
[25] Y. Hamada, H. Otsuki, S. Saito and Y. Hata. Application of disturbance observer for head positioning control system of disk drive. *Trans. Soc. Instrum. Contr. Eng.*, Vol. 30, No. 7, pp. 828-835, Jul. 1994.
[26] H. Hanselman and W. Mortix. High-bandwidth control of the head-positioning mechanism in a Winchester disk drive. *IEEE Control Systems Magazine*, Vol. 7, No. 5, pp. 15-19, Oct. 1997.
[27] F. R. Hansen, G. F. Franklin and R. L. Kosut. Closed-loop identification via the fractional representation: experiment design. *Proc. Amer. Control Conf.*, pp. 386-391, 1989.
[28] M. Hayes. Statistical Digital Signal Processing and Modeling. New York: John Wiley & Sons Inc., 1996.
[29] B. Heo, I. Shen, and J. Riley. Reducing disk flutter by improving aerodynamic design of base castings. *IEEE Transactions on Magnetics*, *Vol*. 36, *No*. 5, pp. 2222-2224, Sept. 2000.
[30] M. Hirata et al. Benchmark problem of Hard Disk Drive System. http://mizugaki.iis.u-tokyo.ac.jp:80/nss/MSS_bench_e.htm.
[31] L. Hitz and B. Anderson. Discrete positive real functions and their application to system stability. *Proc. IEEE*, Vol. 111, pp. 153-155, 1969.
[32] R. Horowitz and B. Li. Adaptive track-following servos for disk file actuators. *IEEE Trans. on Magnetics*, Vol. 32, No. 3, pp. 1779-1786, May 1996.
[33] Y. Huang and W. Messner. A novel disturbance observer design for magnetic hard disk drive servo system with a rotary actuator. *IEEE Trans. on Magnetics*, Vol. 34, No. 4, pp. 1892-1894, Jul. 1998.
[34] X. Huang, M. Hoque, X. Wang, and F. Yap. A feedback control system for suppressing rotating disk flutter in hard disk drives. *Digest of the Asia-Pacific Magnetic Recording*

Conference 2002, pp. AA5-01AA5-02, Piscataway, NJ, USA.
[35] S. Imai, M. Tokuyama, and Y. Yamaguchi. Reduction of disk flutter by decreasing disk-to-shroud spacing. *IEEE Transactions on Magnetics*, *Vol*. 35, *No*. 5, pp. 2301-2303, Sept. 1999.
[36] P. A. Ioannu and P. V. Kokotovic. *Adaptive Systems with Reduced Models*. Springer-Verlag, New York, 1983.
[37] G. Jang, S. Hong, D. Kim, and J. Han. New design of a HDD spindle motor using damping material to reduce NRRO. *IEEE Transactions on Magnetics,* Vol.36, No.5, pp. 2258-60, Sept. 2000.
[38] Q. Jia and S. Yoshida. Design of HDD servo controller with adaptive IMC structure. *Proc. of the 2006 IEEE Int. Conf. on Mechatronics and Automation*, Luoyang, China, pp. 1280-1285, Jun. 2006.
[39] R. Kalman. Design of self-optimization control systems. *Trans. ASME*, *J. Basic Eng.*, Vol. 80, pp. 468-478, 1958.
[40] C. Kempf, W. Messner, M. Tomizuka and R. Horowitz. Comparison of four discrete-time repetitive control algorithms. *IEEE Control System Magazine*, Vol. 13, No. 6, pp. 48-54, Dec. 1993.
[41] R. J. Kenefic and A. H. Nuttall. Maximum likelihood estimation of the parameters of a tone using real discrete data. *IEEE Journal of Oceanic Engineering*, Vol. OE-12, No. 1, Jan. 1987.
[42] Y. Kim, C. Kang, and M. Tomizuka. Adaptive and optimal rejection of non-repeatable disturbance in hard disk drives. In *2005 IEEE/ASME International Conference on Advanced Intelligent Mechatronics*, Monterey, Vol. 1, pp. 1-6, Jul. 2005.
[43] M. Kobayashi, S. Nakagawa, and S. Nakamura. A phase-stabilized servo controller for dual-stage actuators in hard disk drives. *IEEE Transactions on Magnetics*, 39(2), pp. 844-850, Mar. 2003.
[44] K. Krishnamoorthy and T-C. Tsao. Robust adaptive-Q with two period repetitive control for disk drive track following. *Proc. of the 2005 IEEE/ASME Int. Conf. on Advanced Intelligent Mechatronics*, Monterey, CA, pp.13-18, Jul. 2005.
[45] I. D. Landau. A Hyperstability criterion for model reference adaptive control systems. *IEEE Trans. on Aut. Contr.*, AC-14, pp. 552-555, 1969.
[46] I. D. Landau. A stability theorem application to adaptive control. *IEEE Trans. on Aut. Contr.*, AC-25(4), pp. 814-817, 1980.
[47] I. D. Landau. *System Identification and Control Design*. Prentice Hall, 1990.
[48] I. D. Landau, A. Constantinescu, and D. Rey. Adaptive narrow band disturbance rejection applied to an active suspension – an internal model principle approach. *Automatica*, 41(4):563-574, 2005.
[49] I. D. Landau, R. Lozano, and M. M'Saad. *Adaptive Control*. Springer-Verlag London.
[50] I. D. Landau and D. I. Patrascu. Rejection of unknown multiple narrow band disturbances - a direct adaptive control approach. *Proc. of European Control Conf. 2007*, Kos, Greece, Jul. 2007.
[51] Y. D. Landau. Adaptive control, the model reference approach. Marcel Dekker, 1979.
[52] S-H. Lee, Y-H. Kim, and S-E. Baek. Discrete-time robust tracking control using a state space disturbance observer. *Proc. of the American Control Conference*, pp. 4149-4198, Chicago, IL, Jun. 2000.
[53] H-S. Lee and M. Tomizuka. Robust digital tracking controllers for high-accuracy

positioning system. *IEEE Trans. on Industrial Electronics*, Vol. 43, No. 1, pp. 48-55, Feb. 1996.
[54] G. Li. A stable and efficient adaptive notch filter for direct frequency estimation. *IEEE Trans. on Signal Processing*, Vol. 45, No. 8, pp. 2001-2009, Aug. 1997.
[55] L. Ljung. *System Identification – Theory for the User*. Prentice Hall, Englewood Cliffs, NJ, 1987.
[56] L. Ljung and T. Soderstron. *Theory and Practice of Recursive Identification*. MIT Press, Cambridge, MA, 1983.
[57] A. A. Mamun, G. Guo, and C. Bi. *Hard Disk Drive: Mechatronics and Control*. CRC Press, USA, 2007.
[58] W. Messner, R. Horowitz, W. W. Kao, and M. Boals. A new adaptive learning rule. *IEEE Transactions on Automatic Control*, Vol. 36, pp. 188-197, Feb. 1991.
[59] J. B. Moore, L. Xia and K. Glover. On improving control-loop robustness of model-matching controllers. *Systems Control Lett.*, Vol. 1, pp. 83-87, 1986.
[60] M. Morari and E. Zafiriou. *Robust Process Control*. Prentice Hall, Englewood Cliffs, NJ, 1989.
[61] P. Mukund and K. Martin. A second-order hyperstable adaptive filter for frequency estimation. *IEEE Trans. on Circuits and Systems-II: Analog and Digital Signal Processing*, Vol. 40, No. 6, pp. 398-403, Jun. 1993.
[62] T. Murakami and K. Ohnishi. Advanced motion control in mechatronics – a tutorial. *Proc. of the IEEE International Workshop on Intelligent Control*, Vol. 1, Istanbul, Turkey, pp. SL9-SL17, Aug. 1990.
[63] R. Oboe and M. Federico. Initial value compensation applied to disturbance observer-based servo control in HDD. *7th International Workshop on Advanced Motion Control*, pp. 34-39, 2002.
[64] D. Oh and S. Kang. Position error reduction in magnetic disk drives using a head gimbal assembly with radial head motion capability. *Microsystem Technologies*, Vol.11, No.8-10, pp. 728-33, Aug. 2005.
[65] K. Ohnishi. A new servo method in mechatronics. Trans. Of Japanese Society of Electrical Engineering, Vol. 107-D, pp. 83-86.
[66] R. Ortega, L. Praly and I. D. Landau. Robustness of discrete-time direct adaptive controllers. *IEEE Trans. on Aut. Contr.*, AC-30(12), pp. 1179-1187, 1985.
[67] L. Pao and G. F. Franklin. Time optimal control of flexible structures. *Proc. of the 19th IEEE Conf. of Decision and Control*, pp. 2580-2581, Honolulu, Hawaii, 1990.
[68] V. Peterka. Adaptive digital regulation of noisy systems. Preprints *2nd IFAC Symposium on Identification and Process Parameter Estimation*, Prague, 1970.
[69] V. F. Pisarenko. The retrieval of harmonics from a covariance function. *Geophysics J. Roy. Astro. Soc.*, Vol. 33, pp. 347-366, 1973.
[70] V. Popov. Solution of a new stability problem for controlled systems. *Auto. Remote Control*, 24(1), pp. 1-23.
[71] V. Popov. *Hyperstability of Automatic Control Systems*. Springer Verlag, Heidelberg, Germany.
[72] R. Schmidt. Multiple emitter location and signal parameter estimation. *Proc. RADC Spectrum Estimation Workshop*, pp. 243-258, 1979.
[73] R. J. P. Schrama. An open-loop solution to the approximate closed-loop identification problem. *Proc. 9th IFAC/IFORS Symp. On Identification and Systems Parameter*

Estimation, Budapest, pp. 1602-1607, 1991.
[74] C. Smith and M. Tomizuka. Shock rejection for repetitive control using a disturbance observer. *Proc. 35th IEEE Conf. Decision and Control*, Kobe, Japan, pp. 2503-2504, Dec. 1996.
[75] H.C. So. A closed form frequency estimator for a noisy sinusoid. In *45th IEEE. Midwest Symp. Circuits Systems*, Tulsa, OK, 2002.
[76] H.C. So. A comparative study of three recursive least-squares algorithms for single-tone frequency tracking. *Signal Processing*, Vol. 83, pp. 2059-2062, 2003.
[77] H.C. So and Y. T. Chan. Two algorithms for frequency estimation of a real sinusoid from short data records. *IEEE Int. Symp. On Circuits and Systems*, pp. III-391-394, Geneva, Switzerland, May 2000.
[78] S-M. Suh, C. C. Chung, and S-H. Lee. Discrete-time track following controller design using a state-space disturbance observer. *Microsystem Technologies*, Vol. 9, pp. 352-361, 2003.
[79] T. T. Tay, J. B. Moore and R. Horowitz. Indirect adaptive techniques for fixed controller performance enhancement. *Int. J. Control*, Vol. 50, pp. 1941-1959, 1989.
[80] M. Tomizuka. Feedforward digital tracking controllers for motion control applications. *Advanced Robotics*, Vol. 7, No. 6, pp. 575-586, 1993.
[81] M. Tomizuka. Zero-phase error tracking algorithm for digital control. *ASME J. Dynamic Systems*, *Measurement and Control*, Vol. 109, pp. 65-68, Mar. 1987.
[82] M. Tomizuka, K. Chew, and W. Yang. Disturbance rejection through an external model. *ASME Journal of Dynamic Systems, Measurement and Control*, Vol. 112, pp. 559-564, Dec. 1990.
[83] M. Tomizuka and C. Kempf. Design of discrete time repetitive controllers with applications to mechanical systems. *Proceedings of 11th International Federation of Automatic Control World Congress*, Vol. 5, Tallinn, Estonia, U.S.S.R, 1990.
[84] T. Umeno and Y. Hori. Robust speed control of DC servomotors using modern two-degrees-of-freedom controller design. *IEEE Trans. on Industrial Electronics*, Vol. 38, No. 5, pp. 363-368, Oct. 1991.
[85] X. Wang and X. Huang. Feedback control and optimization for rotating disk flutter suppression with actuator patches. *AIAA Journal*, *Vol*. 44, *No*. 4, pp. 892-900, Apr. 2006.
[86] M. T. White, M. Tomizuka, and C. Smith. Improved track following in magnetic disk drives using a disturbance observer. *IEEE/ASME Trans. on Mechatronics*, Vol. 5, No. 1, pp. 3-11, Mar. 2000.
[87] J. Willems. *The Analysis of Feedback Systems*. MIT Press, Cambridge, MA, 1971.
[88] L. B. White. A fast recursive algorithm for the maximum likelihood estimation of the parameters of a periodic signal. *IEEE Trans. on Signal Processing*, Vol. 41, No. 11, Nov. 1993.
[89] M. L. Workman. *Adaptive proximate time optimal servomechanism*. PhD thesis, Stanford University, 1987.
[90] D. Wu, G. Guo, and T.C. Chong. Midfrequency disturbance suppression via micro-actuator in dual-stage HDDs. *IEEE Transactions on Magnetics*, 38(5), pp. 2189-2291, Sept. 2002.
[91] S. Wu and M. Tomizuka. Repeatable runout compensation for hard disk drives using adaptive feedforward cancellation. In *2006 American Control Conference*, pp. 6, Piscataway, NJ, USA.
[92] T. Yamaguchi, K. Shishida, S. Tohyama, Y. Soyama, H. Hosokawa, H. Ohsawa, H.

Numasato, T. Arai, K. Tsuneta, and H. Hirai. A mode-switching controller with initial value compensation for hard disk drive servo control. *Control Eng. Practice*, Vol. 5, No. 11, pp. 1525-1532, Aug. 1997.

[93] T. Yamaguchi, Y. Soyama, H. Hosokawa, K. Tsuneta, and H. Hirai. Improvement of settling response of disk drive head positioning servo using mode switching control with initial value compensation. *IEEE Trans. on Magnetics*, Vol. 32, No. 3, pp. 1767-1772, May 1996.

[94] B. Yao, M. Al-Majed, and M. Tomizuka. High performance robust motion control of machine tools: an adaptive robust control approach and comparative experiments. *IEEE/ASME Trans. on Mechatronics*, Vol. 2, No. 2, pp. 63-76, Jun. 1971.

[95] L. Yi. *Two Degree of Freedom Control for Disk Drive Servo Systems*. PhD Dissertation, University of California at Berkeley, 2000.

[96] L. Yi and M. Tomizuka. Robust motion control of mechanical systems with compliance. *Proc. of the 35th IEEE Conf. on Decision and Control*, pp. 2462-2467, Kobe, Japan, 1996.

[97] L. Yi and M. Tomizuka. Regulation of mechanical systems with compliance. *Proc. of the second Chinese World Congress on Intelligent Control and Intelligent Automation*, pp. 1571-1576, Xi'an, China, 1997.

[98] G. Zames. Feedback and optimal sensitivity: model reference transformations, multiplicative seminorms, and approximate inverses. *IEEE Transactions on Automatic Control*, AC-36, pp. 301-320, 1981.

[99] G. Zames. On the input-output stability of nonlinear time-varying systems, parts I and II. *IEEE Trans. on Automatic Control*, AC-11, pp. 228-238 and pp. 465-477, 1966

[100] J. Zheng, G. Guo, Y. Wang, and W. Wong. Optimal narrow-band disturbance filter for PZT-actuated head positioning control on a spinstand. *IEEE Transactions on Magnetics*, 42(11), pp. 3745-3751, Nov. 2006.

[101] Q. Zheng and M. Tomizuka. Adaptive rejection of dominant frequency component of non-repeatable runout in hard disk drives. *Proc. of the European Control Conf.* 2007, Kos, Greece, pp. 158-165, Jul. 2007.

[102] Q. Zheng and M. Tomizuka. Compensation of dominant frequency components of non-repeatable disturbance in hard disk drives. *IEEE Trans. on Magnetics*, vol. 43, no. 9, pp. 3756-3762, Sep. 2007.

[103] Q. Zheng and M. Tomizuka. Direct adaptive rejection of narrow-band disturbances based on the Youla-Kucera parameterization. *CML Technical Report*, 07-014, Dec. 2007.

[104] Q. Zheng and M. Tomizuka. A disturbance observer approach to detecting and rejecting narrow-band external vibration in hard disk drives. *Proceedings 10th International Workshop on Advanced Motion Control*, Part vol.1, pp. 254-9, Mar. 2008.

[105] Q. Zheng and M. Tomizuka. Direct adaptive disturbance observer design for rejecting the narrow-band disturbance with unknown frequency in hard disk drives. *Proceedings of DSCC 2009: 2009 ASME Dynamic Systems and Control Conference*, Los Angeles, CA, 2009.

[106] K. Zhou, J. C. Doyle and K. Glover. *Robust and Optimal Control*. Prentice Hall, Englewood Cliffs, NJ, 1995.

[107] J. Zhou and Y. Wang. Multirate control for head actuator assembly vibration compensation with an accelerometer. *Digest of the Asia-Pacific Magnetic Recording Conf.*, pp. TU-P-14-01 to TU-P-14-02, 2002.